The background of the entire page is a close-up photograph of water with numerous bubbles of various sizes. The lighting is soft, creating a blue-green hue. The bubbles are in sharp focus in the foreground and become more blurred towards the background, giving a sense of depth. A semi-transparent dark blue horizontal band is overlaid across the middle of the image, containing the main title and other text.

Investigating PTFE Application on Carbon Fiber Paper for Anodic H_2O_2 Generation in Alkaline Water Electrolysis

Graduation Project

Delft University of Technology

Master of Science in Sustainable Energy Technology

Investigating PTFE Application on Carbon Fiber Paper for Anodic H₂O₂ Generation in Alkaline Water Electrolysis

Graduation Project

by

Antonius Waskito Widhiandono

Study Program	Student Number
MSc Sustainable Energy Technology	5849233

Thesis Committee:

Prof. dr. ir. **W. de Jong**

dr. **J.W. Haverkort**

dr. **L. Botto**

Daily Supervisor:

ir. **S. A. Phadke**

Project Duration:

October 2023 – August 2024

Cover photo credit: Water Bubbles Under the Sea by Pixabay from Pexels

Preface

As the climate crisis problem emerges, transformations have been made to overcome the issue. However, it is not simple since numerous aspects need to be considered to go within. So, the one aspect that I want to go contribute to the transformation into is the water electrolysis to produce hydrogen as a clean energy storage. Even though the concept has been found way centuries ago, the importance of the idea is not really well into the society since oil, coal, and natural gas have dominated the energy industries until the realization of now. After around two years of joining the EPC project upgrading a crude oil distillation unit, I have realized the importance of clean energy and straight away changing my future goal into studying in Sustainable Energy Technology in TU Delft in 2022.

Optimizing the selectivity towards H_2O_2 in water electrolysis system is a clear effort to support the transformation by rising its attractiveness to the market for H_2O_2 producers. And I am grateful to be a part of this project. However, completing this study has made several efforts of trial and error through design and experiment as well with revalidating several data that are still unsure of it is correct or not. Through these processes, supervisors and others have guided and motivated me to achieve the certain point where I can finally able to show the results in the end.

I want to give my special gratitude for my supervisors and thesis committee members. Mr. Prof. Wiebren de Jong, who has introduced me to the project and guided me throughout the thesis progress. Not only in electrochemistry, but he also taught me in the biomass courses which I followed back then in the first year. Mr. ir. Sohan A. Phadke, who has given me daily advices with patience and friendliness. He taught me not only in understanding the chemistry behind of it but also the mechanical hard skills which I am not very familiar with it until at the point when I can build the flow cell setup. Mr. dr. J. Willem Haverkort, who has let me join to the hydrogen bubbles research group where I can witness the aspects of electrochemical performance from multiphase flow and gives me advices on how to improve more on my thesis study during presentations. Mr. dr. Lorenzo Botto, who agreed to join as the external thesis committee member for my thesis graduation project. Besides the committee, I also want to give thanks to Mr. Jelmer Postma, Mr. Gilles Deiters, Mr. Emile Craye, Mr. Michel van den Brink, and Mr. Durga P.S. Mainali for the help to guiding and supporting me to do my experiment.

Additionally, I also want to give thanks to my family who lives in Indonesia and my Ooms and Tantes who live in the Netherlands for supporting me during my time to live here. As well, I want to give thanks for my SET and laboratory friends who motivates me to do the work.

I hope this study report could help to contribute the progress towards water electrolysis in the future.

Antonius Waskito Widhiandono

Delft, August 2024

Abstract

Hydrogen (H_2) is an important substance for clean energy storage, but the financial feasibility of large-scale water electrolysis remains a challenge. A promising approach to improve the economics of industrial electrolyzers is the anodic production of hydrogen peroxide (H_2O_2) during alkaline water electrolysis. This dual production could attract H_2O_2 producers and increase the value of electrolyzer output. However, achieving high H_2O_2 selectivity is difficult due to competition with other oxidation products. Recent studies have shown that incorporating polytetrafluoroethylene (PTFE) on carbon fiber paper (CFP) electrodes can enhance H_2O_2 production. Xia et al. suggest that PTFE's hydrophobicity confines O_2 , driving the reaction toward H_2O_2 . However, PTFE's inert characteristic makes complete coverage of the electrode impractical. Vogel et al. further noted that the O_2 bubble perimeter, which attracts more OH^- , a key reactant for H_2O_2 , could also increase H_2O_2 yield.

This project explores the effects of varying PTFE applications on carbon electrodes, focusing on three approaches: increasing the PTFE perimeter patterns ($P1 < P2 < P3 < P4$), increasing the PTFE area patterns ($A1 > A2 > A3 > A4$), and dip-coating the electrode in PTFE emulsion. The study uses a two-electrode system in a flow cell with a K_2CO_3 electrolyte, observing performance lifetime via chronopotentiometry and measuring H_2O_2 yield through permanganate titration. SEM and EDX are also used for electrode observation.

Results show that increasing the PTFE perimeter ($P1$ to $P2$) enhances H_2O_2 yield due to better O_2 bubble formation, but further increases ($P2$ to $P4$) have little effect. Increasing the PTFE area patterns generally shortens operational lifetime and reduces H_2O_2 yield, with $A2$ and $A3$ showing similar results due to potentially non-optimal spacing. PTFE dip-coating leads to rapid performance degradation, confirming that PTFE's lack of active sites makes it unsuitable for initiating reactions. Overall, optimizing PTFE surface area is improving H_2O_2 production in alkaline water electrolysis over than perimeter or dip-coating.

Contents

Preface	iii
Abstract	iv
Contents	v
Chapter 1 - Introduction	1
Chapter 2 - Theory	6
2.1. Alkaline Water Electrolysis.....	6
2.2. Separator and Current Collector.....	9
2.3. Chronopotentiometry.....	9
2.4. Anodic H ₂ O ₂ Production from Water Electrolysis.....	10
2.5. Measuring H ₂ O ₂ Concentration by Titration.....	11
2.6. Enhance Selectivity Towards H ₂ O ₂ by Electrode Materials.....	12
2.7. Scanning Electron Microscopy and Energy-Dispersive X-Ray.....	13
2.8. PTFE Characteristics and Its Role in Anodic H ₂ O ₂ Productivity.....	14
Chapter 3 - Methodology	17
3.1. Experiment Setup and Electrolyzer Flow Cell.....	17
3.2. Electrode Preparation.....	18
3.3. PTFE Stamping Method.....	19
3.4. PTFE Dip-Coating Method.....	21
3.5. Electrode Observation by Optical Microscope, SEM, and EDX.....	22
3.6. Chemicals Preparation.....	24
3.7. Data Measurement.....	26
Chapter 4 - Results and Discussions	27
4.1. Bare CFP as the Anode.....	27
4.2. Limitation of the Experiments.....	30
4.3. Perimeter Variation of PTFE Patterns.....	33
4.4. Area Variation of PTFE Patterns.....	35
4.5. Concentration Variation of PTFE-Dip Coated CFP.....	39
Chapter 5 - Conclusion and Recommendations	44
5.1. Conclusions.....	44
5.2. Recommendations.....	45
References	47

Appendix A - Optical Microscope Images.....	53
A.1. Bare Carbon	53
A.2. Perimeter Pattern Variations.....	54
A.3. Area Pattern Variations	58
A.4. Dip-Coating Variations	62
Appendix B - SEM Images and EDX Mappings.....	63
B.1. Bare Carbon	63
B.2. PTFE-patterned Electrode	65
B.3. Dip-coated Electrode	70

Chapter 1 - Introduction

The growing demand for renewable energy sources has exposed a common issue: intermittency. This issue happens due to a mismatch between when renewable resources are available and when the energy demand is highest. Energy storage technologies have been developed over time to tackle this problem. Hydrogen carriers are among the most popular options due to their high gravimetric energy density and involve non-carbon substances. Based on the Net Zero Emission scenario stated by IEA [1], H₂ demand growth will increase sixfold to 530 MT, with around half needed for the industrial and transportation sectors. However, this target is still far from the national Announced Pledges, which estimate around 250 MT of hydrogen demand [1].

One promising technology that can produce hydrogen is water electrolyzers. In short, water electrolysis involves electricity through an external circuit, electrodes, and the aqueous electrolyte. Then redox reactions would initiate surrounding the electrodes within the electrolyte producing H₂ and O₂. Unlike the previous technologies that involve carbon-based reactants such as water gas shift reactions, water electrolysis is clean since there is no carbon gases emitted from the process and the electricity can be supplied by renewable energy upstream processes such as solar panels, wind turbines, biomass processing, etc. One challenge is the development of feasible electrolyzers, as their levelized cost was higher than that of carbon capture and storage technology in 2019 and is predicted to remain high in 2060 [2].

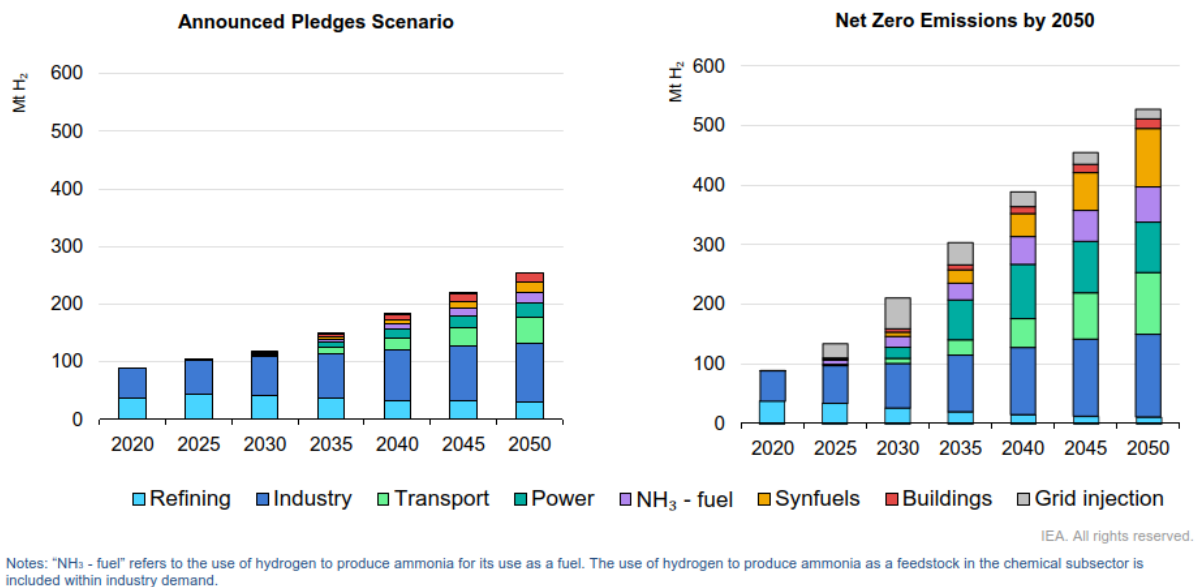


Figure 1.1 Hydrogen demand for each sector based on the Announced Pledges and Net Zero Emission scenarios by 2020 to 2050, plotted by IEA [1]

Several factors are found to enhance the feasibility of using electrolyzers through decreasing the cost of low-carbon electricity, increasing efficiency, lowering capital expenses, etc [1]. One method that is also being investigated is utilizing O₂ gas as a side product to be sold into the industrial market. An article shows the O₂ demand CAGR is projected to be 7.9% for the industry sector due to the use to convert chemicals and optimize combustion processes [3]. Although O₂ generation via electrolysis offers sustainability, the expenditure is still quite expensive compared to other mature technologies such as air separation units and pressure swing adsorption [4].

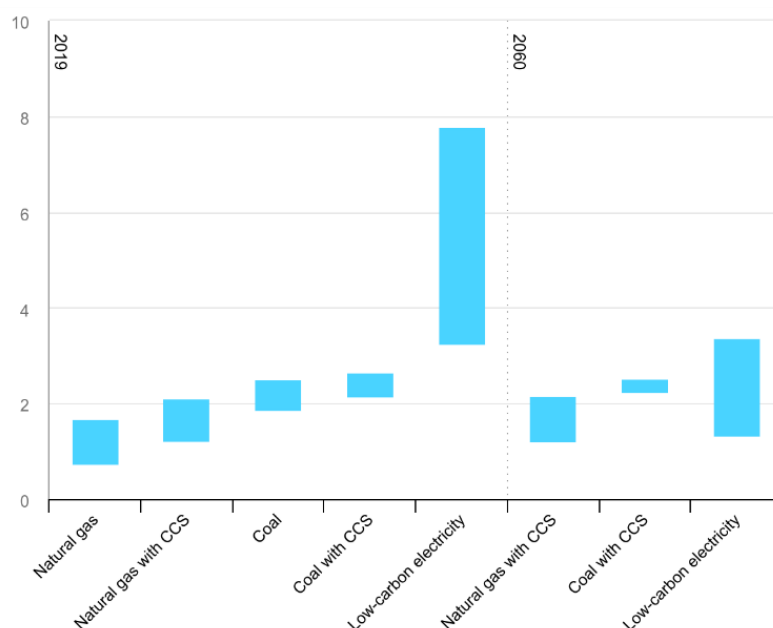


Figure 1.2 Comparison of LCOH of H₂ between different technologies (USD per kg of H₂), plotted by IEA [2]

A novel, promising approach is generating hydrogen peroxide (H₂O₂) via anodic reaction in water electrolysis. H₂O₂ is known to be a green oxidant (decomposes as water and O₂) that is used in several industries such as pulp and paper, wastewater treatment, and textiles [5] [6] [7]. The common industrial process involves the hydrogenation of an anthraquinone compound, followed by oxidation to produce H₂O₂. However, the requirement of H₂, high-temperature conditions, and the amount of CO₂ generated (steam methane reforming involved in the conventional process) would not consider this process sustainable [8] [9] [10].

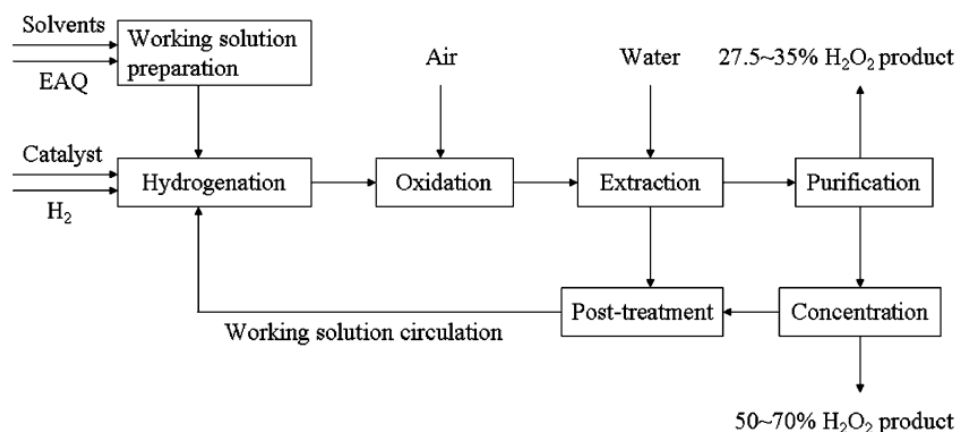


Figure 1.3. Process flow diagram in producing H₂O₂ through the anthraquinone route, made by Gao et al. [11]

Water electrolyzers that produce both H₂ and H₂O₂ could become highly attractive to such industries. According to Intratec's commodity price monitoring history from July 2019, H₂O₂ was at 567 USD per metric ton [12]. In comparison, O₂ for 12.5 Cents per Nm³ or 87.47 USD per metric ton (1 Nm³ of O₂ is equivalent to 1.4291 kg of O₂) [13] [14]. The high-valued H₂O₂ could potentially reduce the high LCOH from water electrolyzers, enabling a more economically viable method.

The common issue with this approach is shifting the water oxidation reaction selectivity towards H_2O_2 . Three known water oxidation reactions (**Equations 2.11 – 2.13**) would occur and H_2O_2 must compete with all of them together. Shi et al. argued as well that the lack of development towards H_2O_2 compared to O_2 throughout time is also a reason why anodic H_2O_2 electro-generation is challenging [15]. Several efforts have been made to overcome the competition such as selecting different electrode materials, surface modifications, and using different electrolytes [15] [16] [17] [18] [19] [20] [21].

A recent finding suggests applying hydrophobic PTFE on the anode surface to increase selectivity towards H_2O_2 . PTFE is hydrophobic and a study shows that confining O_2 bubbles can increase selectivity toward H_2O_2 [22]. Numerous studies have found that using PTFE with carbon-based electrodes yields more H_2O_2 [22] [23] [24]. The abundance and low cost of these PTFE and carbon-based materials could make the concept of selling H_2O_2 to lower LCOH to be more feasible in the future.

This project addresses the application of PTFE on carbon-based materials at a larger scale. PTFE is known to have a high electrical resistivity and nonreactive [25]. Xia et al. demonstrated the PTFE patterns on glassy carbon anodes for H_2O_2 electro-generation as shown in **Figure 1.4** [22]. Xia et al. found a small improvement with the glassy carbon patterning and attributed it to the triple-phase boundary of trapped oxygen bubbles on PTFE, glassy carbon electrode, and electrolyte [22]. When Xia et al. extended to PTFE-coated carbon fiber paper (CFP), a large increase in selectivity towards H_2O_2 was observed [22].

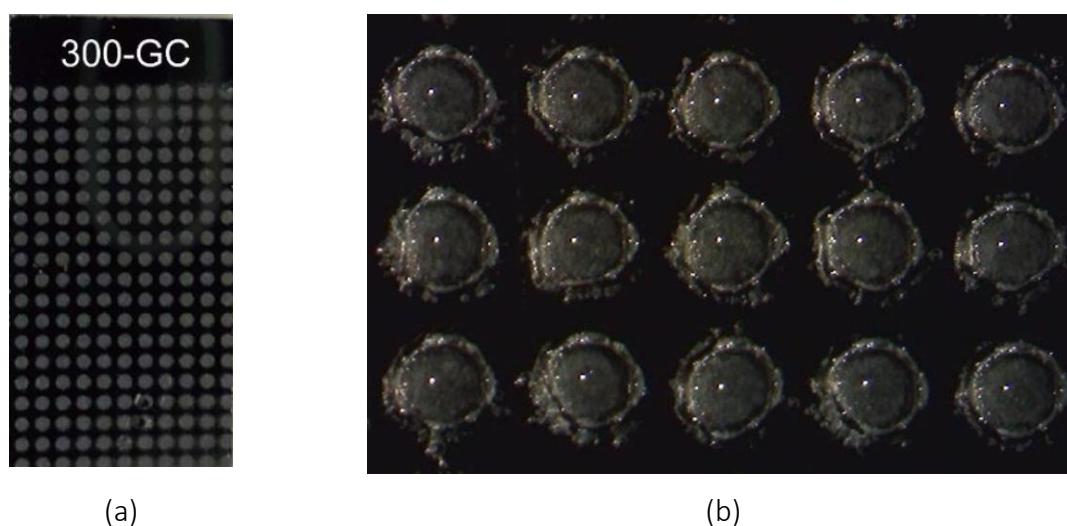


Figure 1.4 Images of PTFE-patterned on the glassy carbon electrode, taken by Xia et al. [22] : (a) 300 microns of PTFE-patterns on the glassy carbon anode (b) an image from a clip showing oxygen bubbles are attached on the patterns during the electrolysis

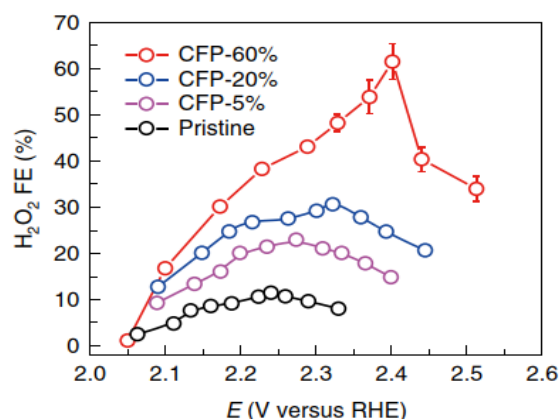


Figure 1.5 Higher concentration of PTFE increased the Faradaic efficiency of H_2O_2 . Plotted by Xia et al. [22]

Since electron transfer is required to do the redox reaction, covering the entire surface of the electrode with PTFE might be not optimal. Less electron conductivity from the electrode to transfer electrons toward ions would lead to higher current localization around the PTFE, potentially releasing heat that could damage the carbon fibers. The lifetime of the electrode is crucial for long-term energy storage solutions. Conversely, the consequence of applying less PTFE on the surface would decrease selectivity towards H_2O_2 . Therefore, the surface area of PTFE should be optimized based on the desired performance.

Furthermore, Vogel et al. have found that the circumference of O_2 bubbles enhances the electrochemical reaction [26]. The author observed that the bubble gathered an excessive amount of OH^- leading to high local anodic current density and lowering the oxidation potential OH^* from OH^- by at least 0.7 V than the supposed redox value [26]. Yet the study focused on the polymerization from OH^* which is produced by the reaction of OH^- [26].

Xia et al. suggest that the perimeter around trapped bubbles is crucial for promoting H_2O_2 production, while Vogel et al. argue that it is the perimeter around adhered bubbles that enhance the reaction. To test these hypotheses, this study aims to investigate the effects of altering the PTFE perimeter while keeping the area constant, and vice versa. This approach will help to determine whether the PTFE perimeter specifically influences the reaction or if it is the overall amount of PTFE on the sample that plays a more significant role. The main objective and research questions are stated below.

Main Objective:

To observe the effects of PTFE distribution variation through patterning in the alkaline water electrolysis on performance lifetime and H_2O_2 yield.

Research Questions:

1. Does PTFE applied on CFP have better stability than bare CFP?

Sub-research questions 1- What changes occur in performance lifetime due to different:

- area variations of PTFE patterns?
- perimeter variations of PTFE patterns?
- concentrations of PTFE applied through dip-coating?

2. How should PTFE be applied to the CFP electrode to yield more H_2O_2 ?

Sub-research questions 2 – What changes occur in H_2O_2 yield due to different:

- (a) **area** variations of PTFE patterns?
- (b) **perimeter** variations of PTFE patterns?
- (c) **concentrations of PTFE** applied through dip-coating?

The next following chapters would be four in total. Chapter 2 overviews the theories that are relevant to the study. Chapter 3 discusses the methodology. Chapter 4 presents the results and discussions. Chapter 5 concludes with the main objective and the results.

Chapter 2 - Theory

This chapter focuses on the theories regarding this project about PTFE on carbon-based electrodes to produce H_2O_2 generation via electrolysis. **Section 2.1** presents the general knowledge of alkaline water electrolysis. **Section 2.2** briefly discusses the separator and current collector. **Section 2.3** briefly discusses the chronopotentiogram. **Section 2.4** explores the H_2O_2 production from water electrolysis on the anodic side. **Section 2.5** briefly explains the H_2O_2 by KMnO_4 titration. **Section 2.6** reviews the material selection for enhancing the H_2O_2 generation. **Section 2.7** briefly explains scanning electron microscopy and energy-dispersive X-ray. Lastly, **Section 2.8** reviews the role of PTFE in increasing the anodic H_2O_2 production.

2.1. Alkaline Water Electrolysis

The electrolysis system consists of two electrodes each dispersed in the separated chambers. The electrodes are the anode which does the oxidization and the cathode which does the reduction. The ions resulting from the half-redox reactions will be transported to each other side and electrons transferred through an external circuit. Several kinds of electrolysis have been developed throughout the years to be more efficient. However, since alkaline water electrolysis (AWE) is performed in this study, the scope of this electrolysis study is limited to AWE.

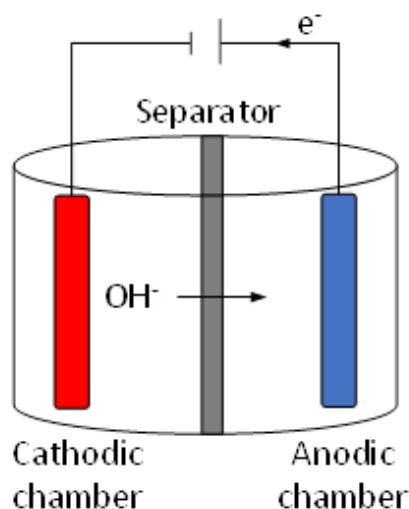
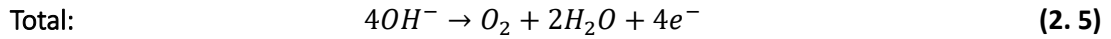
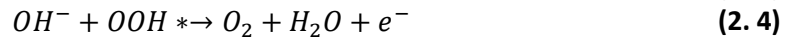
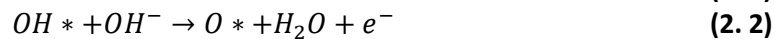
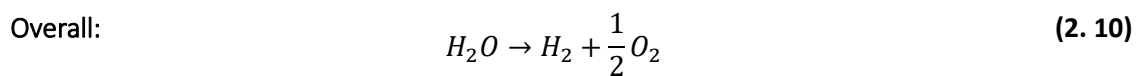
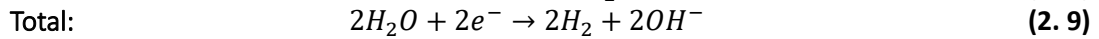
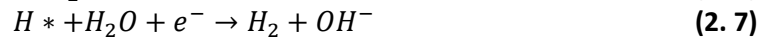


Figure 2.1 Typical water alkaline electrolysis process

AWE uses the basic solution as an electrolyte such as NaOH , KOH , etc. This study used a salt to improve the ionic conductivity. On the cathodic side, the reduced electrolyte releases OH^- . The reaction is known as the Volmer step. Then, the adsorbed hydrogen atom produces hydrogen possibly from the Heyvrosky step (adsorbed H atom reacts with H_2O and e^-) in **Equation 2.2** or the Tafel step (each adsorbed H atoms react to each other) in **Equation 2.3**. This process is known as the hydrogen evolution reaction (HER). The OH^- is transported throughout the system, especially the separator, into the anodic side. Anode binds the OH^- ions and then oxidizes into O_2 and H_2O . This process is known as the oxygen evolution reaction (OER). More detailed step reactions including the intermediates that adsorbed on the surface (noted as *) can be seen in **Equations 2.1 to 2.9** [27].

Oxygen Evolution ReactionHydrogen Evolution Reaction

The standard electrode potential (aqueous solution) to drive the OER and HER (vs NHE) are 1.23 V and 0 V, respectively [28]. Hence, the standard cell potential required for the water electrolysis is -1.23 V. By considering the additional heat that is consumed due to the endothermic water splitting reaction, the least potential that is required for the process at thermoneutral condition is -1.48 V [29]. Nevertheless, the actual required energy is more than the ideal, overpotential and ohmic resistance are the cause for this electrolyzer case. According to Bard and Faulkner, the overpotential happens during the mass transfer from bulk to the interface (between the solid surface and bulk solution), reactions that happened within the interface, and the electron transfer into the redox reaction [28]. While, the ohmic loss relates to the ion movement resistance throughout bulk solution as the drop is caused by the system characteristics such as the distance between electrodes, conductivity of solution, separator conditions, etc. [28] [30].

In reality, the transport of ions is not accordingly straight. Bard and Faulkner explained three known factors that drive the transfer [28]. First is migration which is driven by the electric field between the electrodes (**Figure 2.2(a)**). The charge difference from each electrode attracts the ions with opposite charges. In this case, OH^- would be towards the anode. Second is diffusion which is caused by the concentration gradient of the species (**Figure 2.2(b)**). For example, OH^- left the catholyte due to the migration causing fewer species in that region. This leads to the OH^- movement to the cathodic region. Third is the convection from the flow dynamics aspect. The electrolyte ion can be affected by the fluid motion due to gravity, forced movements (i.e. by a pump or a mixer), etc. These factors are important to determine an effective electrochemical process due to the species' influence on the electrochemical reaction.

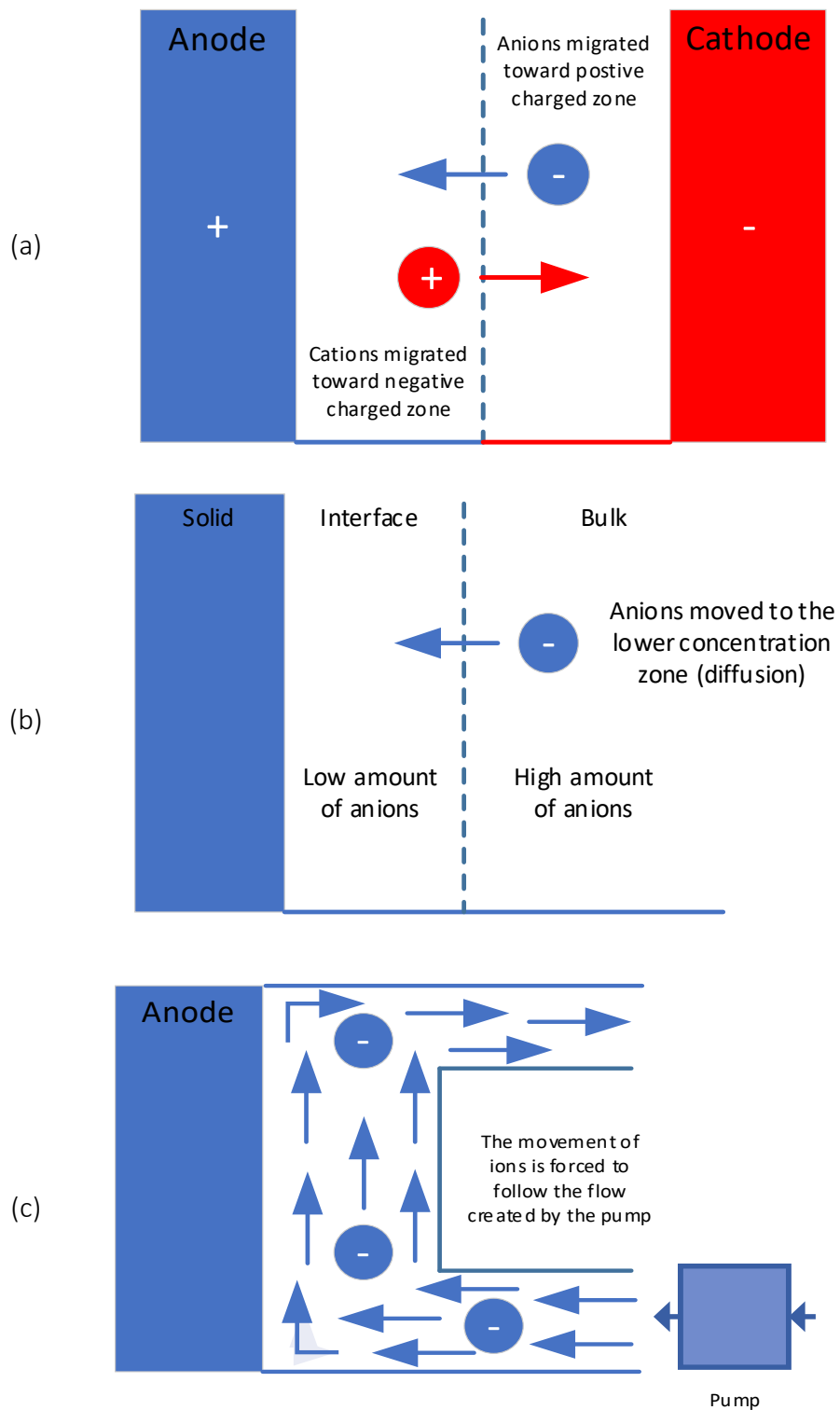


Figure 2.2 Schematic representations of each factor affecting the ionic mass transfer in electrolyzer: (a) migration (b) diffusion (c) convection.

2.2. Separator and Current Collector

The separator (**Figure 2.1**) is used to divide the system into separate chambers for the anolyte and catholyte. Its primary purpose is to prevent short circuits by ensuring that the anode and cathode do not come into direct contact. Another reason is to prevent a crossover of H_2 and O_2 . Otherwise, not only would it complicate the downstream separation process, the mixture would create a flammable hazard (contact with an ignition source could fulfill the fire triangle requirement) which imposes a dangerous safety risk. One example of a separator is Zirfon PERL, which is composed of polyphenylene sulfide coated with a ZrO_2 -polymer [31]. Due to the hydrophilicity of polyphenylene sulfide, the separator allows dissolved ions to pass through while preventing gas crossover.

The current collector facilitates the flow of current to the electrode it contacts. Some designs of the current collector has an extension outside of the cell to be used as a connection point with the external circuit [32] [33]. A more advanced form of current collector is the bipolar which also aids in distributing gas products like O_2 and H_2 . However, due to requirement of this component should have: high conductivity, thermal durability, mechanical strength, and chemical resistant makes the bipolar plate (or current collector) possible to contribute a high cost within the fuel cell components besides the electrode in proton exchange membrane electrolyzers [34] [35] [36].

2.3. Chronopotentiometry

There are two known electrochemical measurement methods: controlled-current and controlled-voltage. Each has its functionalities. Controlled-current is preferred for determining the mass transfer for the reaction [28] [37]. Constant voltage is preferred for characterizing redox reaction and kinetics [28] [38]. However, chronopotentiometry is chosen to prevent a fluctuation of current which can cause a large-power dissipation since it equals to squared value of the current and easier to determine the Faradaic efficiency.

Chronopotentiometry has a parameter of transition time which is a time that afterwards the potential would go overshoot towards infinite. This happens when no reactant can present at the surface to initiate the reaction and the time value is directly proportional to the diffusivity of the reactant [28]. The overshooting potential implies all of the reactants are consumed in the system or the reactant. Chronopotentiograms are also able to determine the stability of the electrodes [39] [40] [41]. In this study, instability due to electrode degradation is more likely to happen than the depleting reactants. However, a disadvantage of using a chronopotentiogram that the applied current could be contributed by a non-faradaic (capacitive) current which could make this method to be more inaccurate [28].

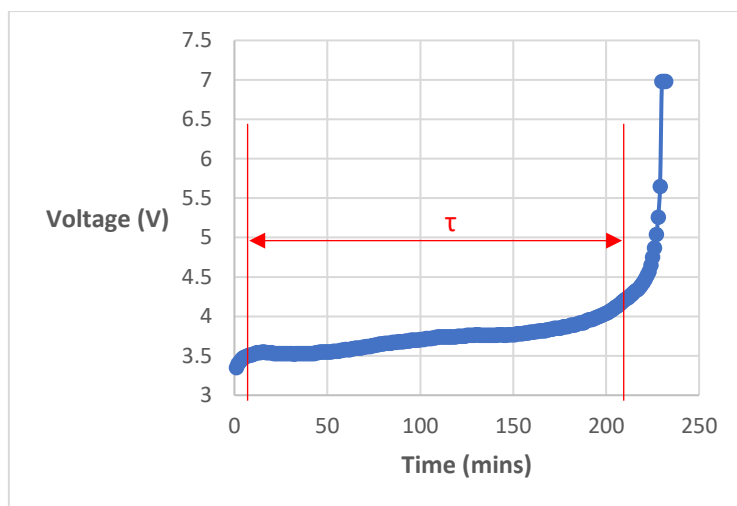


Figure 2.3 Chronopotentiogram of the first experimental test in this project, added with a red line indicating the transition time (τ)

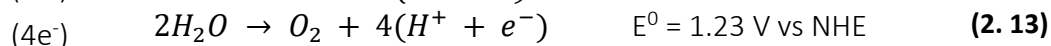
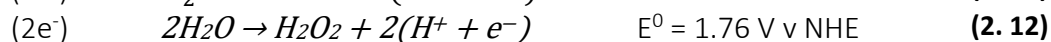
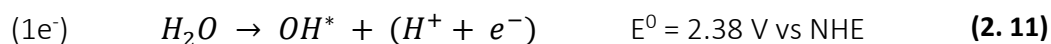
2.4. Anodic H_2O_2 Production from Water Electrolysis

Several studies have found approaches to producing H_2O_2 as shown in the list below [16] :

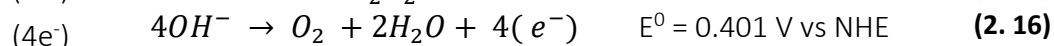
1. Direct synthesis from H_2 and O_2 gases. The H_2 and O_2 molecules adsorbed on the surface and dissociate into atoms. Each of them reacts and forms the HO_2 species at first. The HO_2 molecules react with hydrogen atoms resulting in H_2O_2 .
2. Oxygen reduction reaction (ORR). O_2 molecules are reduced by two electrons resulting in H_2O_2 .
3. Water oxidation reaction (WOR). H_2O molecules are oxidized by two electrons resulting in H_2O_2 .

This study focuses on the WOR since the background is to produce H_2O_2 while the cathode also produces the H_2 .

Three possible reactions could happen on the WOR based on the number of electrons transferred. Shi, et al. [15] mention the reactions in the acidic condition seen through **Equations 2.11 to 2.13** in order based on the standard anodic cell potentials. By measuring the theoretical redox potential with HER at 0 V and each of their Gibb's energy, the four-electron transfer reaction produces O_2 is more thermodynamically favorable than the two-electron transfer.



Since alkaline water is used instead of acid from the related reference, **Equations 2.11 – 2.13** are transformed into alkaline conditions. The modified reactions are written in **Equations 2.14 – 2.16** below. According to the Nernst concept, the standard potential values are adjusted by subtraction with $59\text{mV} \cdot \text{pH}$. The values are based on a pH of 14.



Bicarbonate species were previously found as the preferred supporting electrolyte in effective H_2O_2 production compared to strong base alkalines such as KOH [42] [43]. Gill et al. stated that the possible

mechanism with HCO₃⁻ electrolyte was not direct oxidation of H₂O to H₂O₂, however, the route involves the oxidation of HCO₃⁻ to HCO₄⁻ on the BiVO₄ surface then HCO₄⁻ species is hydrolyzed by H₂O to produce HCO₃⁻ and H₂O₂ [43]. Additionally, the decomposition of H₂O₂ within KHCO₃ is lower compared to Na₂SO₄ and KPi (phosphate buffer) and similar to K₂CO₃ [43]. Afterward, there are studies of using carbonate species for generating H₂O₂. Xia et al. by using the 60% weight PTFE emulsion applied on the CFP electrode has performed an increase within CO₃²⁻ instead of HCO₃⁻ [22]. The proposed explanation by Xia et al. is there are no mechanisms involving carbonate species, rather directly from H₂O oxidized into H₂O₂ [22]. The later study conducted by Mavrikis et al. suggests that the CO₃²⁻ species are involved within the long mechanism involving OH* on boron-doped diamond electrode until forming HCO₄⁻ then proceeds the same route as Gill et al. has proposed then HCO₃⁻ would return to CO₃²⁻ [21]. Another study done by Fan et al. also suggested the CO₂ involved is able to following the same steps as HCO₃⁻ [20]. The mechanisms of bicarbonate or carbonate species are still not yet to be confirmed. However, this project uses carbonate species following Xia et al.

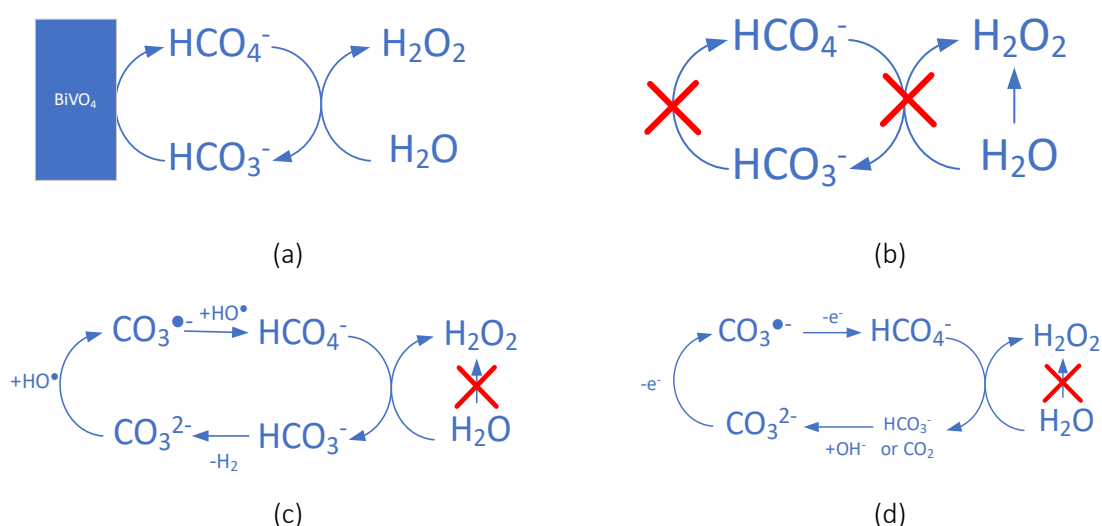
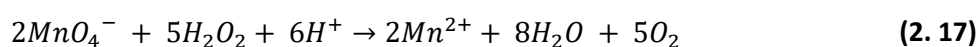


Figure 2.4 Four proposed mechanisms about bicarbonate or carbonate species in water oxidation to H₂O₂, proposed by: (a) Gill et al. [43] (b) Xia et al. [22] (c) Mavrikis et al. [21] (d) Fan et al. [20]

2.5. Measuring H₂O₂ Concentration by Titration

In this project, H₂O₂ will be measured by using the permanganate titration. This method involves a standard reagent with a known concentration (titrant) to gradually added into a sample to do the reaction within until a certain indication knowing that the reaction has reached the equivalent point [44]. Titration has various types depending on the desired analyte that needs to be measured such as acid-base, precipitation, etc. The suitable titration method to determine the H₂O₂ is through the redox reaction with the standard reagents H₂SO₄ and KMnO₄. The KMnO₄ as the titrant has a deep purple color and upon the reaction from **Equation 2.17**, the sample gives the colorless indication. If the sample during titration gives a color slightly pink, all of the H₂O₂ analyte molecules are reacted completely or the endpoint. The known volume used at the endpoint is used to calculate the moles of H₂O₂ through stoichiometry.



2.6. Enhance Selectivity Towards H₂O₂ by Electrode Materials

Combining the mechanisms that happen from OER (Equations 2.1 – 2.5) and electron transfers (Equations 2.14 – 2.16), the binding between OH and the electrode is a key factor in tuning the selectivity that can be seen in an energy state or the binding energy [22]. OH binding energy should not be too weak because there's a certain limit required to dissociate the OH⁻ and also prevent the species from staying in OH* [22] [15]. OH binding energy should not be too strong because the oxidation process would continue to OOH* and more than two electron transfers will happen [22] [15]. A study has shown that ΔG_{OH^*} should be in a range between 1.6 to 2.4 eV [15].

Several metal oxides have been studied to perform WOR into H₂O₂ with the volcano plot shown in Figure 2.5 given by Song et al [16]. The peak of the plot represents the experimentally most selective material for the specified reaction. By referring to the range between 1.6 to 2.4 eV, materials such as WO₃, BiVO₄, SnO₂, and TiO₂ are mentioned to be suitable for H₂O₂ production [22]. Additionally, CaSnO₃ and ZnO with certain structures are reported to reach closer to the volcano peak [45] [17]. Metal oxides are more often to be found producing H₂O₂ through WOR than pure metals or alloys [16]. However, carbon-based materials also have the capability.

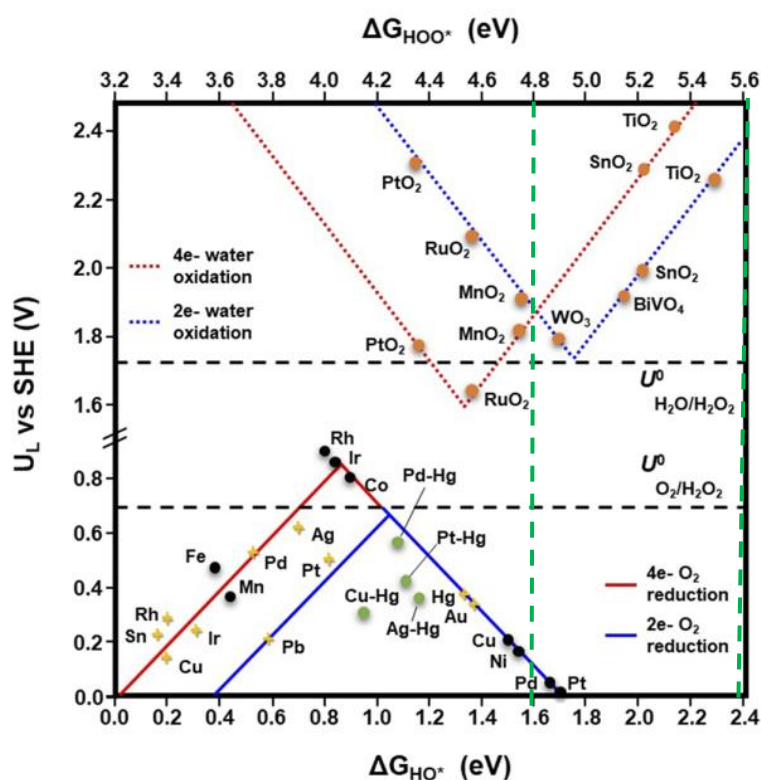


Figure 2.5 Theoretical volcano plot of several materials for certain reactions from a state-of-the-art study [16]. Added with green dashed lines as the ΔG_{OH^*} (or ΔG_{HO^*} relevant to the diagram) limits for H₂O₂ evolution.

Journals often show the use of carbon-based electrodes in generating H₂O₂ through ORR and WOR [16]. Carbon-based materials are found to be equal to or more efficient in H₂O₂ electro-generation compared to others [16]. The first concept of using carbon-based material to produce H₂O₂ was reported by E. Berl using an activated carbon-based cathode for the ORR process [46]. Compared to metals, carbon-based materials have lower electrical conductivity and electric conductivity, and carbon materials tend to be capacitor [47] [48]. Furthermore, carbon can be modified through its structures (different allotropes such as graphite, diamond) and chemical properties (i.e. doping) for performance optimization [16].

2.7. Scanning Electron Microscopy and Energy-Dispersive X-Ray

Scanning electron microscopy (SEM) involves directing an electron beam onto a sample, the electrons interact with the sample, and the emitted electrons from the sample are detected [49]. Conditions for the samples to be observed in SEM must be able to conduct electricity and the SEM within is in a vacuum [49]. The low conductivity of the electrode would overcharge the sample and the vacuum setting is to avoid any gas interactions with the electrons [49]. Otherwise, the image would provide high brightness and poor quality. However, the SEM used in this project (JSM IT-100) can observe a non-conductive sample [50].

There are two different modes of SEM used in this project: Secondary Electron Detector (SED) and Backscattered Electron Detector. The difference between these modes is the depth of electrons that have penetrated the observed material shown in **Figure 2.6**. SED is used as the general method to detect the morphology and topography of the sample while BEC is used to detect sample compositions [49]. SEM has an adjustable parameter which is the accelerating voltage. This voltage helps to penetrate deeply within the sample and reduce the energy loss within the material [49]. However, using a higher accelerating voltage would potentially degrade (i.e. crack) the sample [51].

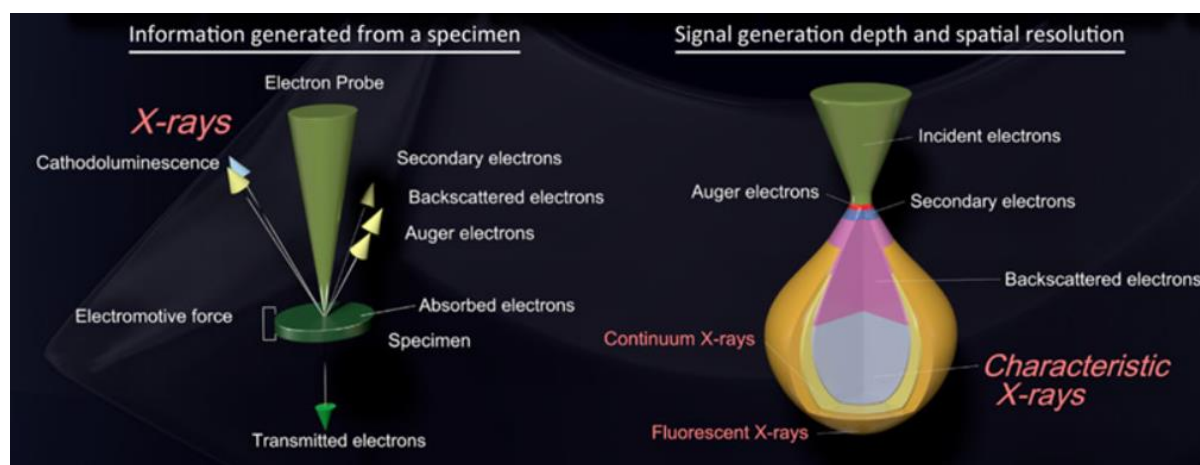


Figure 2.6 Characteristics of each electron toward the sample within SEM, taken from JEOL [52].

In this project, the SEM is provided with energy-dispersive X-ray (EDX). This EDX uses an actual X-ray to determine the elemental composition of the observed specimen. As the X-ray is emitted back from the sample, the characteristic of the wavelength or energy of these emissions will be identified as a certain element [53]. Higher intensity of this specific energy implies that there is a high amount of that element present within the specimen, an example can be seen in **Figure 2.7**. This result can be interpreted as a mass percentage or atomic percentage.

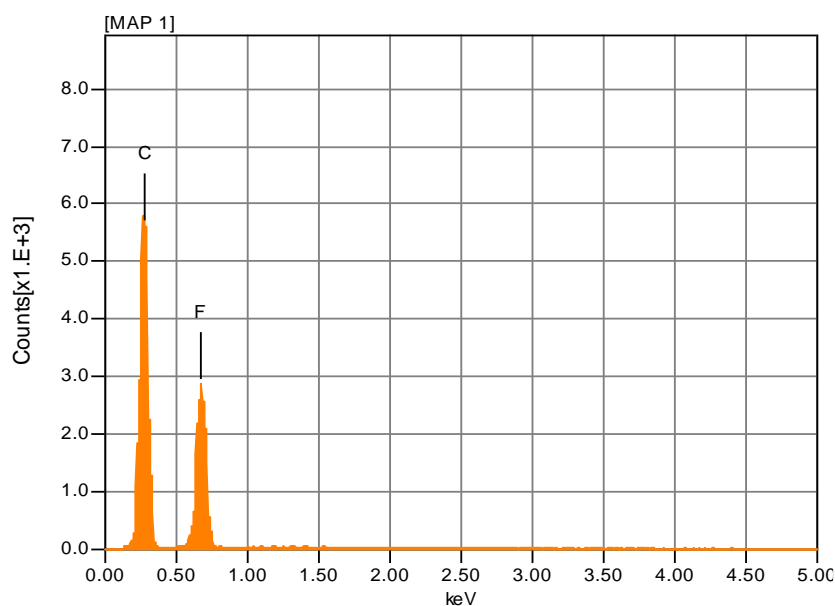


Figure 2.7 EDX spectrum of testing PTFE-patterned electrode.

2.8. PTFE Characteristics and Its Role in Anodic H_2O_2 Productivity

PTFE (commercially known as Teflon) is a polymer containing fluorine and carbon with the chemical formula of $(\text{C}_2\text{F}_4)_n$. The elemental ratio between F/C in a pure form of PTFE is 1.86 [54]. The stable chemical bond characteristic of C-F has made the substance to be highly non-reactive [55] [56]. Although PTFE is reported to be a non-toxic chemical, the pyrolysis (degradation occurs at more than 360°C for long periods) of PTFE would give safety concerns such as C_2F_4 vapors would give dizziness, asphyxiation, and also a flammable substance [25] [57] [58]. The fluorine atom has the highest electronegativity compared to others and the C-F bond is non-polar making PTFE hard to attract the water (hydrophobic) [55]. However, PTFE is aerophilic since the material attracts O_2 and H_2 .

A study by Xia et al. claims that the PTFE applied on the carbon-based anode increases the selectivity of WOR towards the production of H_2O_2 due to the confined O_2 . Even though the exact mechanism is not yet known, this project refers to two major literature sources written by Xia et al. and Vogel et al [22] [26]. According to Xia et al. that the region of O_2 bubbles has affecting the OH^* binding energy due to two proposed reasons [22]. First reason is O_2 helps to reduce OH^* stability on the surface [22]. A stable reactant or at a lower free Gibbs energy state would be difficult to react. This stabilization occurs due to hydrogen bonding of OH^* with H_2O molecules which requires a significant amount of energy to break the bond if OH^* needs to go further OER mechanism [59]. O_2 helps to dissociate the hydrogen bonding which make the OH^* susceptible to do the further reaction [22]. Second reason is O_2 helps to decrease the carbon surface oxidation due to H_2O present on the surface [22]. High presence of oxide-containing functional groups on graphene surfaces would possibly hinder the electrochemical reactions due to less conductivity and reduced surface area [60]. Xia et al. stated that the H_2O increases carbon surface coverage by O^* during the electrochemical process within 2-3 V [22]. Full coverage by O^* means there are no surfaces left for OH^- to reside since the ions are required on the surface. Due to these reasons, PTFE confining O_2 helps the binding energy of OH^* towards in within the suggested ΔG_{OH^*} as mentioned in Figure 2.5. The estimated ΔG_{OH^*} by Xia et al. is shown in Figure 2.8.

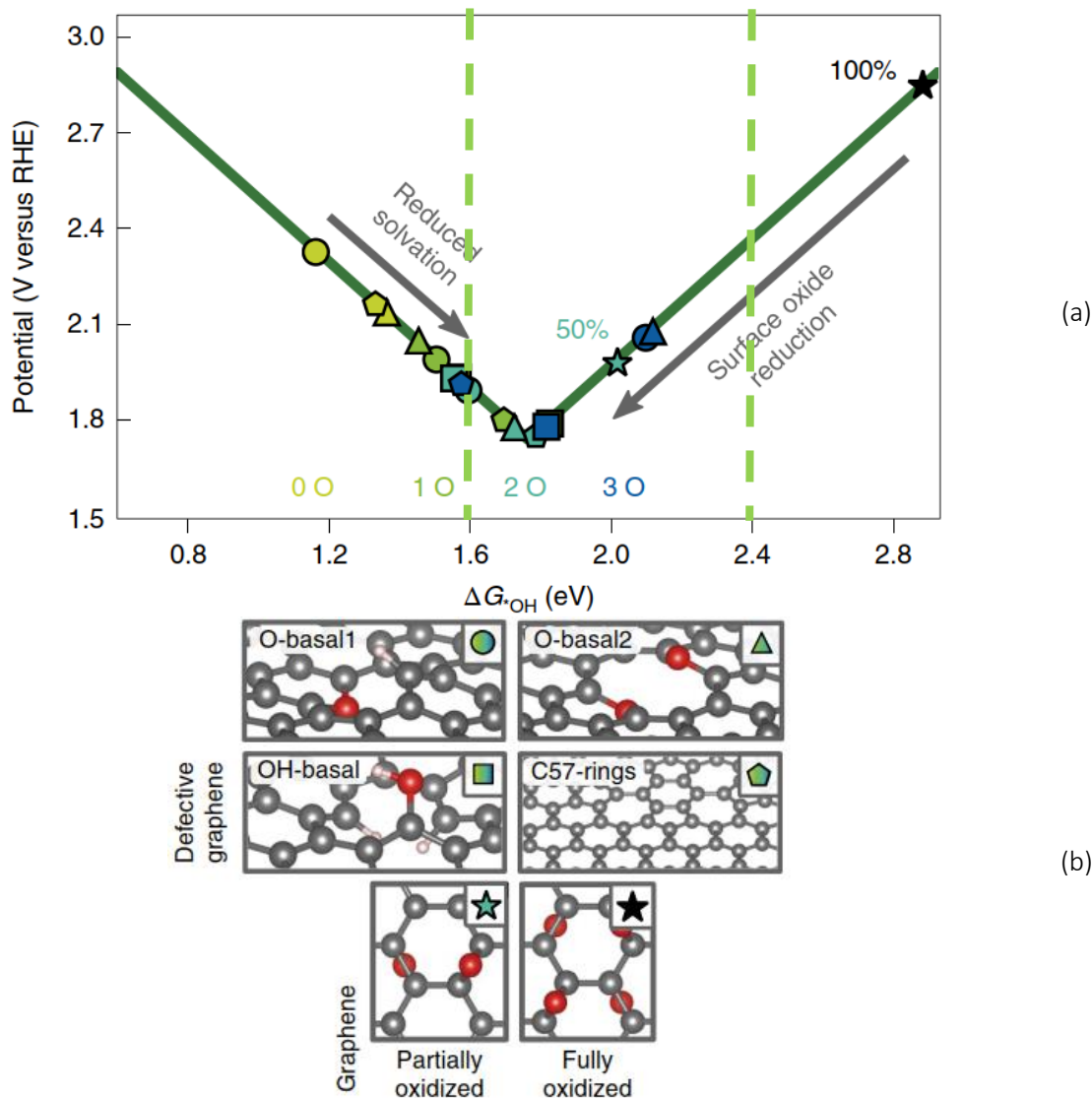


Figure 2.8 (a) Volcano plot showing the influence of O₂ confined bubbles affect the ΔG_{OH^*} towards the peak, plotted by Xia et al. [22], added with green dashed lines as the limits for H₂O₂ evolution. (b) The symbol represents the type of graphene while color represents the number of oxides present that are observed. Taken from Xia et al. [22]

On the other hand, Vogel et al. proposed that O₂ bubbles can gather a high amount of OH⁻ surrounding of its corona [26]. Vogel et al. measured the pH drop of nitrogen bubbles that went through the O₂ bubbles confirming that the OH⁻ ions appeared [26]. Vogel et al. have also observed that the anodic current in the surface static bubbles is increased due to oxidation of OH⁻ to OH^{*} presented by an epifluorescence result during positive bias of the ITO electrode (+1.2 V vs SHE) [26]. Furthermore, Vogel et al. did a polymerization growth method by using luminol and observed a gradient of oxygen species surrounding the bubbles confirming again that the OH^{*} was present [26]. Although the main purpose of this reference is not truly for the H₂O₂, OH⁻ a required reactant for the OER mechanism and as well for H₂O₂ electrogeneration shown in **Equation 2.2** and **Equation 2.15**. The OH⁻ gathered in O₂ bubbles could be the reason if H₂O₂ is increased by the presence of PTFE.

A related study by Venugopal et al. investigated the use of a nickel oxide catalyst for water oxidation, which was coated with PTFE, and explained that Ni-CFx bonds are formed in between [61]. Venugopal et al. applied density functional theory and found that the electronegativity of the fluorine atom, particularly in CF₃, withdraws electrons from the oxygen atom in the adsorbed OH^{*} intermediate [61].

This electron withdrawal increases the energy barrier to form O^* which is essential for four-electron transfer reactions as shown in **Equation 2.2** [61].

Chapter 3 – Methodology

This chapter overviews the methodology used for this project is written in this chapter. **Section 3.1** explains the experiment setup and the electrolyzer flow cell. **Section 3.2** briefly explains the electrode preparation. **Section 3.3** explains the PTFE stamping method. **Section 3.4** explains the PTFE dip-coating method. **Section 3.5** explains the use of the optical microscope, SEM, and EDX. **Section 3.6** overviews the chemical preparation. **Section 3.7** overviews the data measurement conducted in this project.

3.1. Experiment Setup and Electrolyzer Flow Cell

The electrolyzer design used in this study is a flow cell, consisting of various layers stacked together and secured with M5-sized bolts. Plates in the back and middle of the cell are made of PMMA. Gaskets to prevent leakage of the electrolyte are made of EPDM. The overall area of the flow cell is 6 x 12 cm². For the external circuit, alligator clips are connected with the potentiostat to the titanium plates titanium plates, which extend outside the flow cell. The positive terminal is connected to the titanium plate in contact with the anode. While the negative terminal is connected to the plate in contact with the cathode.

The electrolyte enters the cell through an inlet at the bottom of the backplate and exits through an outlet at the top. The separator used in this cell is Zirfon Perl UTP 500, which allows dissolved ions to transport from the cathode to the anode. The electrolyte flow is maintained by a peristaltic pump at a rate of 100 mL/min (81.7 rpm). The temperature and pressure conditions of each experiment are set at ambient conditions. The setup is illustrated as below.

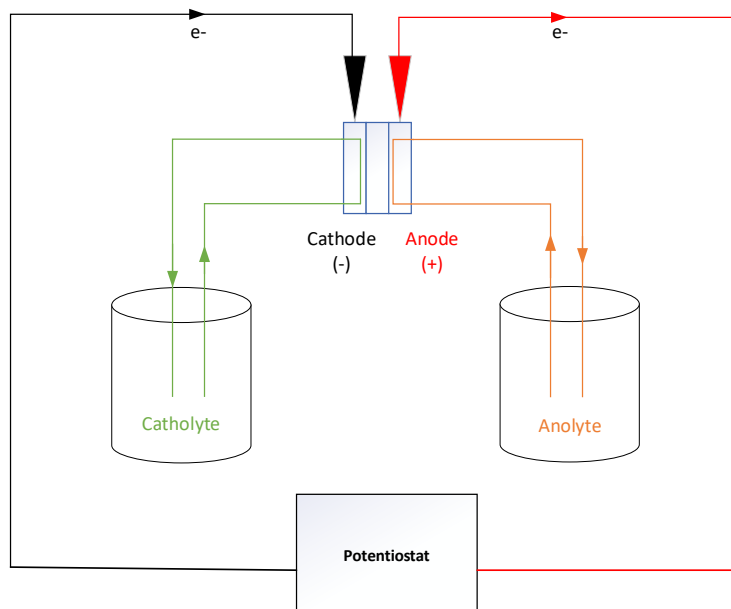


Figure 3.1 The water-splitting process scheme

The distance between each electrode and the separator is maintained by a PMMA frame and an EPDM gasket, with a combined total thickness of 7 mm. In this design, there are two EPDM gaskets designated to be aligned with the titanium plates in each electrolyte chamber. These gaskets have two openings

(20 x 20 mm² each), located above and below the titanium plates. These openings serve as passageways for the electrolyte to flow into the gap between the electrode and the separator, enabling the mass transport to occur in this space. **Figure 3.2** provides the visual representation of electrolyzer flow cell.

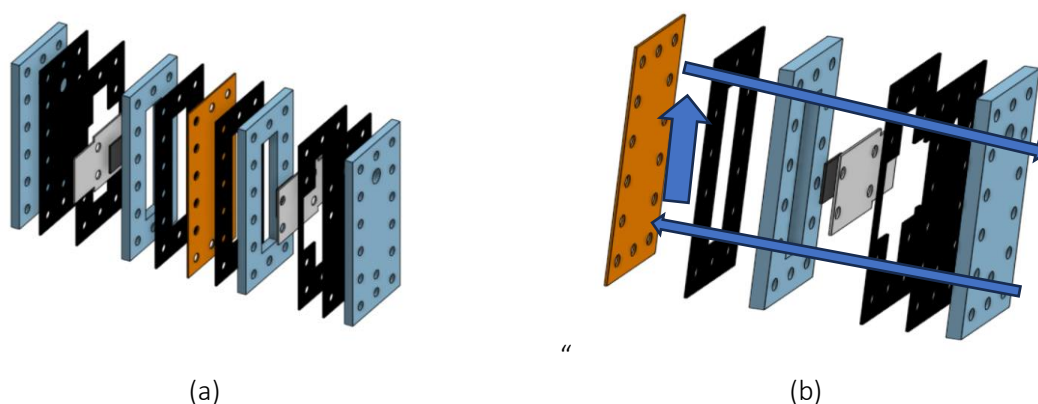


Figure 3.2 3D design of the electrolyzer flow cell: (a) overall stack (b) electrolyte flow direction represented in half of the flow cell

Each color describes:

- = PMMA frame
- = EPDM gasket
- = Titanium plate
- = Electrode
- = Separator

3.2. Electrode Preparation

One of the basic components required for electrochemistry is the electrode. In this experiment, the cathode is a nickel fiber felt sheet. The geometric area is 2x2 cm² with a length extension of 1 cm to be held by the PMMA plate. The nickel fiber felt sheet is supplied by Hebei Aegis Metal Materials Co., LTD. with porosity of 60% and 40 micron fiber diameter. The nickel electrode is first cleansed by being immersed within the acetone in a beaker to be vibrated by a sonicator. Later, replace the isopropyl alcohol with milli-Q water and redo the cleansing.

The anode is CFP the same size as the cathode. The CFP is supplied by Toray with the specification product name TGP-H-60 (untreated). The characteristics of the material are presented in **Table 3.1**. However, due to the fragility of the CFP, this material does not follow the cleansing procedure as the cathode.

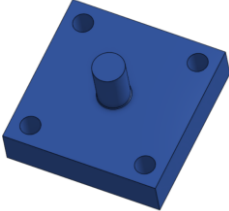

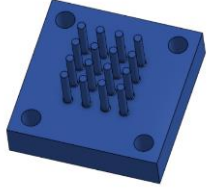
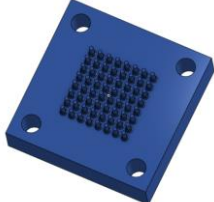
Table 3.1 Characteristics of the CFP [62]

Characteristics	Numbers and Unit
Thickness	0.19 mm
Bulk density	0.44 gr/cm ³
Porosity	78%
Gas permeability	1900 mL.mm/(cm ² .hr.mmAq)
Electrical resistivity (through plane)	80 mΩ.cm
Electrical resistivity (in plane)	5.8 mΩ.cm

3.3. PTFE Stamping Method

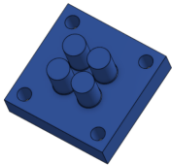

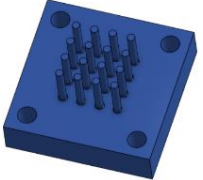
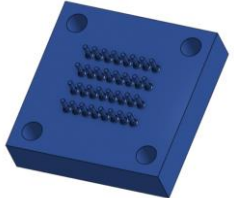
To answer the questions regarding the PTFE area and perimeter effects, a stamping method is used in this study. The stamps are 3D-printed and made of resin materials. The stamps were soaked in a 60% mass of PTFE emulsion and then applied to the CFP electrode. Each of the stamps has a different total stamping area and perimeter. The perimeter variation stamps with different total stamping perimeters and the same total stamping areas are listed in **Table 3.2**. The stamps are based on the order with the smallest to largest total stamping perimeter: $P1 < P2 < P3 < P4$.

Table 3.2 Perimeter variation stamps

Stamp	Image	Stamp diameter (mm)	Total stamp area (mm ²)	Perimeter (mm)
P1		8	50.27	25.13
P2		4	50.27	50.27
A3/P3		2	50.27	100.53
P4		1	50.27	201.06

The area variation stamps with different total stamping areas and the same total stamping perimeters are listed in **Table 3.3**. The stamps are based on the order with the smallest to largest total area perimeter: $A1 > A2 > A3 > A4$.

Table 3.3 Area variation stamps

Stamp	Image	Stamp diameter (mm)	Total stamp area (mm ²)	Perimeter (mm)
A1		8	201.06	100.53
A2		4	100.53	100.53
A3/P3		2	50.27	100.53
A4		1	25.13	100.53

Should be noted that P3 stamp and A3 stamp are same, the reason is to correlate the effect of perimeter with area of the PTFE in the end.

To prevent inaccuracy of PTFE stamping on the electrode geometric area, a holder is made as well by 3D printing with resin material. The stamp is dipped within the PTFE emulsion with a concentration of 60%. The electrode is placed on the electrode holder, then the holder is set above the stamp by using bolts for precise patterning. The holder with the electrode is pushed towards the stamp and pressed afterward. Both the holder and the patterning setup are seen in the images below.

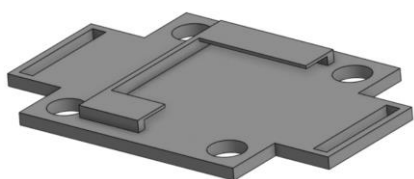


Figure 3.3 Electrode holder scheme

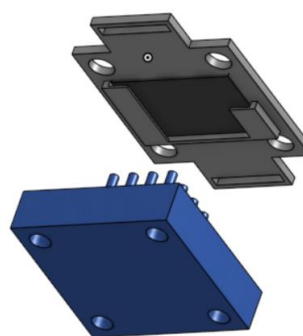


Figure 3.4 Patterning tools positions



Figure 3.5 PTFE patterning test on a nickel plate. The plate extension shows the location of the electrode.

After the pressing, the PTFE-patterned electrode is dried and annealed. Following the same procedure as Xia et al., the drying is set at 120°C in ambient conditions then the annealing is set at 350°C within a nitrogen atmosphere for 30 minutes [22].

3.4. PTFE Dip-Coating Method

The dip-coating method for this study is also implemented for comparison with the patterned electrodes. There are five variations of PTFE concentration for this method: 1%, 5%, 20%, 40%, and 60% PTFE by mass in the emulsion. Since the chemical supply was provided as a 60% PTFE mass solution, dilution was necessary to achieve the lower concentrations. The electrode were dipped within the PTFE emulsion in 10 minutes, following the procedure used by Xia et al. [22]. After dip-coating, the CFP electrodes were heated and annealed according to the procedure mentioned in **Section 3.3.**

Table 3.4 Mass change in % for each dip-coating CFP variants

PTFE Concentration	Mass change (%)
1%A	5.12
1%B	5.14
5%A	19.64
5%B	19.14
20%	64.04
40%	136.30
60%	378.14

3.5. Electrode Observation by Optical Microscope, SEM, and EDX

The stamped carbon electrodes were observed using an optical microscope (OM), specifically the VHX-7000 model provided by Keyence International. Before the experiment, the diameter of the PTFE pattern(s) on each electrode sample was measured using the OM. The diameter was determined by measuring the outermost circle from the center of the pattern. The images are attached in **Appendix A** -. Afterward, the actual total stamp area and perimeter are calculated.

To ensure the accuracy and precision of the stamping, the coefficient of variation (COV) is estimated for both area and perimeter across all patterns for each variation. COV is calculated based on **Equation 3.1** which allows for comparison of variability across data sets with different units. Perimeter and area variations are shown respectively in **Table 3.5** and **Table 3.6**. The results indicate that the COV of perimeter variations for the area is lower than that for the perimeter, suggesting that the stamped areas are more consistent than the perimeters. As well as the area variation, the stamped perimeter for each stamp is more similar than the area.

However, an important to note that due to the high porosity of the CFP (78%) and the uncoordinated movement of the water solvent carrying PTFE, the PTFE patterning inside the bare carbon may not precisely match the intended surface design [62]. Therefore, achieving "perfect" accuracy in this patterning method is unlikely. These values are just to ensure consistency.

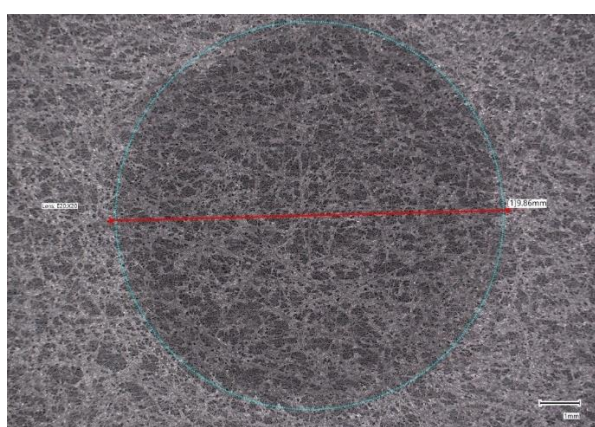


Figure 3.6 Aftermath of the PTFE patterning on CFP. The pattern applied is P1 (sample A).

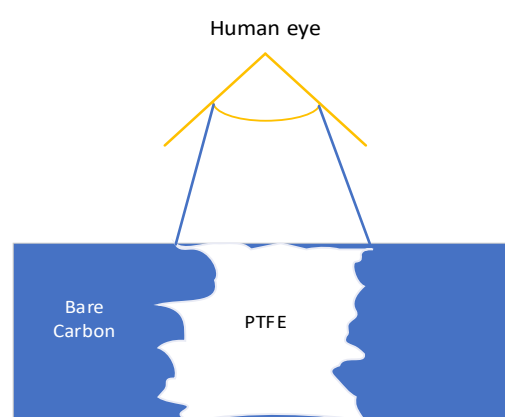


Figure 3.7 Possible PTFE patterning within the bare carbon does not exactly match the intended cross-sectional area as designed for the electrode surface

$$COV = \left(\frac{\text{Standard deviation}}{\text{Average}} \right) \times 100\% \quad (3.1)$$

Table 3.5 Actual of the constant area and different perimeters designed (perimeter variation) PTFE-patterned electrodes measurement analysis (samples A and B represent the repeat samples of the pattern).

Pattern		Design		Actual		Ratio of Actual to Design		Mass change (%)
		Area (mm ²)	Perimeter (mm)	Area (mm ²)	Perimeter (mm)	Area	Perimeter	
P1	A	50.27	25.13	76.36	30.98	1.52	1.23	6.37
	B			55.63	26.44	1.11	1.05	4.36
P2	A		50.27	139.35	83.63	2.77	1.66	15.59
	B			126.47	79.70	2.52	1.59	15.57
P3	A		100.53	116.37	152.71	2.32	1.52	14.37
	B			59.97	109.64	1.19	1.09	16.16
P4	A		201.06	92.42	269.59	1.84	1.34	9.31
	B			50.27	223.71	1.00	1.11	3.08
			Average	89.60	122.05			
			Standard deviation	34.46	87.75			
			Coefficient of Variation	38.46%	71.90%			

Table 3.6 Actual of the constant perimeter and different areas designed (area variation) PTFE-patterned electrodes measurement analysis (samples A and B represent the repeat samples of the pattern).

Pattern		Design		Actual		Ratio of Actual to Design		Mass change (%)
		Area (mm ²)	Perimeter (mm)	Area (mm ²)	Perimeter (mm)	Area	Perimeter	
A1	A	201.06	100.53	282.66	119.10	1.41	1.18	62.85
	B			218.20	104.64	1.09	1.04	48.78
A2	A	100.53		138.21	117.62	1.37	1.17	34.86
	B			156.68	125.42	1.56	1.25	28.28
A3	A	50.27		79.43	125.92	1.58	1.25	16.39
	B			74.66	122.19	1.34	1.15	13.81
A4	A	25.13		28.60	107.03	1.58	1.25	0.97
	B			24.97	99.56	1.49	1.22	1.93
			Average	129.72	116.29			
			Standard deviation	81.40	9.49			
			Coefficient of Variation	62.75%	8.16%			

To determine the chemical composition of the electrode, SEM was used. This technique also allowed for the investigation of any anomalies on the electrode that could lead to unexpected results. The SEM is provided by JEOL, JSM-IT100. The images are attached in **Appendix B-**. The SEM is equipped with the EDX to analyze the composition through spectrum analysis and mapping. The example of SEM/EDX pictures of PTFE-patterned A1 are shown in **Figure 3.8**. BED images will be shown as well and should be noted that there is a composition type (BEC) and a topography type (BET).

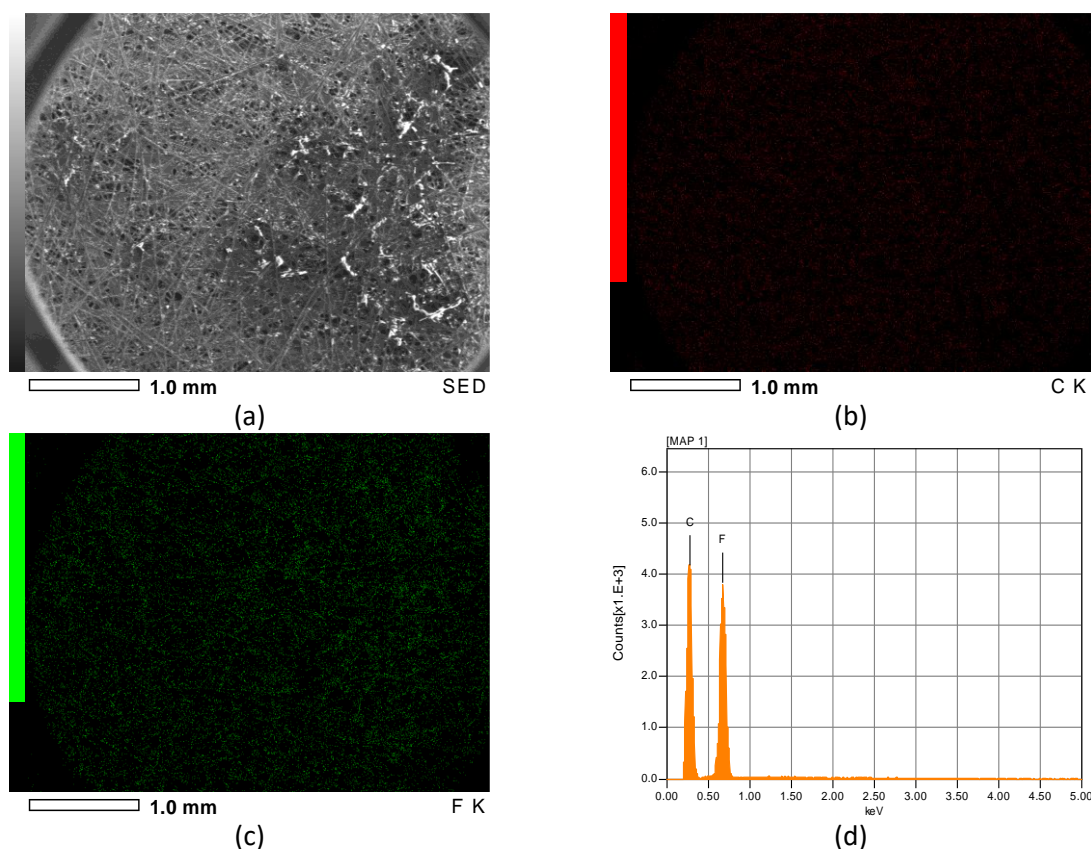
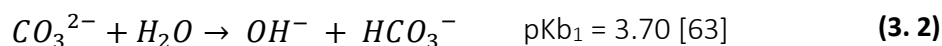


Figure 3.8 Images taken from SEM: (a) SED image of the center of PTFE pattern A1A at x30 (b) Carbon mapped by EDX (c) Fluorine mapped by EDX (d) Composition spectrum (the mass ratio F/C is 0.783 lower than 1.86 implies the carbon elements detected from the CFP electrode)

3.6. Chemicals Preparation

Electrolyte Solution

In this experiment, the electrolyte is potassium carbonate (K_2CO_3). The concentration is prepared for 1 M with an addition of 11 gr/L Na_2SiO_3 to stabilize H_2O_2 product. The solution is made by dissolving a certain amount of K_2CO_3 and Na_2SiO_3 with milli-Q water. The pH of this solution should be based on the calculation below.



For 1 M of K_2CO_3 :

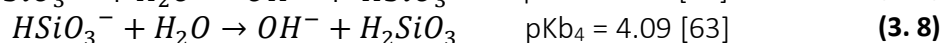
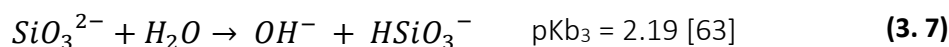
$$Kb_1 = \frac{[OH^-][HCO_3^-]}{[CO_3^{2-}]} \quad (3.4)$$

$$Kb_2 = \frac{[OH^-][H_2CO_3]}{[HCO_3^-]} \quad (3.5)$$

Due to the Kb_2 value being low or more acidic than Kb_1 , assumed that $[OH^-]$ produced would be very low. Hence, the amount of $[OH^-]$ is calculated with **Equation 3.4**. From the calculation, the concentration of OH^- from 1M of K_2CO_3 is 0.0141 M or equal to pH of 12.15.

$$[OH^-]_{K_2CO_3} = \sqrt{Kb_1[CO_3^{2-}]} \quad (3.6)$$

Since Na_2SiO_3 is a weak base, pH should be affected as well. Should be noted that $[SiO_3^{2-}]$ is 0.090 M.



$$Kb_3 = \frac{[OH^-][HSiO_3^-]}{[SiO_3^{2-}]} \quad (3.9)$$

$$Kb_4 = \frac{[OH^-][H_2SiO_3]}{[HSiO_3^-]} \quad (3.10)$$

With the same assumption from the K_2CO_3 pH calculation, the OH^- concentration is determined by using Equation 3.9.

$$[OH^-]_{Na_2SiO_3} = \sqrt{Kb_1[SiO_3^{2-}]} \quad (3.11)$$

In order to estimate the pH of solution combining K_2CO_3 and Na_2SiO_3 , Equation 3.12 is used. The $[OH^-]$ of the solution is 38.25 mM or pH of 12.58.

$$[OH^-]_{Solution} = [OH^-]_{K_2CO_3} + [OH^-]_{Na_2SiO_3} \quad (3.12)$$

KMnO₄ Solution

KMnO₄ solution is made to be used for permanganate titration. KMnO₄ is supplied by Sigma-Aldrich with starting concentration of 0.02 mol/L (0.1 N). The solution is made through diluting the KMnO₄ by using milli-Q water within a volumetric flask. The target solution is 2 mM and the dilution is followed by Equation 3.13. Due to sensitivity of solution towards light, KMnO₄ solution is stored in a glass bottle covered by an aluminum foil and stored in the chemical cabinet.

$$[KMnO_4]_{initial} \times V_{KMnO_4} = [KMnO_4]_{final} \times V_{target} \quad (3.13)$$

H₂SO₄ solution

H₂SO₄ solution is also made to be used for permanganate titration. H₂SO₄ is supplied by Sigma-Aldrich with starting concentration of 95-98% by volume. The solution is made by diluting the H₂SO₄ to 16% of volume/volume or volume ratio of 1:5 in milli-Q water. However, H₂SO₄ mixed with water would enact an exothermic reaction releasing high heat. To prevent the dangerous risk, milli-Q water should be added first into the volumetric flask with the required volume then the rest is filled with the acid.

3.7. Data Measurement

In this project, there are two kinds of measurements applied: chronopotentiogram and titration.

Chronopotentiogram

For chronopotentiogram, the data is obtained using a potentiostat provided by OWON, SPE6103. The potentiostat was configured using a Python software, operating in linear current mode for constant-current chronopotentiograms. The current was set at 0.4 A (equivalent to 0.1 A/cm²) from start to end. The number of data points was set to approximately 600, with a 60-second delay between readings. When the potential values suddenly overshoot, indicating that the anode has reached the end of its lifetime, the data is saved in a TXT file. This should be noted that these potential represents the whole cell potential, not the half-redox reaction potential.

KMnO₄ Titration

For titration, a 2.5 mL sample is taken from each reservoir every 15 minutes using a syringe. For every new sample taken, a new syringe should be used. Catholyte is also taken as a sample to detect if any H₂O₂ is also present. The collected sample is poured into an Erlenmeyer flask, followed by the addition of approximately 2.5 mL of H₂SO₄ to ensure the sample acts as the limiting reagent. The Erlenmeyer flask is then shaken to mix thoroughly, and a magnetic stir bar is placed inside. Put the Erlenmeyer on top of the magnetic plate and beneath the outlet of the burette glass containing KMnO₄ 2mM. Note the initial liquid volume within the burette. Turn on the magnetic stir plate to start the stirring process and then slowly add KMnO₄ drop by drop until a faint pink color appears in the solution. After that, the volume of the burette should be noted. The obtained volume data is then calculated in **Equation 3.14** based on the **Equation 2.17**.

$$[H_2O_2]_{detected} = \frac{5 \times (V_{final} - V_{initial})}{2 \times V_{sample}} \quad (3.14)$$

Chapter 4 - Results and Discussions

In this chapter, the results of the experiments conducted with the discussions are presented. **Section 4.1** presents for the bare CFP as the anode. **Section 4.2** explains a limitation of this experiment. **Section 4.3** presents for the perimeter variation. **Section 4.4** presents for the area variation. **Section 4.5** presents for the PTFE dip-coating variation.

4.1. Bare CFP as the Anode

In this experiment, bare carbon samples are used as the baseline variation. The SEM images of bare CFP before the experiment are shown in **Figure 4.1.a**. As can be seen, CFP contains multiple carbon fibers in every layer which characterizes the graphite structure. EDX analysis confirmed that the only detected element was carbon.

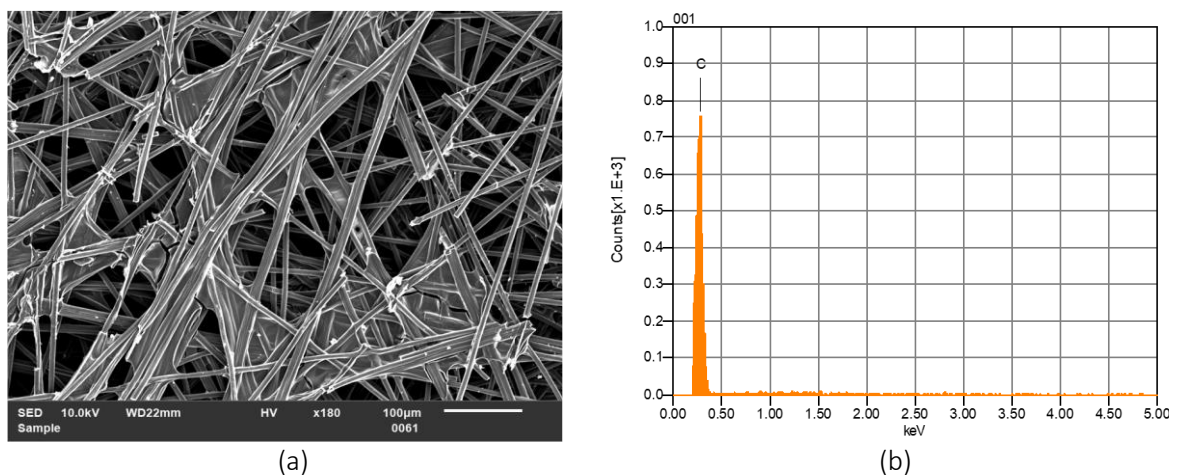


Figure 4.1 SEM image of bare CFP (a) and EDX analysis of bare CFP (b).

In all experiments, three bare carbon samples (A, B, and C) are used as baselines for different variations: bare carbon A for perimeter variation, bare carbon B for area variation, and bare carbon C for dip-coating variation. **Figure 4.2** shows the chronopotentiogram results for these bare carbon samples. The lifetimes of bare carbon A, B, and C are respectively 4.20, 5.27, and 3.60 hours. Based on the anolyte volume, the electrode degradation occurred quickly than if it were caused by electrolyte depletion.

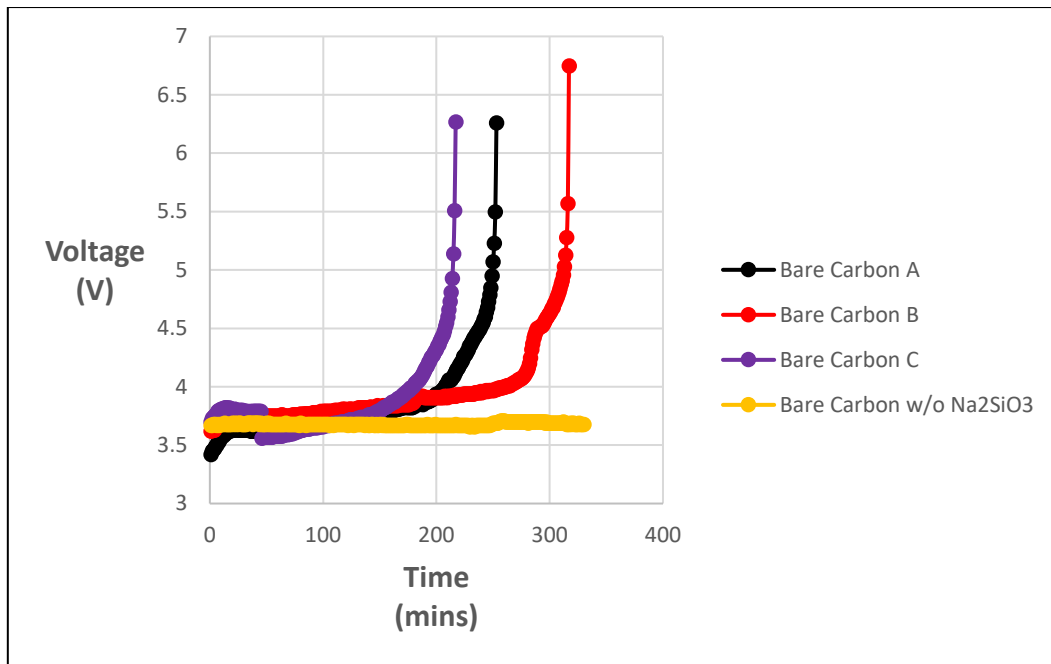


Figure 4.2 Chronopotentiogram for bare carbon samples as the anode

H₂O₂ product was detected through permanganate titration as shown in Figure 4.3. As the process nears the end of the lifetime, the concentration becomes more stagnant. This implies the process the process is no longer effectively producing H₂O₂.

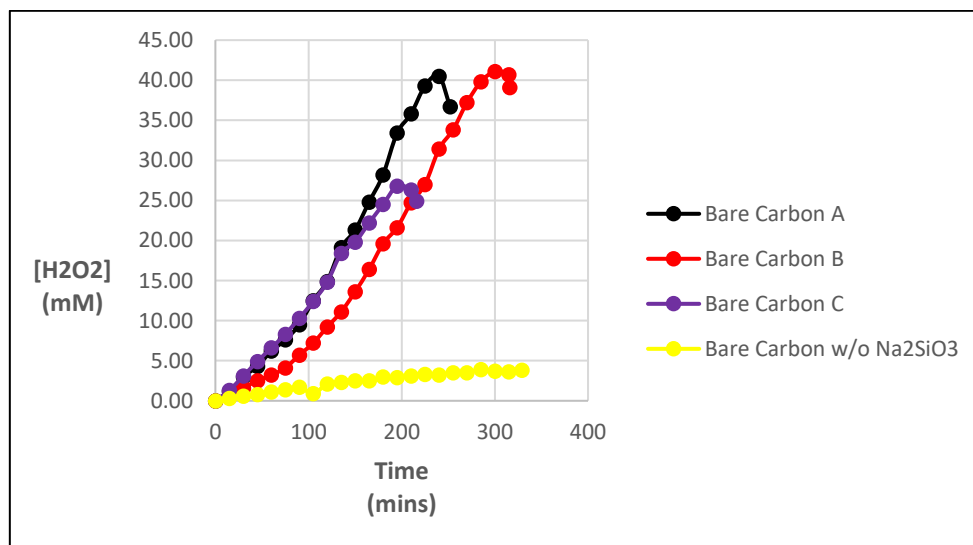


Figure 4.3 H₂O₂ concentration results throughout time

The post-experiment condition of the bare carbon electrodes was examined using SEM/EDX analysis, with the results shown in Figure 4.4. The mapping shows a significant presence of Si and O elements across the bare carbon fiber. This is likely due to the migration flow of SiO₃²⁻ ions toward the anode. The coverage is so high that the most of carbon fibers are not clearly visible in the EDX mapping. Na and K elements are also detected based on the EDX result implying a different driving force made these elements to go toward the anode (diffusion or convection).

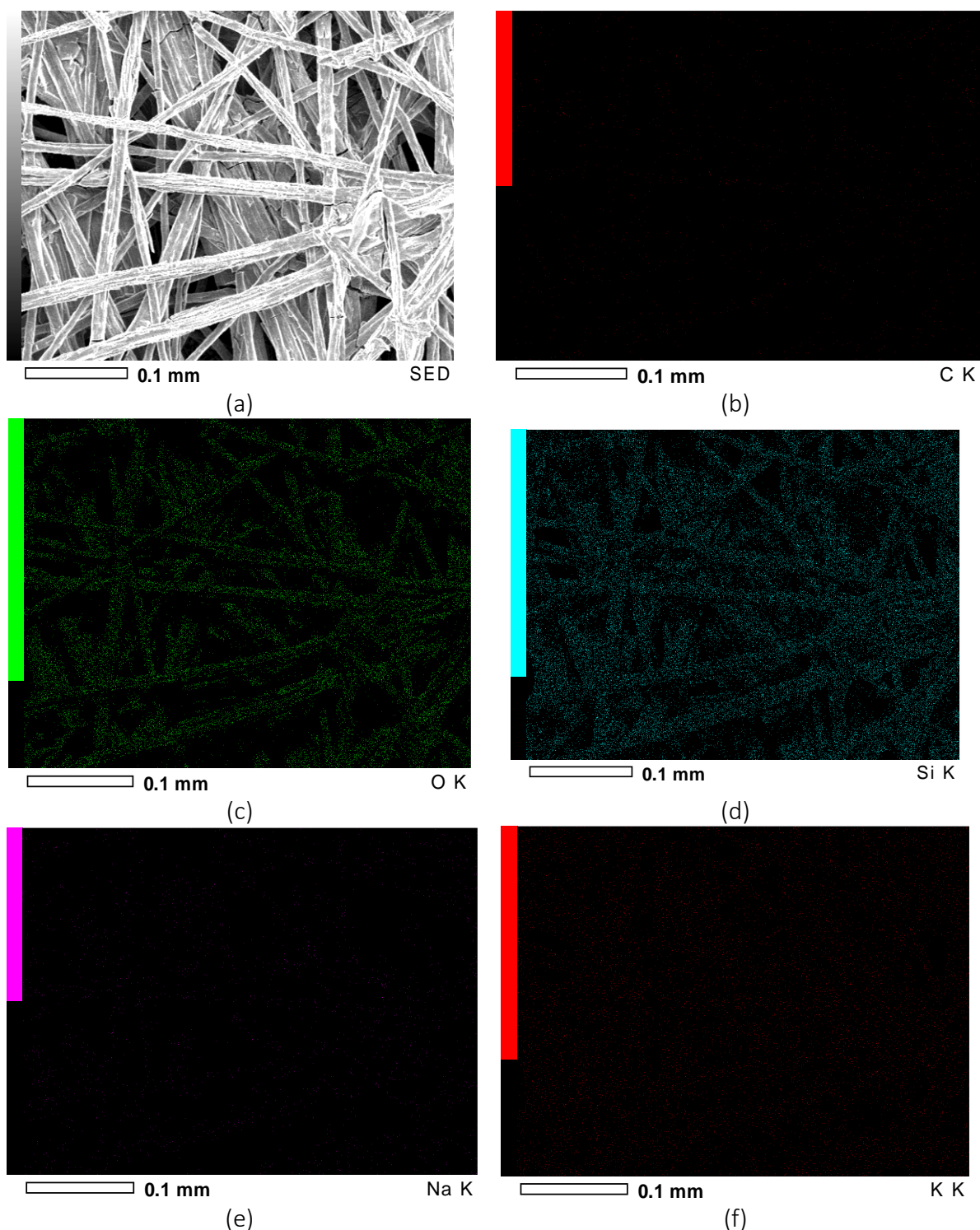


Figure 4.4 SEM/EDX mapping images of post-experiment bare carbon A: (a) SED image (b) Carbon (c) Oxygen (d) Silicon (e) Sodium (f) Potassium

Another bare carbon sample was tested in the electrolyte without Na_2SiO_3 . As shown in **Figure 4.2**, there's no indication of overshooting potential within around 5 hours of the experiment. This suggests that the presence of SiO_3^{2-} ions inhibits the electroactive area. Based on the SEM/EDX images (**Figure 4.5**), a high indication of carbon fibers implying that this bare carbon can have more stable in electrolysis operation. However, the absence of Na_2SiO_3 led to a lower H_2O_2 yield, as shown in **Figure 4.3**. This trade-off needs to be considered for less Na_2SiO_3 concentration in the electrolyte.

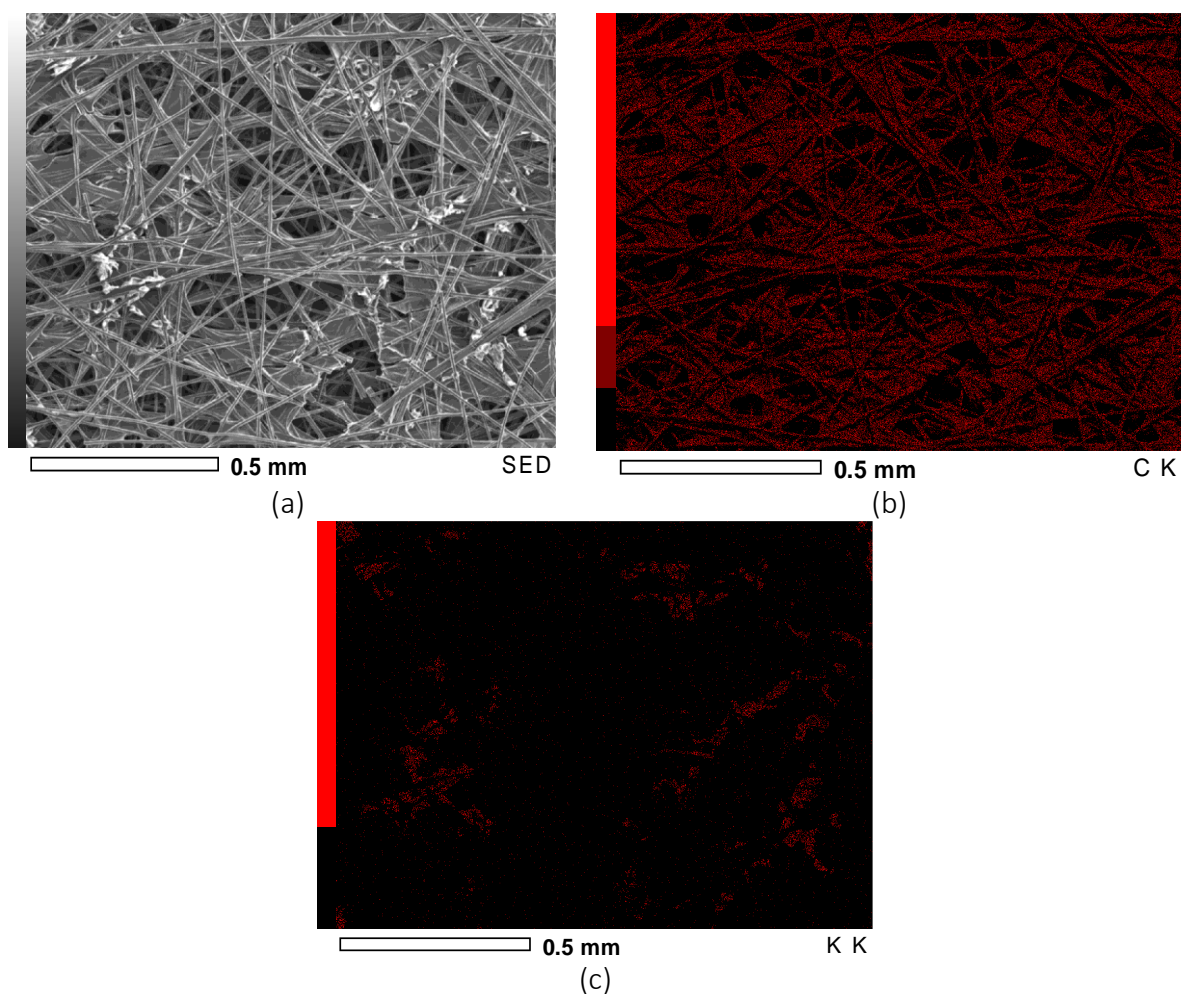


Figure 4.5 SEM/EDX mapping images of post-experiment bare carbon without Na_2SiO_3 : (a) SED image (b) Carbon (c) Potassium

4.2. Limitation of the Experiments

Before further into the results and discussions, there's a limitation of this project that needs to be know. The forced pressing applied in this method can cause PTFE penetrate through the CFP. This could be a problematic because current collector contacts to the backside of PTFE-patterned CFP. In most experiments, traces of PTFE have been observed on the current collector, as shown in **Figure 4.6**.

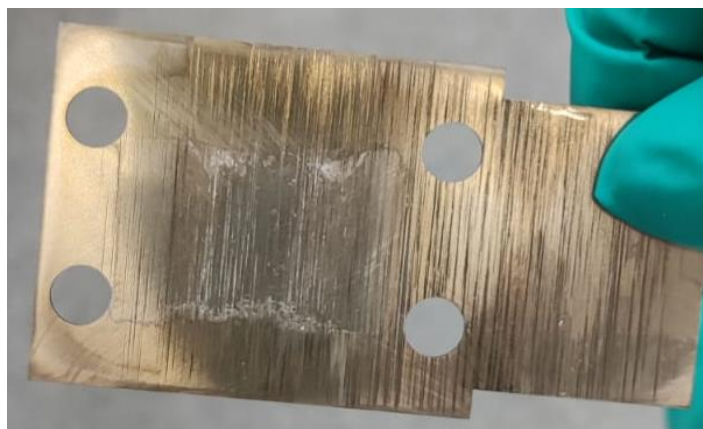
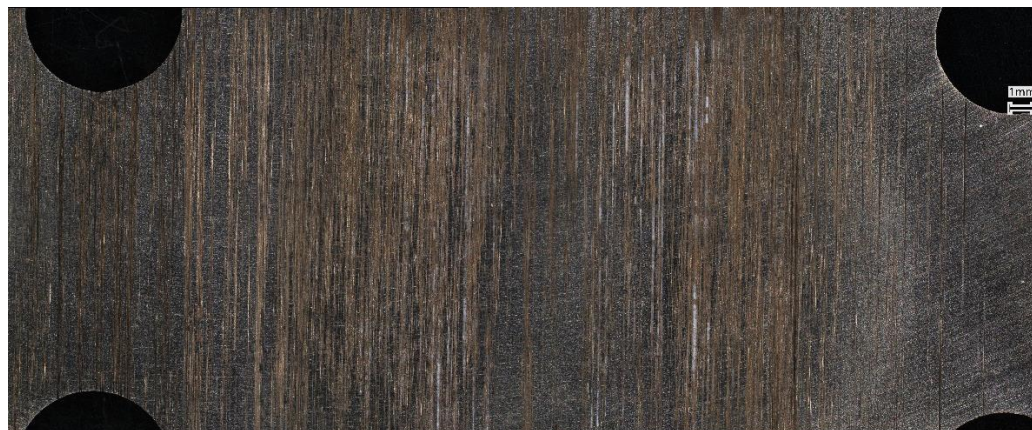
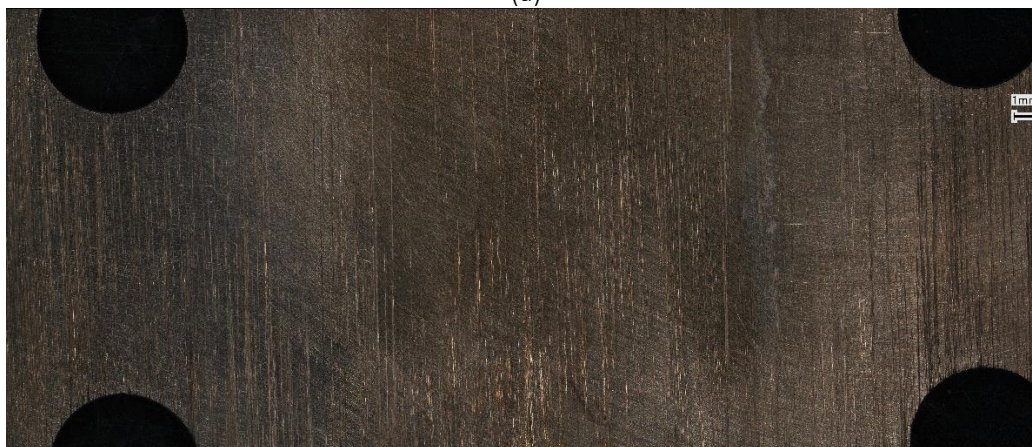


Figure 4.6 PTFE traces appeared on the titanium plate surface after the experiment

Before starting a new experiment, the plate is consistently cleaned using a sanding method with 2000-grit sandpaper. However, repeated contact with PTFE, particularly from dip-coated electrodes, makes it increasingly difficult to remove PTFE traces from the plate, even with fine-grit sandpaper. **Figure 4.7** compares the current collector side that has more frequent contact with PTFE (side X) to the side with less frequent contact (side Y).



(a)



(b)

Figure 4.7 Comparison of two different sides of the current collector for anode by using an optical microscope: (a) frequently contact with PTFE or named as **side X** (b) less frequently contact with PTFE or named as **side Y**

When comparing performance, differences in lifetime and H_2O_2 yield are observed. Although A3 and P3 have the same design, **Figure 4.8** highlights these differences. The P3 electrodes have a shorter lifetime compared to the A3 electrodes. This reduced lifetime is likely due to the traces of PTFE on **side X**, which increase electrical resistance and contribute to electrode instability.

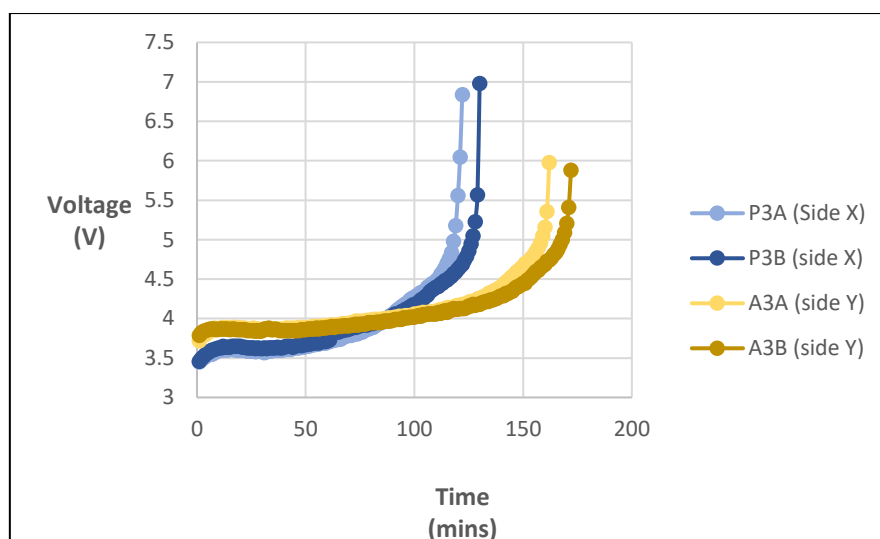


Figure 4.8 Comparing different sides of the current collector by using A3 and P3 stamps through chronopotentiogram

Regarding H_2O_2 concentrations, a difference between the P3 and A3 samples is evident in **Figure 4.9**. The graph shows a distinct variation in yield over time between A3 and P3. Furthermore, ANOVA analysis confirms that this difference is statistically significant. The high porosity of CFP, approximately 78% [62], likely contributing to this effect. Traces of PTFE on the surface of the current collector may trap O_2 within the porous structure, thereby increasing the H_2O_2 yield rate.

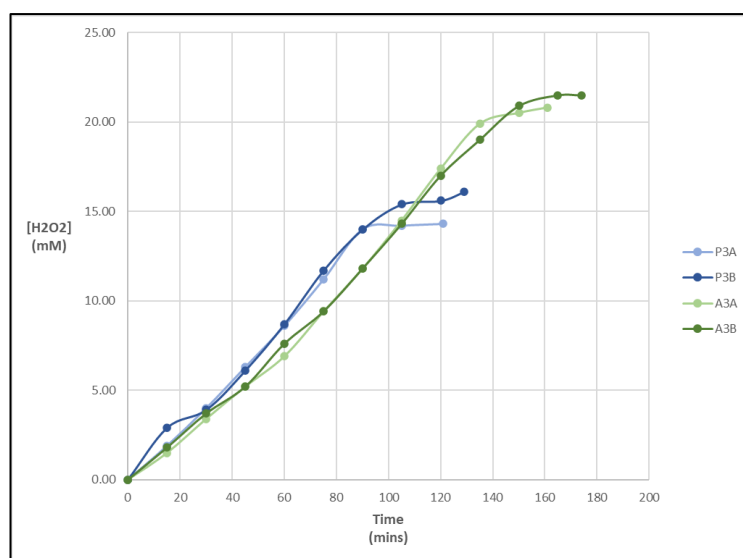


Figure 4.9 H_2O_2 yield throughout the time for P3 and A3

To keep experiments clear and sustain the use of titanium plates, the events are ordered as below:

1. Perimeter variation: applied on **side X**, bare carbon A as the baseline
2. Area variation: applied on **side Y**, bare carbon B as the baseline
3. Dip-coating variation: applied on **side X**, bare carbon C as the baseline

During each variation, the experiments were conducted as close together in time as possible to minimize any differences due to changes in the current collector.

Nevertheless, as the surface continues to worsen over time, the precision of these experiments is compromised due to the impact of the current collector's capability. This can be seen in the difference

between bare carbon A and C in **Figure 4.2**, implying the deterioration of the current collector decreased the performance lifetime. Similarly, for bare carbon B, the better condition of the current collector on side Y suggests a longer lifetime.

4.3. Perimeter Variation of PTFE Patterns

In the **Figure 4.10**, PTFE-patterned carbon electrode samples have a shorter lifetime compared to the bare CFP electrode. The presence of PTFE on the electrodes hinders electron transfer throughout the material. While, the chronopotentiogram of CFP electrodes with different perimeter variations shows a similar behavior.

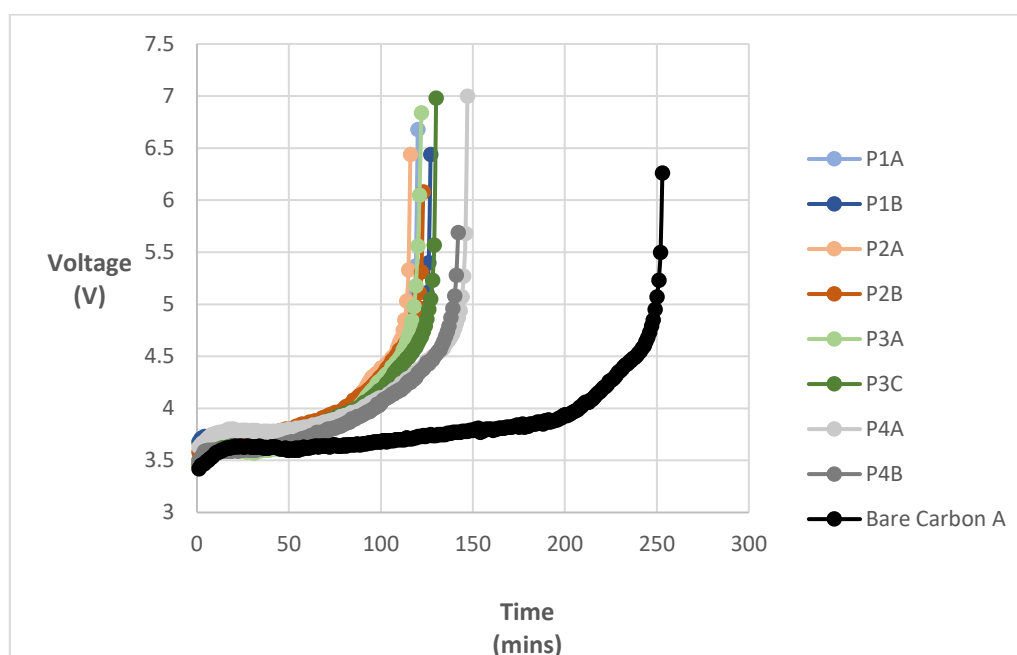


Figure 4.10 Chronopotentiogram of each PTFE-patterned CFP with a different perimeter and bare carbon

The performance lifetime based on the chronopotentiogram are calculated and shown in **Table 4.1**. For the values that are listed, the average lifetime of PTFE-patterned carbon electrodes are 2.09 hours which is almost two times shorter than the lifetime of bare CFP A. However, both samples of P4 patterns exhibit longer performance lifetimes of 2.15 and 2.45 hours for A and B.

Table 4.1 Performance lifetime for each PTFE-patterned CFP electrodes with different perimeter

Pattern	Sample	Performance lifetime (hours)
P1	A	1.98
	B	2.10
P2	A	1.92
	B	2.03
P3	A	2.02
	B	1.85
P4	A	2.15
	B	2.43
Bare Carbon A		4.20

H₂O₂ yield concentrations from the experiment are displayed in **Figure 4.11**. In this result, the bare carbon is able to produce higher concentrations until 40 mM of H₂O₂ while most of the PTFE-patterned electrodes are shown in the range below 20 mM due to the longer lifetime compared to the PTFE patterns. However, when comparing yields at the initial time, the bare CFP produced less H₂O₂ than most of the PTFE-patterned electrodes. This shows that PTFE does have an effect on H₂O₂ selectivity.

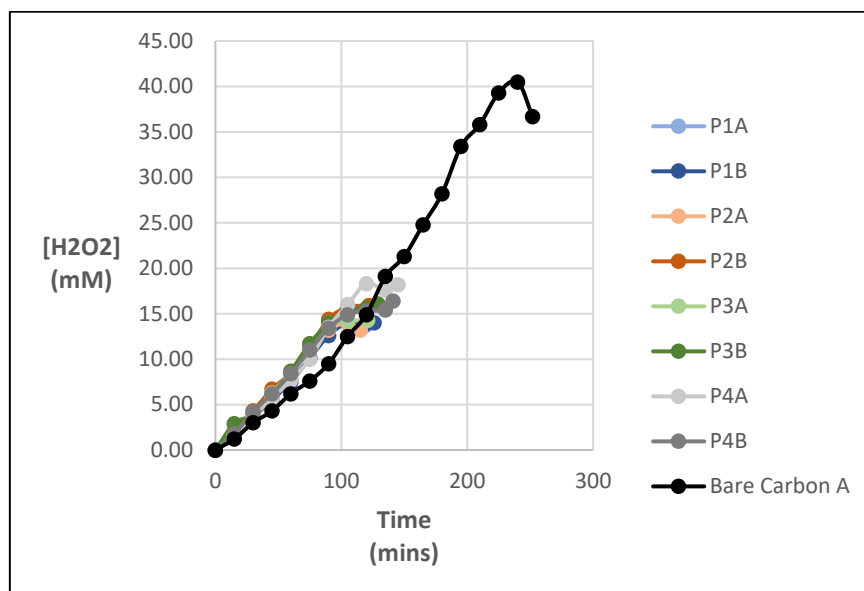


Figure 4.11 H₂O₂ yield throughout the time for each PTFE-patterned CFP with different perimeter and bare CFP B

However, the graph's scale makes it difficult to distinguish the differences between each curve. **Figure 4.12** shows the average H₂O₂ concentration yield for each pattern to show a clearer visual comparison between the curves. Since each pattern has a different lifetime and the H₂O₂ concentration tends to be stagnant near the end, the average curves are displayed only up to a selected time point. For the perimeter variation, the averages are calculated up to 105 minutes, as most patterns have a lifetime of around 120 minutes.

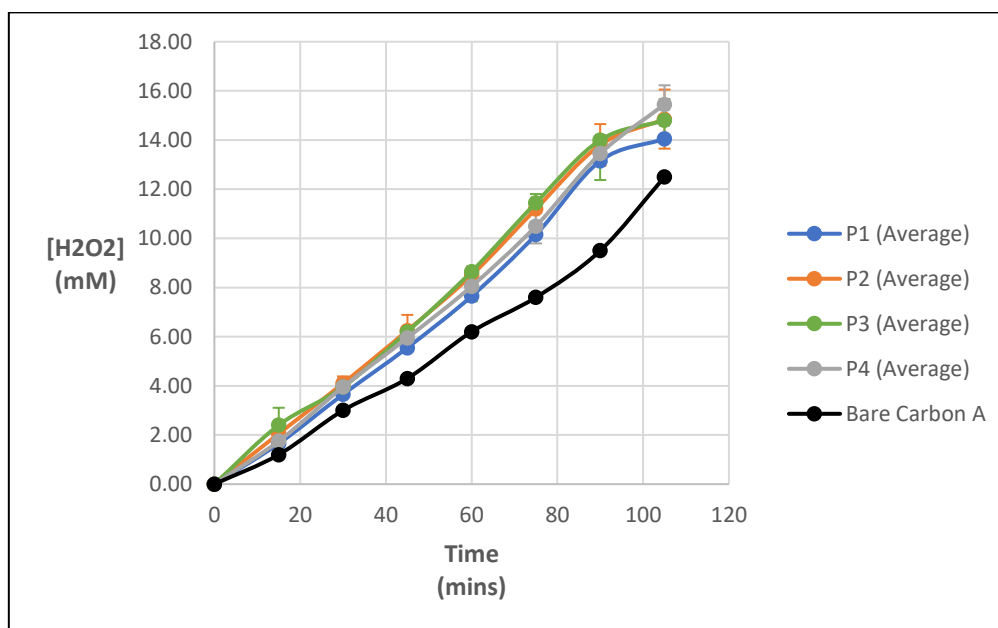


Figure 4.12 Average [H₂O₂] in mM of each electrode (perimeter variation) until 105 minutes

To determine whether there are significant differences in H₂O₂ concentrations over time among the different patterns, the analysis of variance (ANOVA) method is used. The analysis will provide the p-value to determine whether the values among other samples are different or not. The analysis was conducted using the “ANOVA two-factor with replication” option in the data analysis tool of Microsoft Excel. The two-factor ANOVA was chosen instead of the one-factor ANOVA to also observe the concentration trend over time. However, the time factor results are not presented in this report, as it is evident that longer reaction times naturally influence the concentration due to the reaction rate. The results of this analysis are presented in **Table 4.2**.

Table 4.2 Results of ANOVA two-way factor with replication for perimeter variation (yellow color indicates the P-value is lower than 0.05 as the significance level)

Samples observed	P-value
Overall	0.000475
P1 and P2	0.001698
P1 and P3	5.06E-05
P1 and P4	0.00823
P2 and P3	0.629464
P2 and P4	0.276255
P3 and P4	0.072386
P1, P2, P3	0.000281
P1, P2, P4	0.003025
P1, P3, P4	0.000163
P2, P3, P4	0.234146

In general statistical analysis, the p-value is compared to a significance level (α), which is equal to 1 minus the confidence level, to determine whether to accept or reject the null hypothesis [64]. The null hypothesis is defined that there is no significant difference, while rejecting the null hypothesis (in favor of the alternative hypothesis) indicates a significant difference [64]. In this study, when comparing all samples, the p-value was approximately 0.000475. Given a typical α value of 0.05, the p-value is lower implying that the statistics suggest to reject the null hypothesis or the H₂O₂ concentrations for each perimeter variation pattern have significant difference.

However, further analysis revealed that the P1 samples (A and B) were primarily responsible for the low p-value. The P1 samples produced the lowest H₂O₂ concentrations compared to the other three perimeter variants, leading to the rejection of the null hypothesis according to the ANOVA results. If the P1 samples were excluded from the analysis, the statistics would fail to reject the null hypothesis. Nevertheless, excluding P1 would not be appropriate, as the result might indeed reflect a true effect where the perimeter of PTFE or the O₂ bubble circumference influences the reaction. However, this effect only becomes statistically insignificant as the perimeter increases from P2 to P4.

4.4. Area Variation of PTFE Patterns

Figure 4.13 shows a more distinct difference of operation lifetime in between PTFE-patterned with different patterned area variants. The same as perimeter variation that the bare carbon B exhibits to have longer stability than PTFE-patterned carbon electrodes. As higher surface area of the patterns makes faster occurrence of overshooting potential. However, A2 samples does not follow the expected trend, as its lifetime is longer than that of A3, despite A3 having a smaller PTFE area.

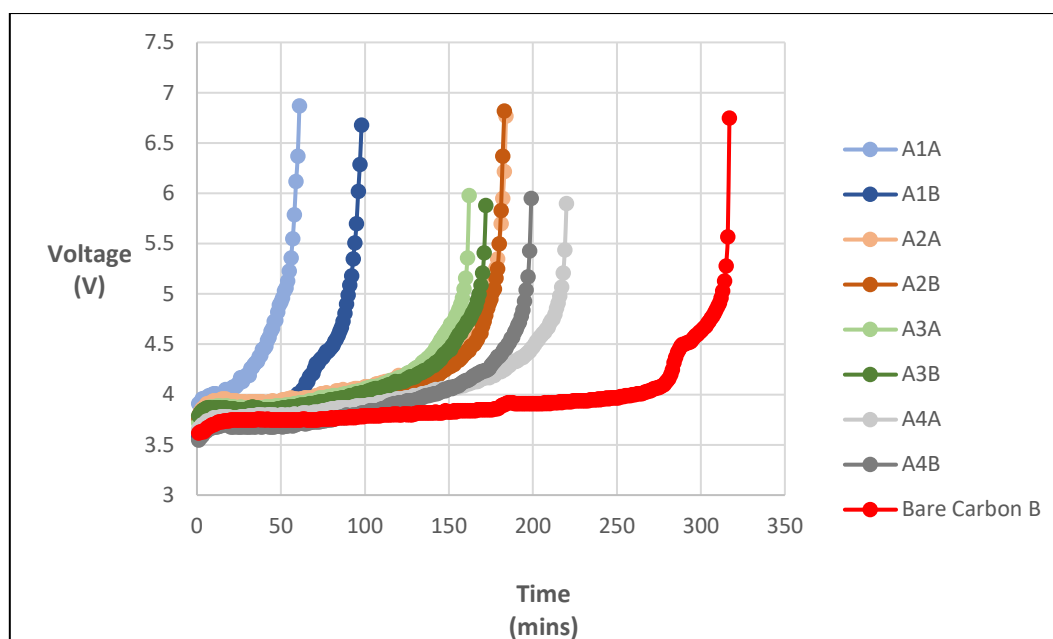


Figure 4.13 Chronopotentiogram of each PTFE-patterned CFP with a different area and bare carbon

Table 4.3 presents the performance lifetime of each electrode, estimated from the chronopotentiogram data. Compared to the results from the perimeter variation, the PTFE area variation shows a much greater range of lifetimes. This suggests that area variation affects more to the electrode stability.

Table 4.3 Performance lifetime for each PTFE-patterned CFP electrode with different area

Pattern	Sample	Performance lifetime (hours)
A1	A	1.00
	B	1.62
A2	A	3.03
	B	3.02
A3	A	2.68
	B	2.90
A4	A	3.65
	B	3.30
Bare Carbon B		5.27

Figure 4.14 displays the H_2O_2 yield for each PTFE-patterned area variant. On this scale, the yield differences over time for each electrode variant appear similar. However, when the data is presented in **Figure 4.15**, the differences become more visually distinct. Unlike the perimeter variation, the average data is shown only up to 60 minutes, as the least stable electrode (A1A) lasts around a hour.

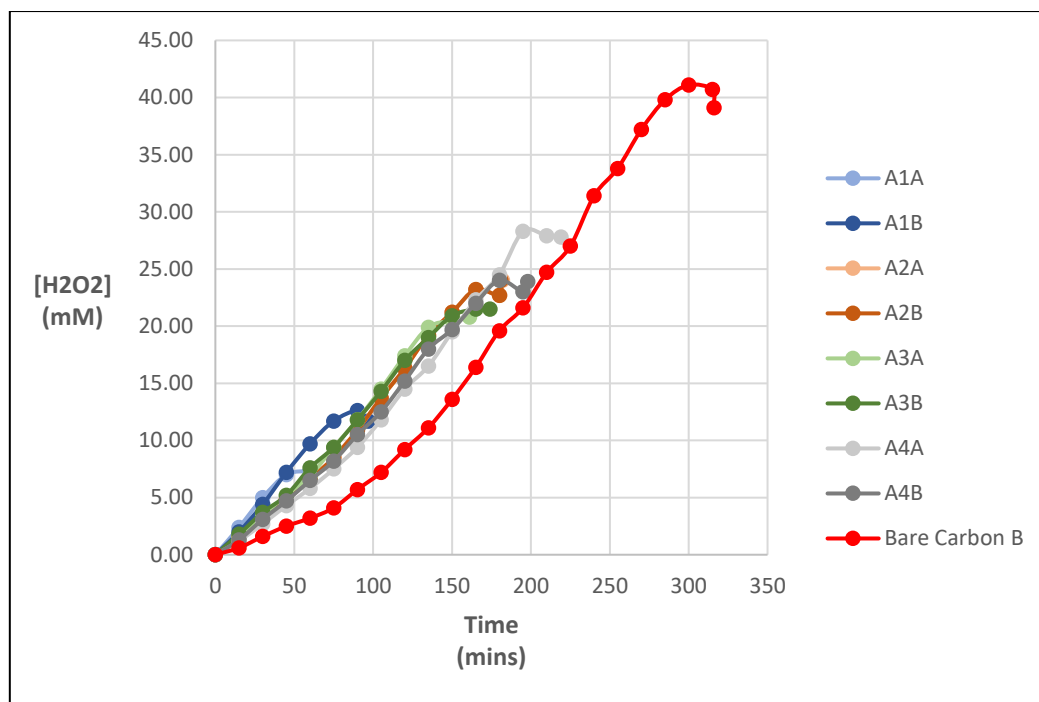


Figure 4.14 H₂O₂ yield throughout the time for each PTFE-patterned CFP with different perimeter and bare CFP B

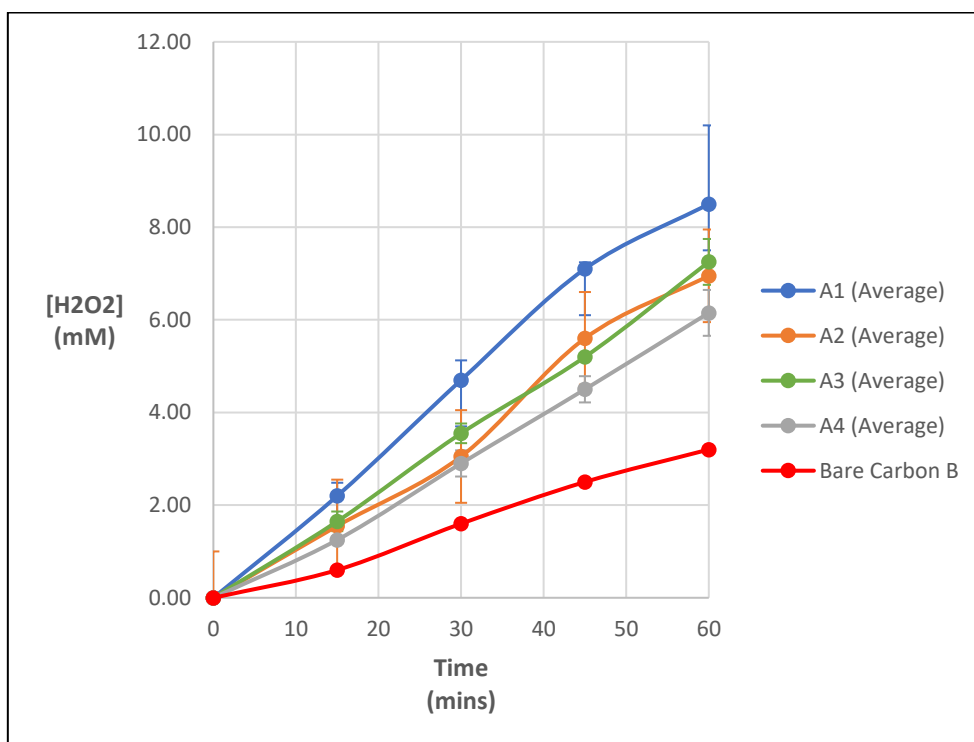


Figure 4.15 Average [H₂O₂] in mM of each electrode (area variation) until 60 minutes

Based on the ANOVA results (Table 4.4), most samples have a p-value lower than the general significance level of 0.05. This implies that different area variations have a statistically significant impact toward H₂O₂ concentration. However, the comparison between A2 and A3 yielded a p-value higher than 0.05, meaning the null hypothesis could not be rejected. This could be seen in Figure 4.15 as well that A2 and A3 show a similar result.

Table 4.4 Results of ANOVA two-way factor with replication for area variation (yellow color indicates the P-value is lower than 0.05 as the significance level)

Samples observed	P-value
Overall	2.36E-05
A1 and A2	0.006247
A1 and A3	0.004325
A1 and A4	0.000182
A2 and A3	0.627041
A2 and A4	0.043306
A3 and A4	0.000881
A1, A2, A3	0.001614
A1, A2, A4	0.000107
A1, A3, A4	2.51E-05
A2, A3, A4	0.013697

An interesting observation about A2 stamp that the vertical distance (design condition) between PTFE stamp is the farthest compared to A1, A3, and A4. This could be a possible reason why A2 has a slightly longer lifetime and produce insignificant difference H_2O_2 concentration compared to A3 stamp. Since the flow direction is vertical, there could be a high chance where a flow is contacted to the electroactive zone between the patterns, refer to a “red zone” in **Figure 4.17**, which is far away from the crucial multiphase boundary to enable the H_2O_2 reaction. Xia et al. have also explained that the triple-phase boundary enables the two-electron transfers [22]. As the local concentration of H_2O is still high on this red zone, where the local concentration of H_2O remains high, the reaction mechanism may shift, potentially favoring the four-electron transfer process instead of producing H_2O_2 .

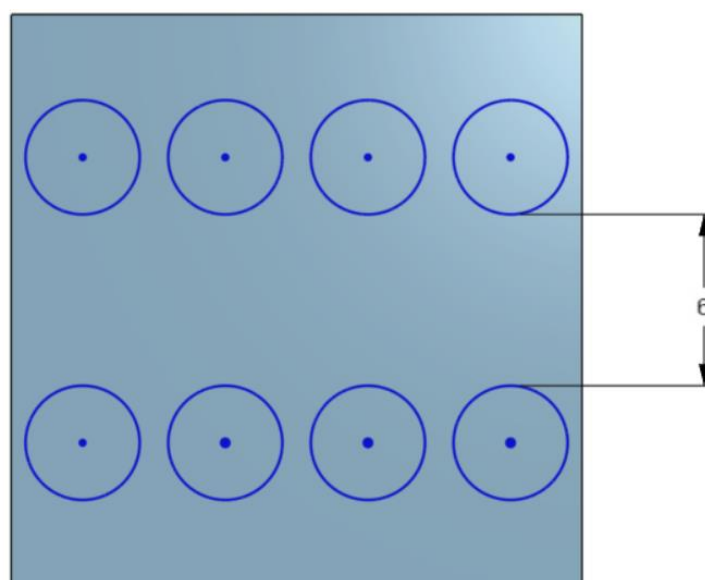
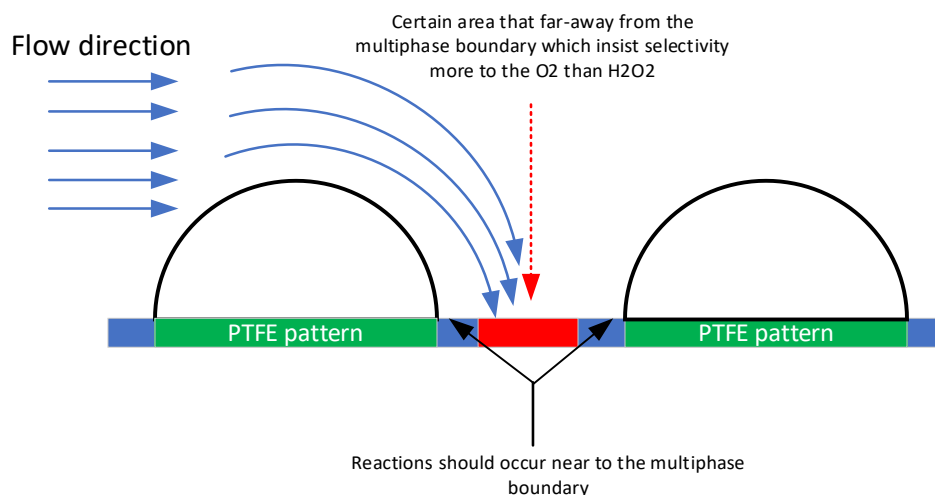


Figure 4.16 The distance between stamp pillars in the A2 variant for 6 mm

Table 4.5 Vertical distance between stamp pillars for each variants

Variant	Vertical distance between stamps (mm)
A1	2
A2	6
A3	3
A4	4

**Figure 4.17** A schematic explaining a flow that would go onto the red zone in between the confined O₂ bubbles

Nevertheless, from the **Figure 4.12** and **Figure 4.15** show that neither perimeter nor area variation led to any significant increase in H₂O₂ production compared to the bare carbon samples, especially when considering the scale difference. Therefore, the dip-coating method will be tested, which Xia et al. reported to have much higher selectivity for H₂O₂.

4.5. Concentration Variation of PTFE-Dip Coated CFP

Compared to other variations, the PTFE dip-coated electrode samples gave surprising results. As shown in **Figure 4.18** as the concentration of PTFE on the surface increases, the potential overshoots more quickly. This supports the suggestion that dip-coating the carbon electrode covers the electroactive area, thereby hindering the reactions.

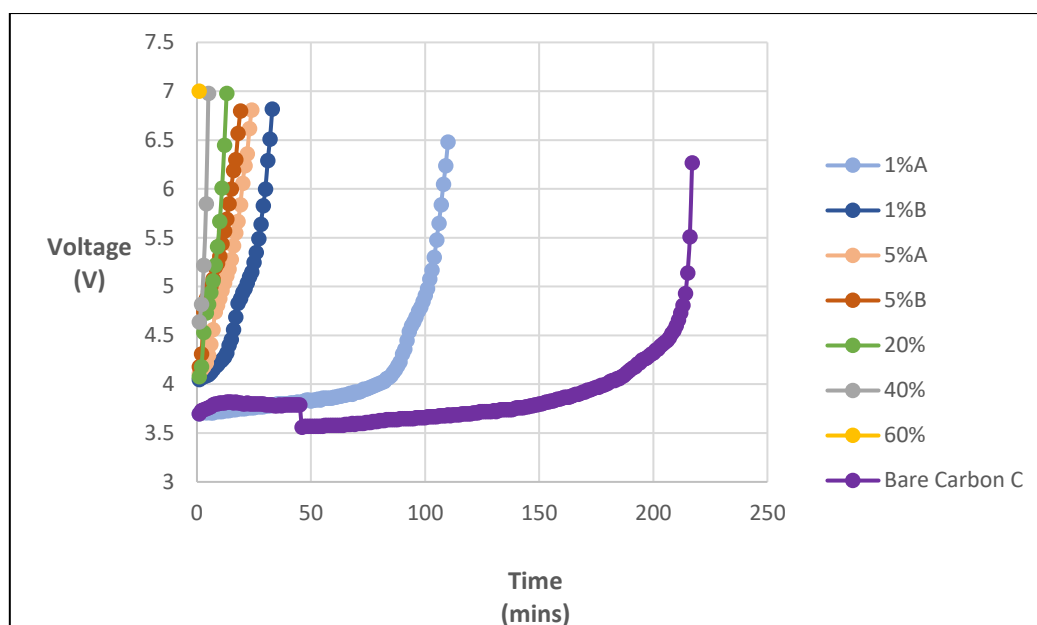


Figure 4.18 Chronopotentiogram of each PTFE-coated CFP with a different concentrations and bare carbon C

From the chronopotentiogram, samples 1%A and 1%B exhibit significantly different lifetimes. Based on the mass change percentage from **Table 3.4**, both 1%A and 1%B should have similar surface compositions. SEM/EDX images of 1%A PTFE concentration are provided in **Figure B.7**. The used PTFE dip-coated electrode is still intact (due to being covered by PTFE), and these extension parts of the electrodes were analyzed to observe the composition. According to the EDX results shown in **Figure 4.20**, the composition of carbon and fluorine elements changed significantly for sample 1%A. The F/C ratios before and after electrolysis were 0.307 and 0.051, respectively, whereas the post-experiment F/C ratio for 1%B was 0.449. An unclear occurrence during the experiment led to a reduction in PTFE coverage for 1%A. Due to this observation, 1%A electrode in a sense has a longer lifetime compared to 1%B.

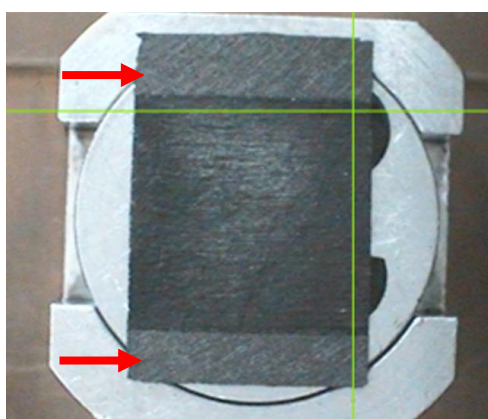


Figure 4.19 Post-experiment 1%B CFP electrode is still intact with the extension area (shown by the red arrows)

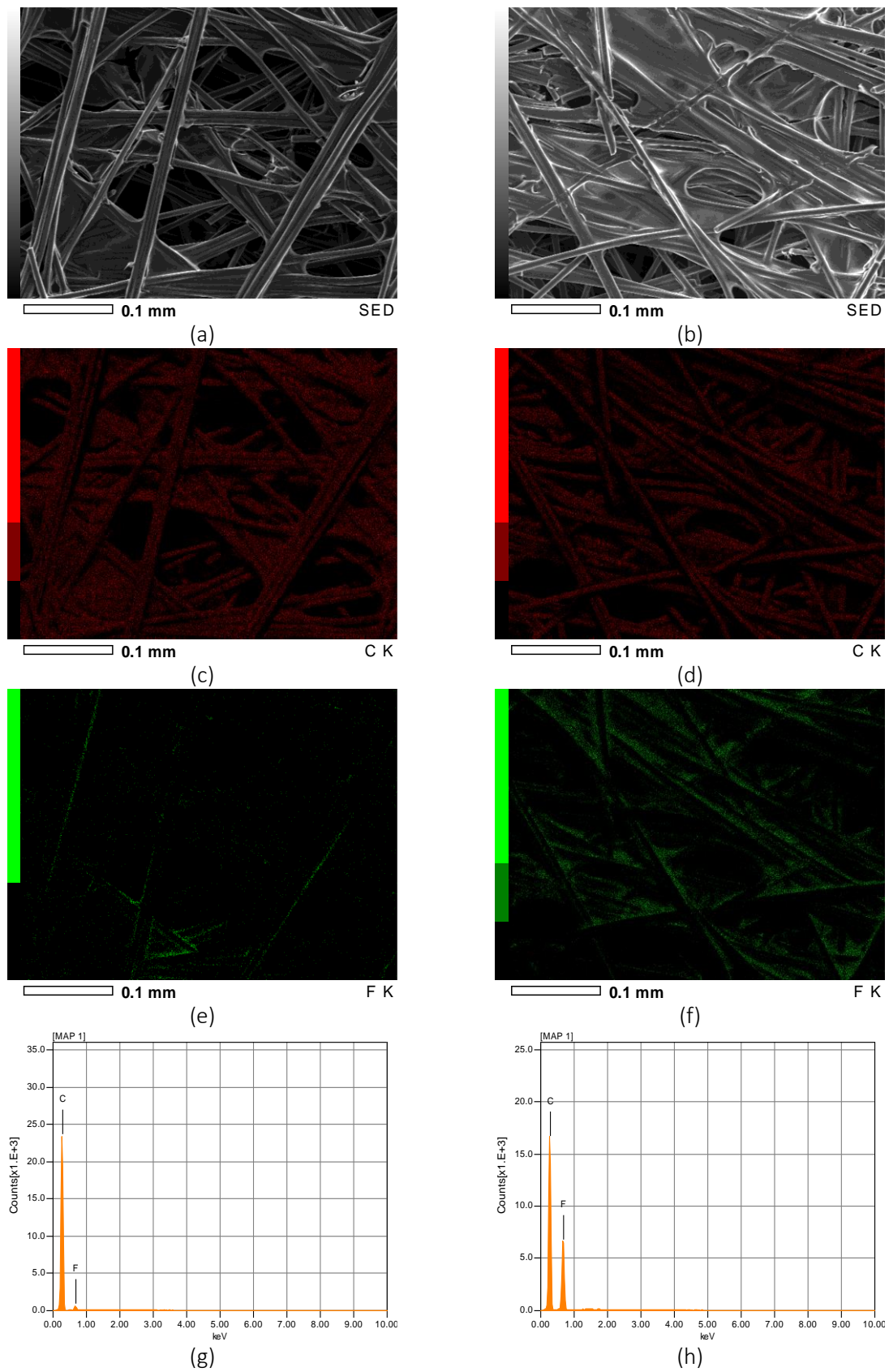


Figure 4.20 Comparison between post-experiment 1%-wt PTFE emulsion dip-coated CFP in SEM image (15kV with 300x magnification) and EDX results. For 1%A is shown in (a), (c), (e), and (g). For 1%B is shown in (b), (d), (f), and (h)

Given the short lifetimes of most PTFE dip-coated electrodes, these samples were unable to produce significant amounts of H_2O_2 over extended periods (1%A is an exception due to **Figure 4.20**). The H_2O_2 concentrations for each PTFE dip-coated electrode, along with bare carbon C, are displayed in **Figure 4.21**. An enlarged version of the graph is presented in **Figure 4.22**. Although the PTFE dip-coated electrode does give a higher H_2O_2 yield than bare carbon C, the duration of this increased yield shortens as the PTFE concentration increases.

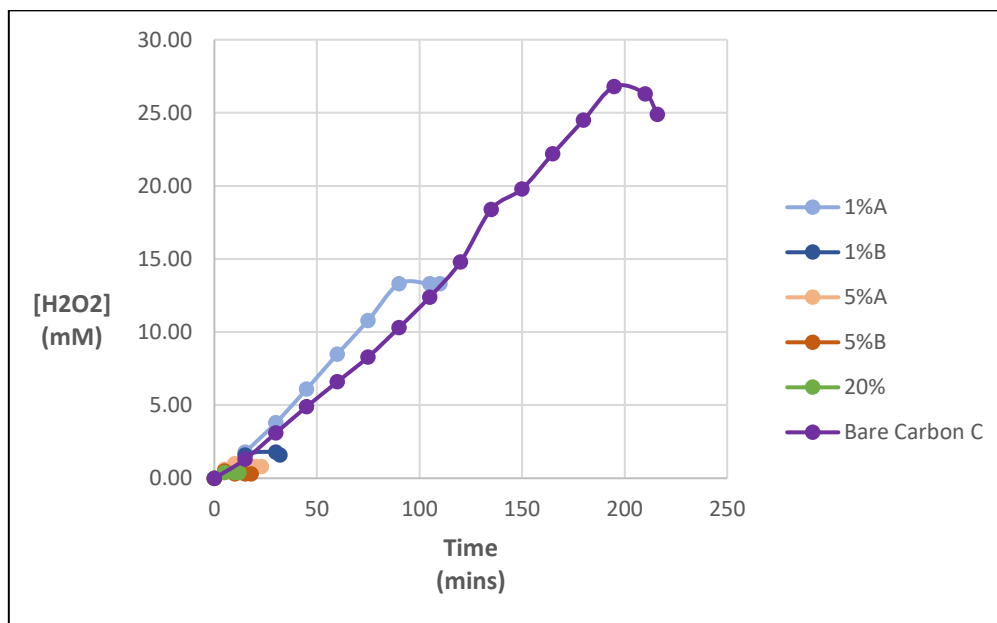


Figure 4.21 H_2O_2 concentration results throughout time for each PTFE dip-coated CFP variant and bare carbon C

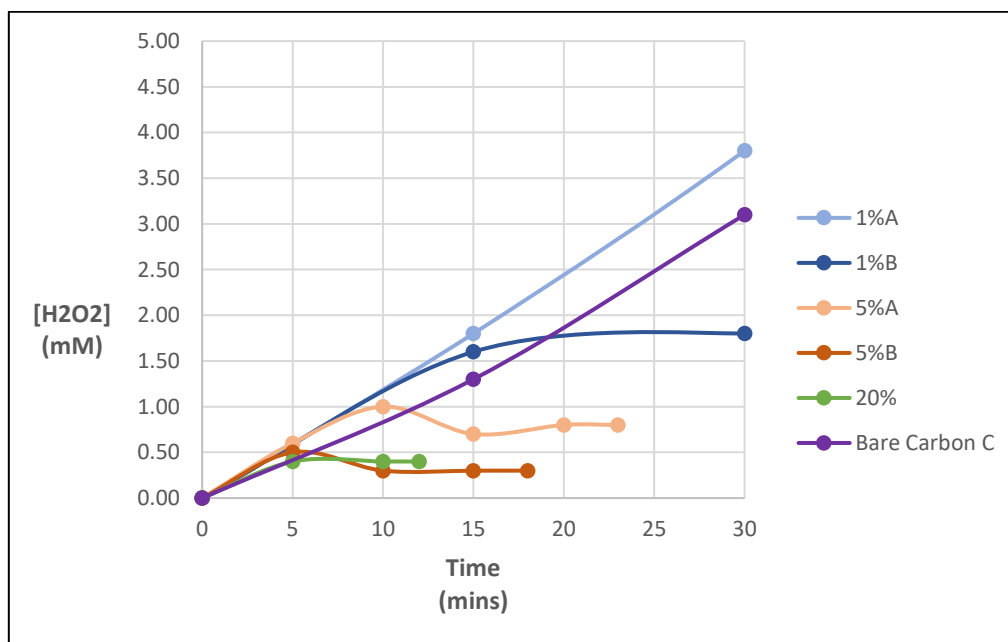


Figure 4.22 H_2O_2 concentration for each PTFE dip-coated CFP variant and bare carbon C within 30 minutes

This suggests that a dip-coated electrode with a high concentration of PTFE may not be suitable for large-scale applications. The inertness and high electrical resistivity of PTFE hinder electrochemical reactions, as ion molecules require a conductive surface. Additionally, water must come into contact

with the electrode. Otherwise, the reactant cannot be delivered to the surface due to the hydrophobic nature of the coating.

In contrast, Xia et al. reported that a dip-coated electrode with a 60% PTFE emulsion achieved a significantly longer lifetime of over 400 minutes [22]. A comparison of the experimental conditions between this study and that of Xia et al. is presented in **Table 4.6**. According to this comparison, one peculiar difference is the pretreatment by oxygen plasma. Xia et al. proposed that PTFE enhances H_2O_2 selectivity because confined O_2 decreases reactant stability and prevents graphene oxidation by reducing local water concentration [22]. Oxygen plasma pretreatment could alter the surface chemical composition, potentially enabling continuous electrolysis operation. However, implementing plasma pretreatment on an industrial scale could introduce financial challenges.

Table 4.6 Comparison of the experimental conditions from this study with the study conducted by Xia et al. [22]

Experiment condition	This study	Xia et al.
Electrolysis cell type	<ul style="list-style-type: none"> Flow cell – two-electrode system: Nickel fiber felt as the counter electrode 	<ul style="list-style-type: none"> H-type glass cell (customized) – three-electrode system Saturated electrode calomel as the reference electrode Platinum foil as the counter electrode Flow cell for WOR coupled ORR – three electrode system
Separator	Zirfon PERL	Nafion 117
Electrolyte	K_2CO_3 1M with 11 gr/L of Na_2SiO_3 (pH = 12.58)	Na_2CO_3 1M with 4 mg/mL of Na_2SiO_3 (pH = 11.96)
Temperature	Ambient	25°C
Mass change of 60% PTFE	378.14%	150%
CFP electrode supplier	Toray (TGP-060-H, untreated)	Fuel Cell Store
CFP geometric area	2x2 cm ²	Size of 2x5 cm ² is mentioned from the methodology. The geometric area the study stated is 0.36 cm ² for ECSA* consideration.
Electrode drying and annealing method	120°C under 15 minutes and 350°C minutes under 30 minutes within N_2 gas	120°C under unknown duration and 350°C minutes under 30 minutes within Ar gas
Electrode pretreatment	None	Pretreated with oxygen plasma at 50 W for 2 minutes
H_2O_2 quantification method	2.5 mL at 15 minutes with $KMnO_4$ titration	$KMnO_4$ titration
Electrolysis operation	Constant current at 0.1 A/cm ² with the resulting voltage above 3.40 V	Constant voltage at 2.4V with the resulting current around 0.1 A/cm ² . The electrolyte is refreshed randomly.

*ECSA = electrochemical surface area

Chapter 5 - Conclusion and Recommendations

5.1. Conclusions

The overall objective is to observe the different treatments of PTFE to be applied on CFP electrodes. The concept is important for applying a reproducible method for a larger scale if the idea of anodic H₂O₂ production is demanded for a larger scale. Given the challenges in precisely measuring the surface area of microscopic bare carbon fibers or accurately determining bubble circumference on the surface, a patterning method was employed. Research questions are revisited as below.

Research Questions:

1. Does PTFE applied on CFP have better stability than bare CFP?

PTFE-applied CFP is **less stable** than bare CFP, as indicated by a shorter performance lifetime.

Sub-research questions 1- What changes occur in performance lifetime due to different:

(a) **perimeter** variations of PTFE patterns?

Most of the perimeter variation of PTFE patterns (P2, P3, and P4) have an insignificant effect on the performance lifetime (shown in **Figure 4.10** and **Table 4.1**).

(b) **area** variations of PTFE patterns?

A larger PTFE pattern area significantly increases the operation lifetime (shown in **Figure 4.13** and **Table 4.3**).

(c) **concentrations of PTFE** applied through dip-coating?

Higher concentrations of PTFE significantly reduce the operation lifetime (shown in **Figure 4.18**).

2. How should PTFE be applied to the CFP electrode to yield more H₂O₂?

PTFE should be applied with a **larger surface area** on the electrode, but **dip-coating the entire electrode is not recommended**, as it inhibits electrochemical activity.

Sub-research questions 2 – What changes occur in H₂O₂ yield due to different:

(a) **perimeter** variations of PTFE patterns?

Most of the perimeter variations of PTFE patterns (P2, P3, and P4) have an insignificant effect on H₂O₂ yield (shown in **Figure 4.12** and **Table 4.2**).

(b) **area** variations of PTFE patterns?

A larger PTFE pattern area significantly increases H₂O₂ yield (shown in **Figure 4.15** and **Table 4.4**).

(c) **concentrations of PTFE** applied through dip-coating?

Higher concentrations of PTFE on dip-coated electrodes significantly decrease H_2O_2 yield (shown in **Figure 4.22**).

Based on all the results, the following conclusions can be drawn to the studies by Xia et al. and Vogel et al.:

1. The perimeter of the bubble might have OH^- surrounding the circumference as this study did not exactly prove it and showed from P1 that the lowest perimeter can increase to P2. However, from P2 to P4, there was no significant difference, suggesting that increasing the PTFE perimeter is not advantageous for large-scale applications.
2. Increasing the PTFE area generally led to an improvement in H_2O_2 concentration, indicating that more multiphase boundaries with O_2 reduce local H_2O concentration, thus increasing the reaction rate, as suggested by Xia et al. However, a larger PTFE area also shortens the performance lifetime.
3. Coating the entire electrode with PTFE would likely worsen performance, as the presence of conducting material (bare CFP) is essential for the reaction to proceed efficiently.

These conclusions are based on the experimental conditions outlined in the methodology. Additionally, the precision limitations of this study may also be influenced by the condition of the current collector, as discussed in **Section 4.2**.

5.2. Recommendations

If any further research would be conducted related to this study, recommendations are listed below for consideration.

Electrode Soaking Duration in Pre-Experiment Influences the Performance Lifetime

During the study, it was observed that soaking the A3/P3 CFP electrodes (K_2CO_3 1M with 11 gr/L of Na_2SiO_3) prior to electrolysis positively impacted their performance lifetime. Longer soaking durations correlated with extended lifetimes. According to a study about pre-soaking carbon electrodes for capacitors with an electrolyte found that the fibers swelled and wettability increased, leading to a more stable performance [65]. However, the concentrations of H_2O_2 for each of them were not significantly affected. The concept of pretreatment of carbon electrodes within electrolyte would be a recommendation for future studies to optimize the operation lifetime.

Selecting Metal Oxides or Different Carbon Material Structure as the Base Material

Based on **Figure 4.15**, comparing bare carbon B, pattern A1, and pattern A4 shows that as the time goes longer before near the end of the lifetime, the yield difference becomes larger. This implies that using a more durable base electrode could significantly enhance H_2O_2 concentration when combined with PTFE. Materials that are mentioned in **Section 2.6** such as WO_3 , BiVO_4 , TiO_2 , and SnO_2 or different form of carbon materials such as boron-doped diamond provide more durability could give larger amount of H_2O_2 .

Adjusting the Flow

Although perimeter variation showed no significant effect as the PTFE perimeter increased, Vogel et al. noted that bubbles possess highly reactive redox sites in their static form [26]. In this study, the vertical flow geometry of the cell, which is perpendicular to bubble growth on the electrode, might have caused the forced release of bubbles. Adjusting the flow to be lower might have an effect.

Activating Carbon to Have Hydrophobic Surface

Xia et al. highlighted the significant role of O_2 in enhancing H_2O_2 selectivity through the use of PTFE. Besides applying PTFE, carbon electrodes could be modified to become more hydrophobic. A study conducted by Goncalves et al. that the hydrophobic-modified into activated carbon is made by pyrolysis of propene (propylene) [66]. Additionally, research on biopropylene from biomass sources has been reviewed [67] [68]. This could enable the use of abundant biomass sources to increase the feasibility of water electrolyzers.

References

- [1] IEA, "Global Hydrogen Review 2021," 2021. [Online]. Available: <https://iea.blob.core.windows.net/assets/5bd46d7b-906a-4429-abda-e9c507a62341/GlobalHydrogenReview2021.pdf>.
- [2] IEA, "Global average levelised cost of hydrogen production by energy source and technology, 2019 and 2050," 2020. [Online]. Available: <https://www.iea.org/data-and-statistics/charts/global-average-levelised-cost-of-hydrogen-production-by-energy-source-and-technology-2019-and-2050>.
- [3] FMI, "Industrial Oxygen Market to Surge at a Projected 7.9% CAGR," 2023. [Online]. Available: <https://finance.yahoo.com/news/industrial-oxygen-market-surge-projected-103000483.html>.
- [4] T. Kato, M. Kubota, N. Kobayashi and Y. Suzuoki, "Effective utilization of by-product oxygen from electrolysis hydrogen production," *Energy*, vol. 30, pp. 2580-2595, 2005.
- [5] B. Burek, S. Bormann, F. Hollmann, J. Bloh and D. Holtmann, "Hydrogen peroxide driven biocatalysis," *Green Chemistry*, no. 12, 2019.
- [6] A. Goti and F. Cardona, "Hydrogen peroxide in green oxidation reactions: recent catalytic processes," *NATO Science for Peace and Security Series ((NAPSC))*, pp. 191-212, 2008.
- [7] Y. Shi, Y. Xia, G. Xu, L. Wen, G. Gao and B. Zong, "Hydrogen peroxide and applications in green hydrocarbon nitridation and oxidation," *Chinese Journal of Chemical Engineering*, vol. 41, pp. 145-161, 2022.
- [8] J. M. Campos-Martin, G. Blanco-Brieva and J. L. G. Fierro, "Hydrogen peroxide synthesis: an outlook beyond the anthraquinone process," *Angewandte Chemie International Edition*, vol. 45, pp. 6962-6984, 2006.
- [9] D. Pangotra, L. Csepei, A. Roth, V. Sieber and L. Vieira, "Anodic generation of hydrogen peroxide in continuous flow," *Green Chemistry*, vol. 24, pp. 7931-7940, 2022.
- [10] A. Murray, S. Voskian, M. Schreier, T. Hatton and Y. Surendranath, "Electrosynthesis of Hydrogen Peroxide by Phase-Transfer Catalysis," *Joule*, vol. 3, no. 12, pp. 2942-2954, 2019.
- [11] G. Gao, Y. Tian, X. Li, Y. Hu, K. Yang and B. Zong, "Development and application of slurry-bed production technology of hydrogen peroxide by anthraquinone auto-oxidation process," *Results in Engineering*, vol. 19, 2023.
- [12] Intratec, "Hydrogen Peroxide Prices," [Online]. Available: <https://www.intratec.us/chemical-markets/hydrogen-peroxide-price>. [Accessed 10 August 2024].
- [13] Intratec, "Oxygen Price," [Online]. Available: <https://www.intratec.us/products/water-utility-costs/commodity/oxygen-price>. [Accessed 10 August 2024].

- [14] I. Universal Industrial Gases, "Unit Conversion Data for Oxygen," [Online]. Available: https://www.uigi.com/o2_conv.html. [Accessed 8 August 2024].
- [15] X. Shi, S. Siahrostami, G. Li, Y. Zhang, P. Chakthranont, F. Studt, T. Jaramillo, X. Zheng and J. Nørskov, "Understanding activity trends in electrochemical water oxidation to form hydrogen peroxide," *Nature Communications*, vol. 8, 2017.
- [16] J. Song and S. Cho, "Catalytic materials for efficient electrochemical production of hydrogen peroxide," *APL Materials*, vol. 8, no. 5, 2020.
- [17] S. Kelly, X. Shi, S. Back, L. Vallez, S. Park, S. Siahrostami, X. Zheng and J. Nørskov, "ZnO as an active and selective catalyst for electrochemical water oxidation to hydrogen peroxide," *ACS Catalysis*, vol. 9, pp. 4593- 4599, 2019.
- [18] D. Liu, D. Solanki, E. Stabitski, M. Li, S. Hu, V. Batista and K. Yang, "Selective water oxidation to H₂O₂ on TiO₂ surfaces with redox-active allosteric sites," *ACS Applied Energy Materials*, vol. 6, no. 16, pp. 8368-8376, 2023.
- [19] L. Li, Z. Hu, Y. Kang, S. Cao, L. Xu, L. Yu, L. Zhang and J. Yu, "Electrochemical generation of hydrogen peroxide from a zinc gallium oxide anode with dual active sites," *Nature Communications*, vol. 14, 2023.
- [20] L. Fan, X. Bai, C. Xia, X. Zhang, X. Zhao, Y. Xia, Z. Wu, Y. Lu, Y. Liu and H. Wang, "CO₂/carbonate-mediated electrochemical water oxidation to hydrogen peroxide," *Nature Communications*, vol. 13, 2022.
- [21] S. Mavrikis, M. Goltz, S. Rosiwal, L. Wang and C. Leon, "Carbonate-induced electrosynthesis of hydrogen peroxide via two-electron water oxidation," 2021.
- [22] C. Xia, S. Back, S. Ringe, K. Jiang, F. Chen, X. Sun., S. Siahrostami, K. Chan and H. Wang, "Confined local oxygen gas promotes electrochemical water oxidation to hydrogen peroxide," *Nature Catalysis*, vol. 3, pp. 125-134, 2020.
- [23] J. Hou, Z. Xu, J. Ji, Y. Zhao, M. Gao and C. Jin, "Enhanced in-situ electro-generation of H₂O₂ using PTFE and NH₄HCO₃ modified C/PTFE electrode for treatment of landfill leachate," *Journal of Environmental Management*, vol. 295, 2021.
- [24] J. F. Pérez, C. Sáez, J. Llanos, P. Cañizares, C. López and M. A. Rodrigo, "Improving the efficiency of carbon cloth for the electrogeneration of H₂O₂: role of polytetrafluoroethylene and carbon black loading," *Industrial & Engineering Chemistry Research*, vol. 56, 2017.
- [25] L. Radulovic and Z. Wojcinski, *Encyclopedia of Toxicology (Third Edition)*, 2014.
- [26] Y. B. Vogel, C. W. Evans, M. Belotti, L. Xu, I. C. Russell, L. Yu, A. K. K. Fung, N. S. Hill, N. Darwish, V. R. Goncales, M. L. Coote, K. S. Iyer and S. Ciampi, "The corona of surface bubble promotes electrochemical reactions," *Nature communications*, vol. 11, 2020.
- [27] O. Diaz-Morales, D. Ferrus-Suspreda and M. Koper, "The importance of nickel oxyhydroxide deprotonation on its activity towards electrochemical water oxidation," *Chemical Science*, no. 4, 2016.

- [28] J. Bard and L. Faulkner, *Electrochemical Methods: Fundamentals and Applications* Second Edition., John Wiley and Sons, 2001.
- [29] P. Cavalier, *Water Electrolysis for Hydrogen Production*, Springer, 2023.
- [30] S. Trasatti, "Electrochemical Theory- Electrokinetics," in *Encyclopedia of Electrochemical Power Sources*, Elsevier, 2009, pp. 23-31.
- [31] AGFA, "Technical Data Sheet- Zirfon PERL UTP 500," [Online]. Available: https://www.agfa.com/specialty-products/wp-content/uploads/sites/8/2020/06/TDS_ZIRFON_PERL_UTP_500_20200525.pdf. [Accessed 18 03 2024].
- [32] K. Ham, S. Hong, S. Kang, K. Cho and J. Lee, "Extensive Active-Site Formation in Trirutile CoSb₂O₆ by Oxygen Vacancy for Oxygen Evolution Reaction in Anion Exchange Membrane Water Splitting," *ACS Energy Letter*, vol. 6, no. 2, pp. 364-370, 2021.
- [33] J. Ampurdanes, M. Chourashiya and A. Urakawa, "Cobalt oxide-based materials as non-PGM catalyst for HER in PEM electrolysis and in situ XAS characterization of its functional state," *Catalysis Today*, vol. 336, pp. 161-168, 2019.
- [34] T. Liu, Y. Tao, Y. Wang, M. Hu, Z. Zhang and J. Shao, "Towards cost-effective and durable bipolar plates for proton exchange membrane electrolyzers: a review," *Fuel*, vol. 368, 2024.
- [35] S. Kamarudin, W. Daud, A. Som, M. Takriff and A. Mohammad, "Technical design and economic evaluation of a PEM," *Journal of Power Sources*, vol. 157, pp. 641-649, 2006.
- [36] L. Bertuccioli, A. Chan, D. Hart, F. Lehner, B. Madden and E. Standen, "Development of Water Electrolysis in the European Union- Final Report," 2014.
- [37] K. Barros, M. Marti-Calatayud, T. Scarazzato, A. Bernardes, D. Espinosa and V. Pierre-Herranz, "Investigation of ion-exchange membranes by means of chronopotentiometry: A comprehensive review on this highly informative and multipurpose technique," *Advances in Colloid and Interface Science*, vol. 293, 2021.
- [38] G. Papanastasiou, G. Kokkinidis and N. Papadopoulos, "Determination of kinetic parameters from chronoamperometric data," *Journal of Electroanalytical Chemistry*, vol. 352, no. 1-2, pp. 153-165, 1993.
- [39] M. Stelzle, C. Bieg, K. Fuchsberger, G. Linke, R. Ramba and S. Werner, "Solid contact ion selective electrodes (ISE) for applications in life sciences, biotechnology and environmental monitoring – technology and performance," in *AMA Conferences 2017*, Nurnberg, Germany, 2017.
- [40] J. Bobacka, "Potential stability of all-solid-state ion-selective electrodes using conducting polymers as ion-to-electron transducers," *Analytical Chemistry*, vol. 71, no. 21, 1999.
- [41] K. Kordek-Khalil, D. Janas and P. Rutkowski, "Revealing the effect of electrocatalytic performance boost during hydrogen evolution reaction on free-standing SWCNT film electrode," *Scientific Reports*, vol. 11, 2021.

- [42] K. Sayama and H. Arakawa, "Effect of carbonate addition on the photocatalytic decomposition of liquid water over a ZrO₂ catalyst," *Journal of Photochemistry and Photobiology A: Chemistry*, vol. 94, pp. 67-76, 1996.
- [43] T. Gill, L. Vallez and X. Zheng, "The role of bicarbonate-based electrolytes in H₂O₂ production through two-electron water oxidation," *ACS Energy Letters*, vol. 6, no. 8, pp. 2645-3010, 2021.
- [44] J. Kozak and A. Townshend, "Titrimetry," in *Encyclopedia of Analytical Science (Third Edition)*, Elsevier, 2019, pp. 111-120.
- [45] S. Park, H. Abroshan, X. Shi, H. Jung, S. Siahrostami and X. Zheng, "CaSnO₃: an electrocatalyst for two-electron water oxidation reaction to form H₂O₂," *ACS Energy Letters*, vol. 4, no. 1, pp. 352-357, 2019.
- [46] E. Berl, "A new cathodic process for the production of H₂O₂," *Transactions of the Electrochemical Society*, vol. 76, no. 1, pp. 359-369, 1939.
- [47] Engineering Toolbox, "Solids, Liquids and Gases- Thermal Conductivities," [Online]. Available: https://www.engineeringtoolbox.com/thermal-conductivity-d_429.html. [Accessed 08 10 2024].
- [48] R. McCreery, "Advanced Carbon Electrode Materials for Molecular Electrochemistry," *Chemical Reviews*, vol. 108, no. 7, 2008.
- [49] K. Akhtar, S. Khan, S. Khan and A. Asiri, "Scanning Electron Microscopy: Principle and Applications in Nanomaterials Characterization," in *Handbook of Materials Characterization*, Springer, 2018.
- [50] JEOL, "JSM-IT100 InTouchScope™ Scanning Electron Microscope," [Online]. Available: <https://www.jeol.com/products/scientific/sem/JSM-IT100.php>. [Accessed 15 08 2024].
- [51] ThermoFisher Scientific, "Electron Beam Damage in Scanning Electron Microscopes: An overview of the damage caused to samples by electron beams.," [Online]. Available: <https://www.thermofisher.com/nl/en/home/materials-science/learning-center/applications/sample-degradation-scanning-electron-microscope-sem.html>. [Accessed 14 08 2024].
- [52] JEOL, "Posters: Periodic Table / L-Value Tables," [Online]. Available: <https://www.jeolusa.com/RESOURCES/Posters>. [Accessed 14 08 2024].
- [53] M. Mutalib, M. Rahman, M. Othman, A. Ismail and J. Jaafar, "Chapter 9- Scanning Electron Microscopy (SEM) and Energy-Dispersive X-Ray (EDX) Spectroscopy," in *Membrane Characterization*, 2017, pp. 161-179.
- [54] H. Hunke, N. Soin, T. Shah, E. Kramer, A. Pascual, M. Karuna and E. Siores, "Low-Pressure H₂, NH₃ Microwave Plasma Treatment of Polytetrafluoroethylene (PTFE) Powders: Chemical, Thermal and Wettability Analysis," *Materials*, vol. 8, no. 5, pp. 2258-2275, 2015.
- [55] B. Crawford and B. Quinn, "Physiochemical properties and degradation," in *Microplastic Pollutants*, Elsevier, 2017, pp. 57-100.

- [56] I. Mcneill, "Thermal Degradation," in *Comprehensive Polymer Science and Supplements*, Elsevier, 1989, pp. 451-500.
- [57] F. Lewis and M. Naylor, "Pyrolysis of Polytetrafluoroethylene," *Journal of the American Chemical Society*, vol. 69, no. 8, pp. 1841-2078, 1947.
- [58] National Library of Medicine, "Tetrafluoroethylene," [Online]. Available: <https://pubchem.ncbi.nlm.nih.gov/compound/Tetrafluoroethylene>. [Accessed 16 August 2024].
- [59] S. Siahrostami and A. Vojvodic, "Influence of absorbed water on the oxygen evolution reaction on oxides," *The Journal of Physical Chemistry*, vol. 119, no. 2, pp. 883-1270, 2015.
- [60] C. Qiu, L. Jiang, Y. Gao and L. Sheng, "Effects of oxygen-containing functional groups on carbon materials in supercapacitors: A review," *Materials & Design*, vol. 230, 2023.
- [61] A. Venugopal, L. Egberts, J. Meeprasert, E. Pidko, B. Dam, T. Burdyny, V. Sinha and W. Smith, "Polymer modification of surface electronic properties of electrocatalysts," *ACS Energy Letters*, vol. 7, no. 5, pp. 1586-1593, 2022.
- [62] Toray, "Toray Carbon Fiber Paper "TGP-H"," [Online]. Available: https://www.fuelcellearth.com/wp-content/uploads/converted_files/pdf/Toray_specs.pdf. [Accessed 08 08 2024].
- [63] J. Hall and S. Zumdahl, *Zumdahl's Chemistry 6th Edition*, Cengage Learning, 2002.
- [64] D. Montgomery, G. Runger and N. Hubele, *Engineering Statistics*, John Wiley and Sons, 2011.
- [65] J. Menzel, A. Slesinski, P. Galek, P. Bujewska, A. Kachmar, E. Frackowiak, A. Washio, H. Yamamoto, M. Ishikawa and K. Fic, "Operando monitoring of activated carbon electrodes operating aqueous electrolytes," *Energy Storage Materials*, vol. 49, pp. 518-528, 2022.
- [66] M. Goncalves, M. Molina-Sabio and F. Rodriguez-Reinoso, "Modification of activated carbon hydrophobicity by pyrolysis of propene," *Journal of Analytical and Applied Pyrolysis*, vol. 89, pp. 17-21, 2010.
- [67] E. Vasiliadou and A. Lemonidou, "Production of biopropylene using biomass-derived sources," *Encyclopedia of Inorganic and Bioinorganic Chemistry*, 2016.
- [68] T. Phung, T. Pham, K. Vu and G. Busca, "(Bio)propylene production processes: a critical review," *Journal of Environmental Chemical Engineering*, vol. 9, no. 4, 2021.
- [69] S. Dermühl and U. Riedel, "A comparison of the most promising low-carbon hydrogen," *Fuel*, vol. 340, 2023.
- [70] A. J. Bard, R. Parsons and J. Jordan, *Standard Potentials in Aqueous Solution*, CRC Press, 1985.
- [71] E. Brillas, E. Mur, R. Sauleda, L. Sanchez, J. Peral, X. Domenech and J. Casado, "Aniline mineralization by AOP's: anodic oxidation, photocatalysis, electro-Fenton and photoelectro-Fenton processes," *Applied Catalysis B: Environment and Energy*, vol. 16, pp. 31-42, 1998.

-
- [72] N. Klassen, D. Marchington and H. McGowan, "H₂O₂ determination by the I₃- method and by KMnO₄ titration," *Analytical Chemistry Volume 66*, no. 18, pp. 884A- 915A, 1994.
- [73] N. Klassen, D. Marchington and H. McGowan, "H₂O₂ determination by the I₃- method and by KMnO₄ titration," *Analytical Chemistry*, vol. 66, no. 18, pp. 884A-915A, 1994.
- [74] F. Budiyanto, Harmesa, Lestari and A. Bayu, "Chapter 3- Bioelectrochemical systems for managing the metal's issues," in *Bioremediation, Nutrients, and Other Valuable Product Recovery*, Elsevier, 2021, pp. 41-82.

Appendix A - Optical Microscope Images

A.1. Bare Carbon



Figure A.1 OM image of a bare carbon electrode (x20)

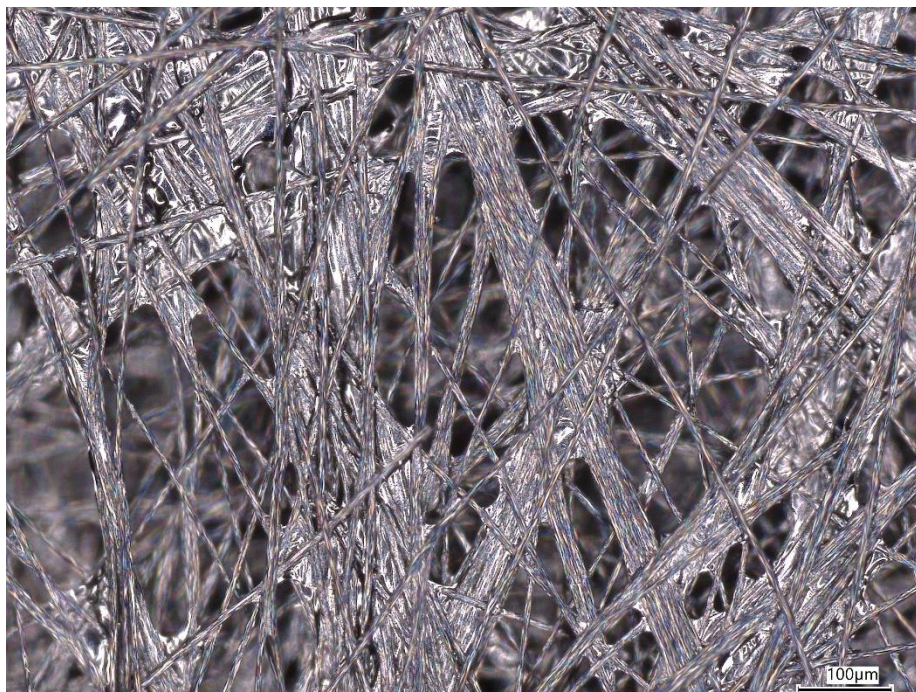
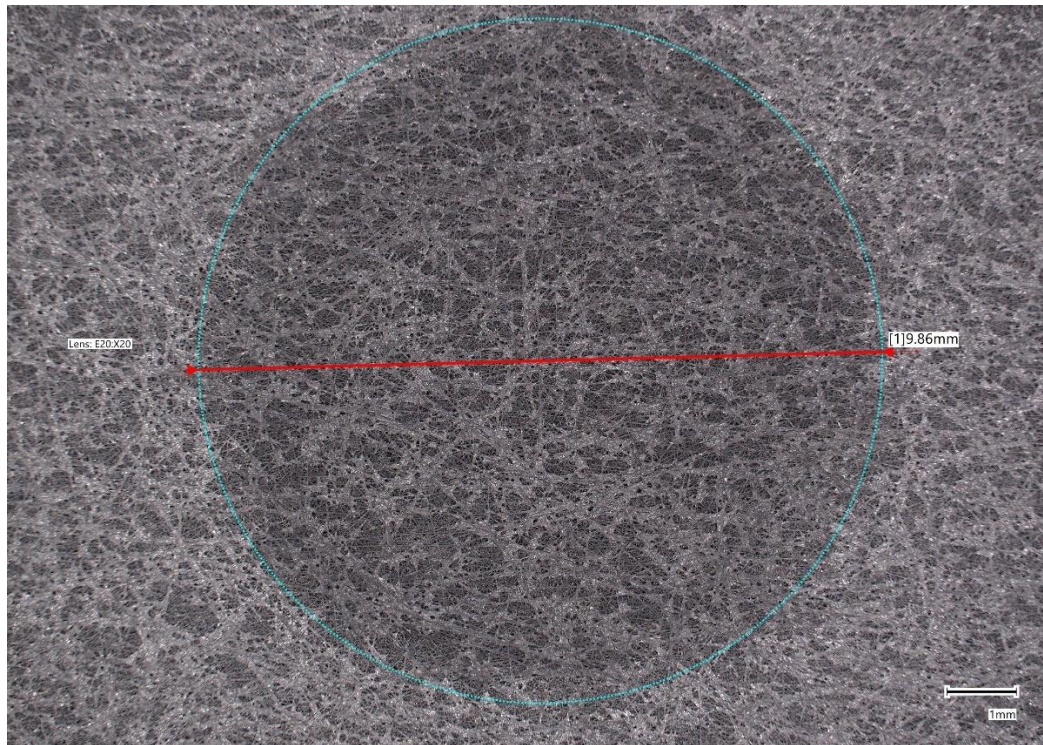


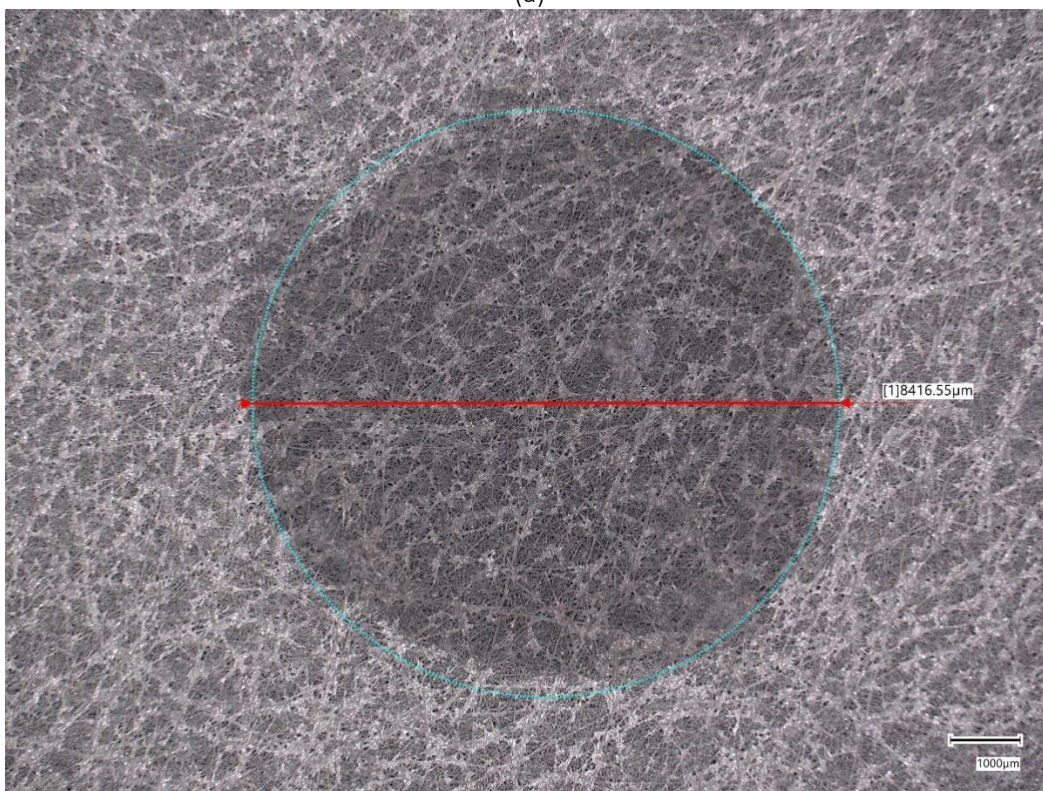
Figure A.2 OM image of a bare carbon electrode (x300)

A.2. Perimeter Pattern Variations

P1 pattern (design diameter = 8 mm)



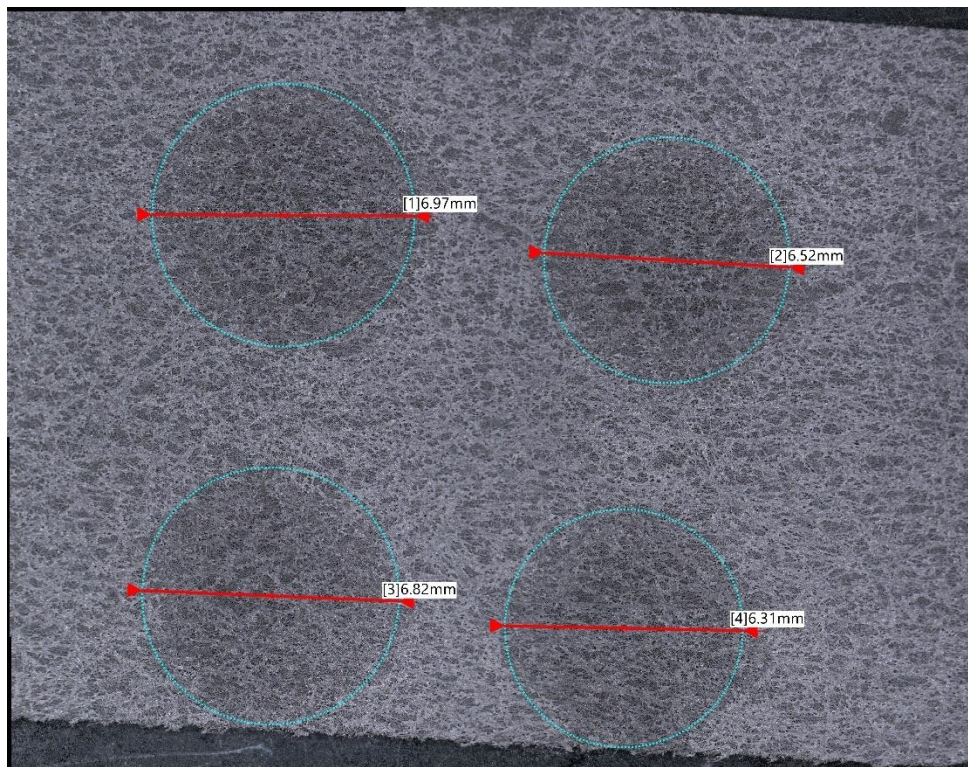
(a)



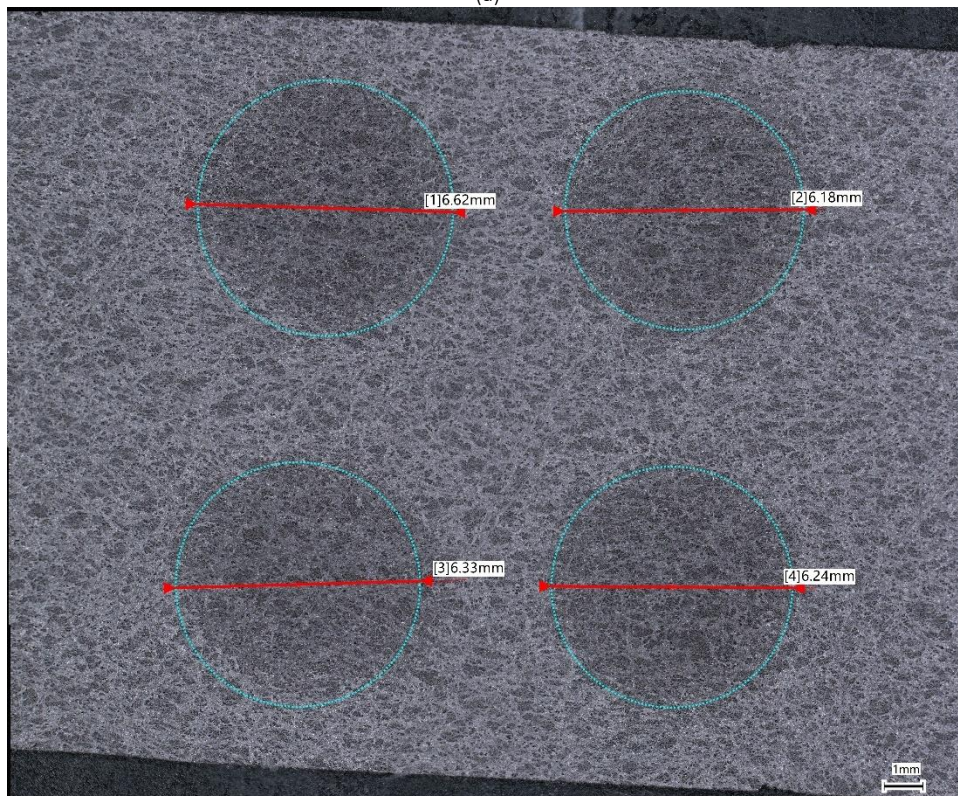
(b)

Figure A.3 P1 variant: (a) sample A (b) sample B

P2 pattern (design diameter = 4 mm)



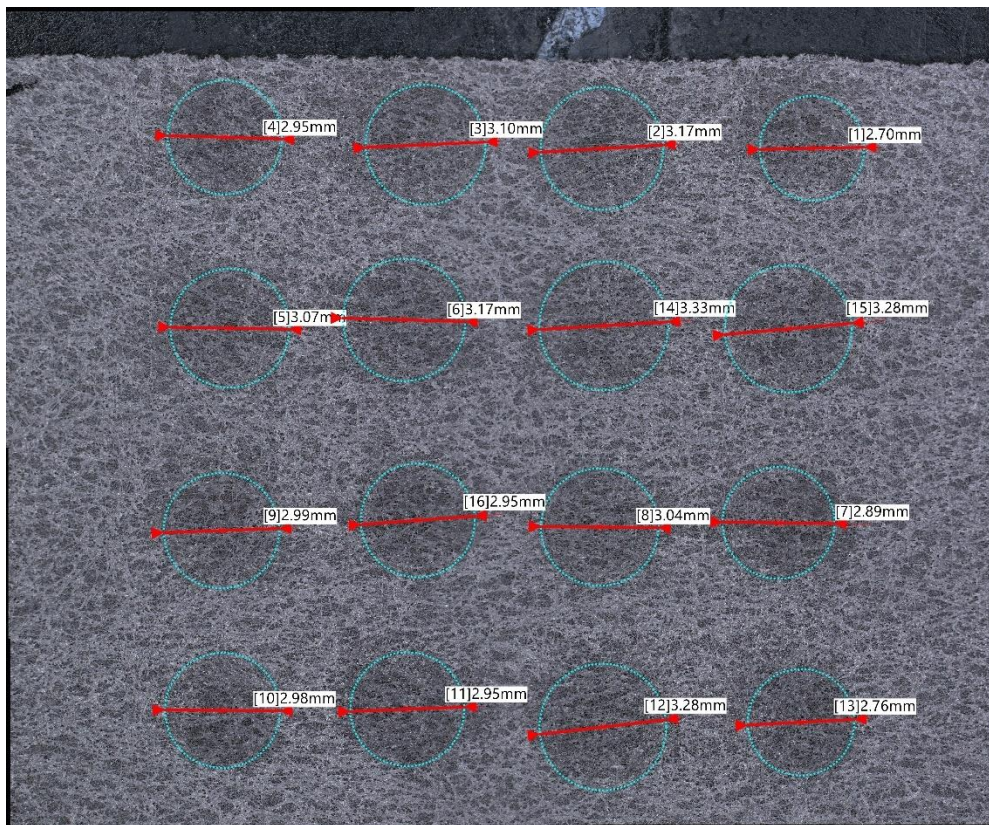
(a)



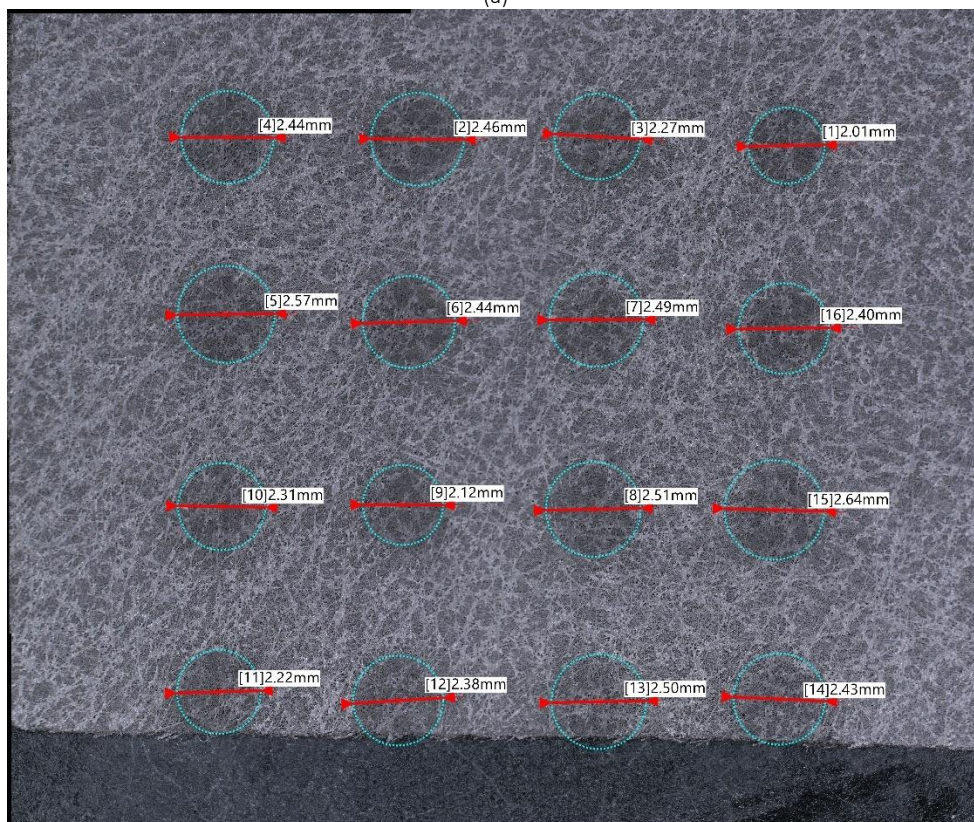
(b)

Figure A.4 P2 variant: (a) sample A (b) sample B

P3 pattern (design diameter = 2 mm)



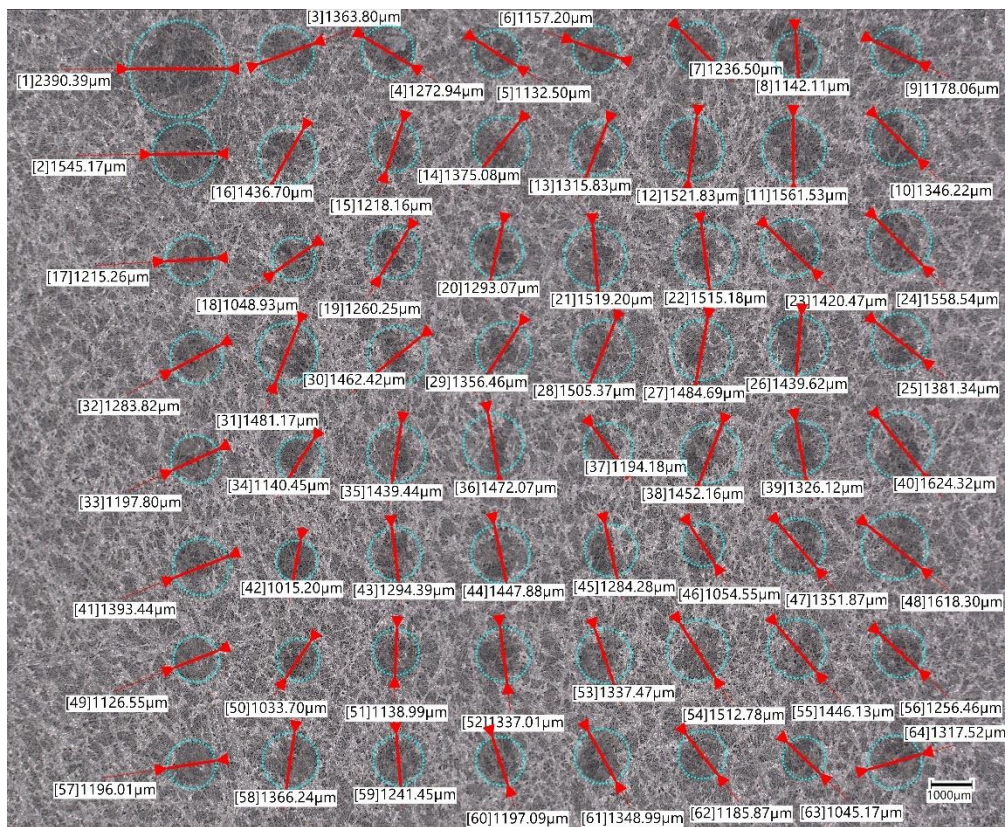
(a)



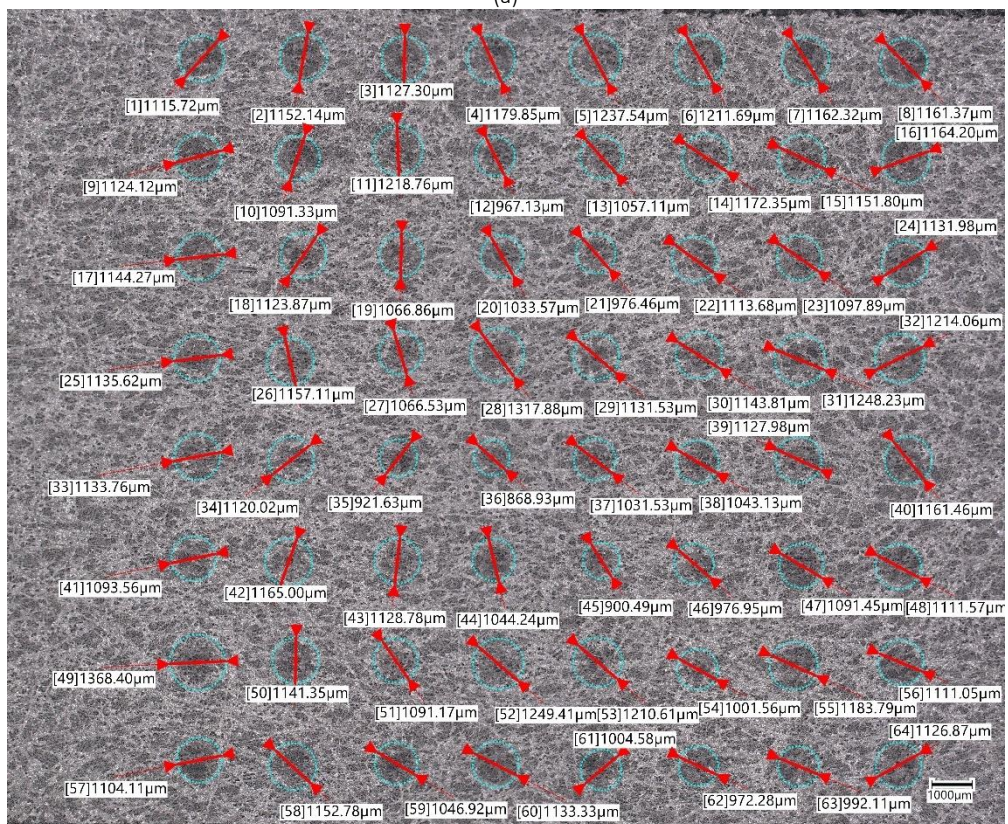
(b)

Figure A.5 P3 variant: (a) sample A (b) sample B

P4 pattern (design diameter = 1 mm)



(a)

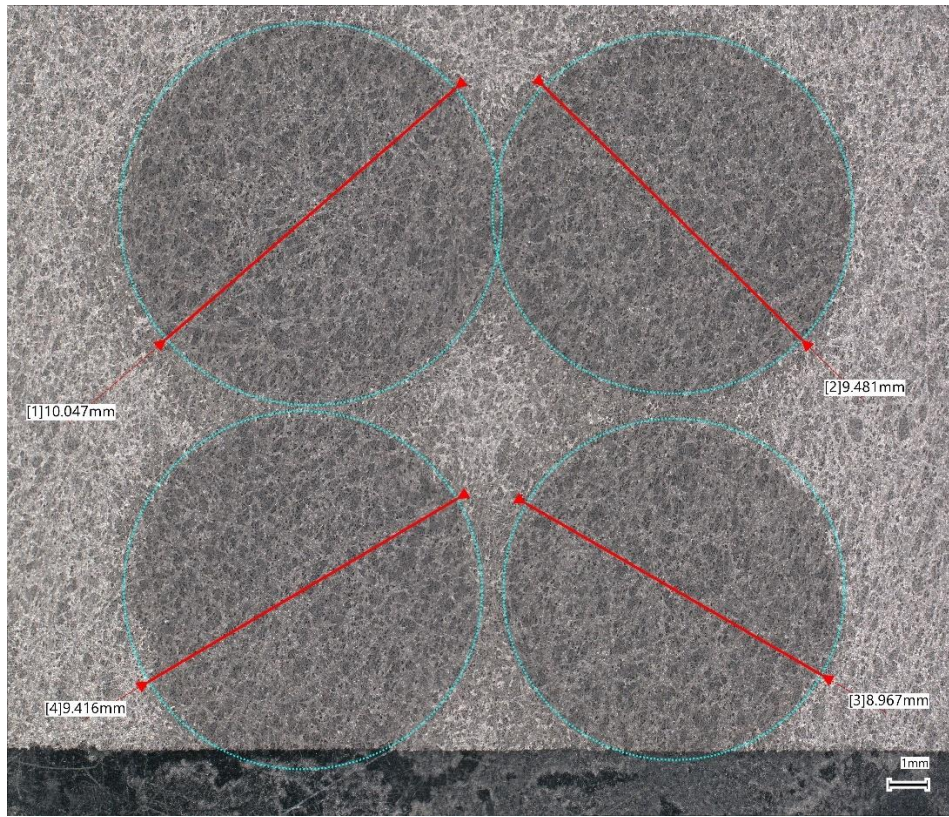


(b)

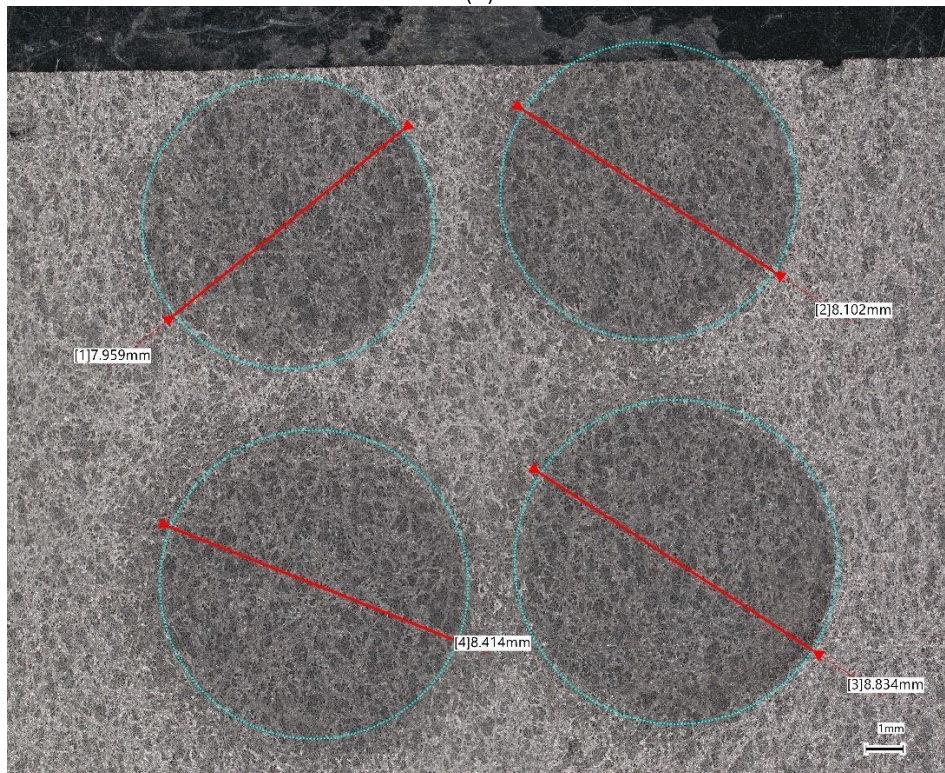
Figure A.6 P4 variant: (a) sample A (b) sample B

A.3. Area Pattern Variations

A1 pattern (design diameter = 8 mm)

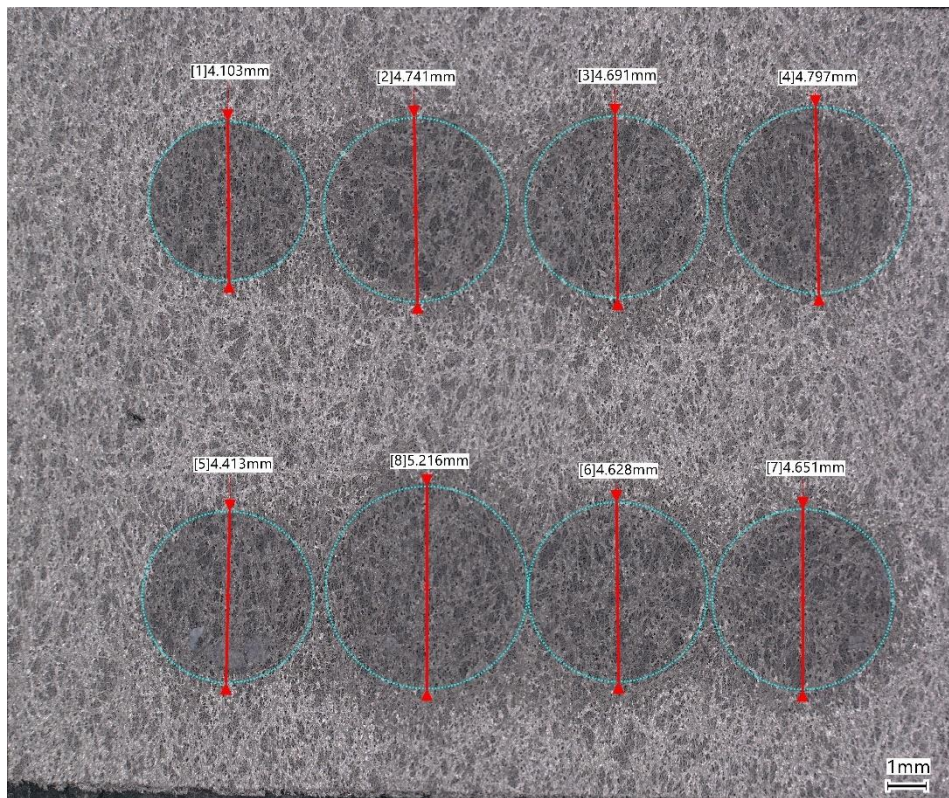


(a)

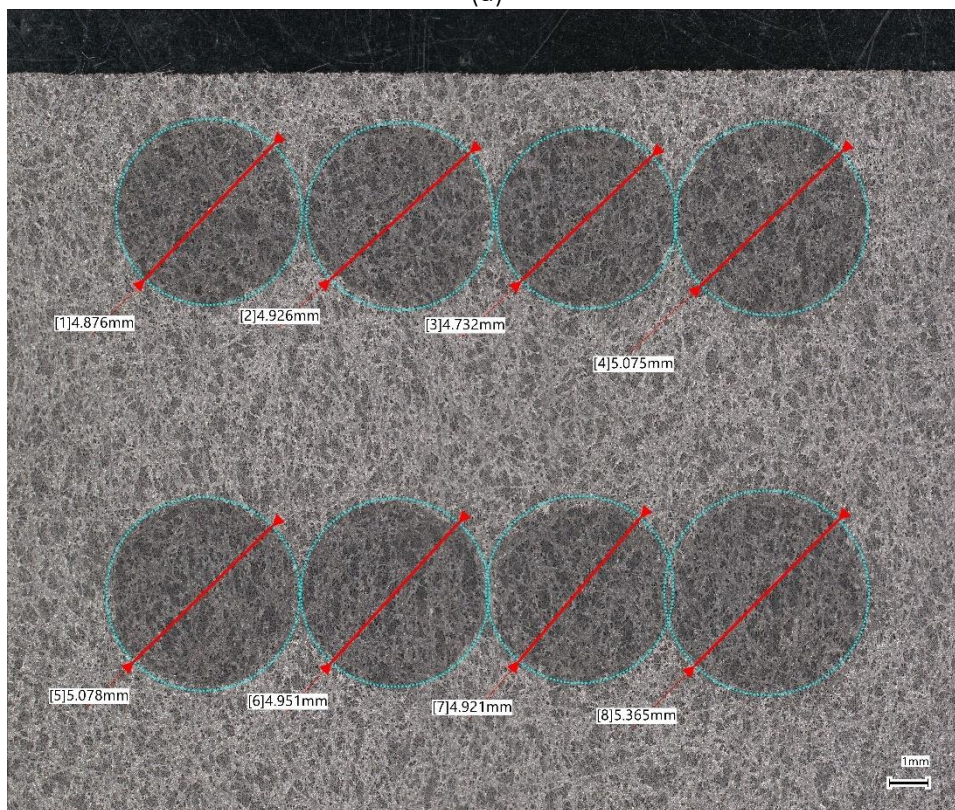


(b)

Figure A.7 A1 variant: (a) sample A (b) sample B

A2 pattern (design diameter = 4 mm)

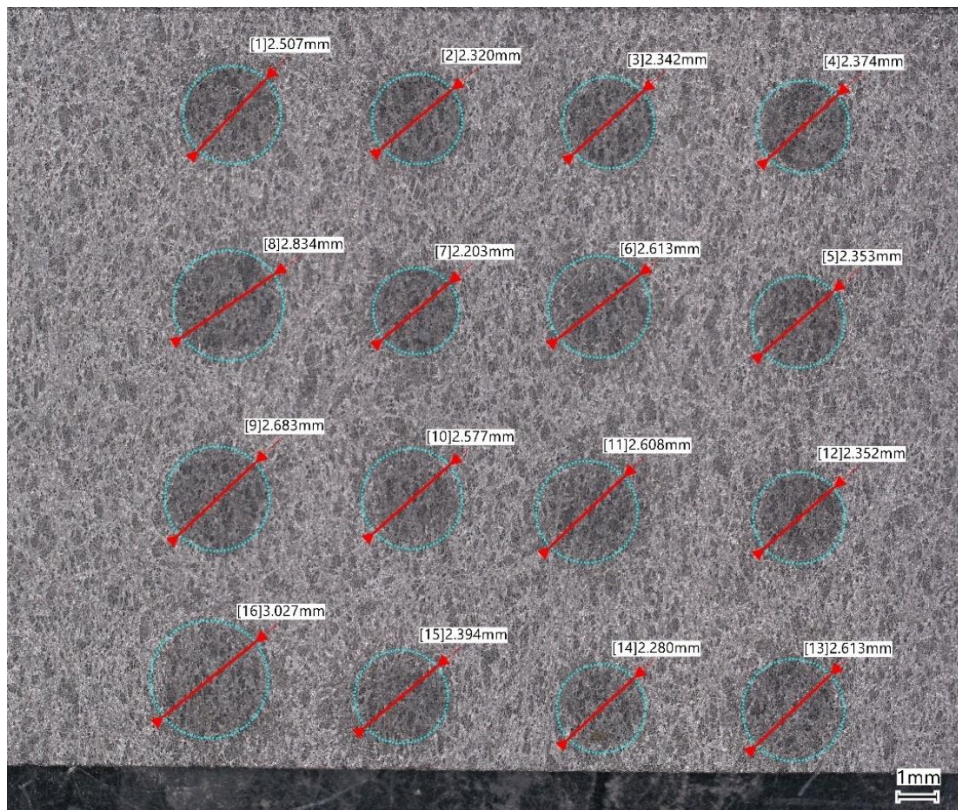
(a)



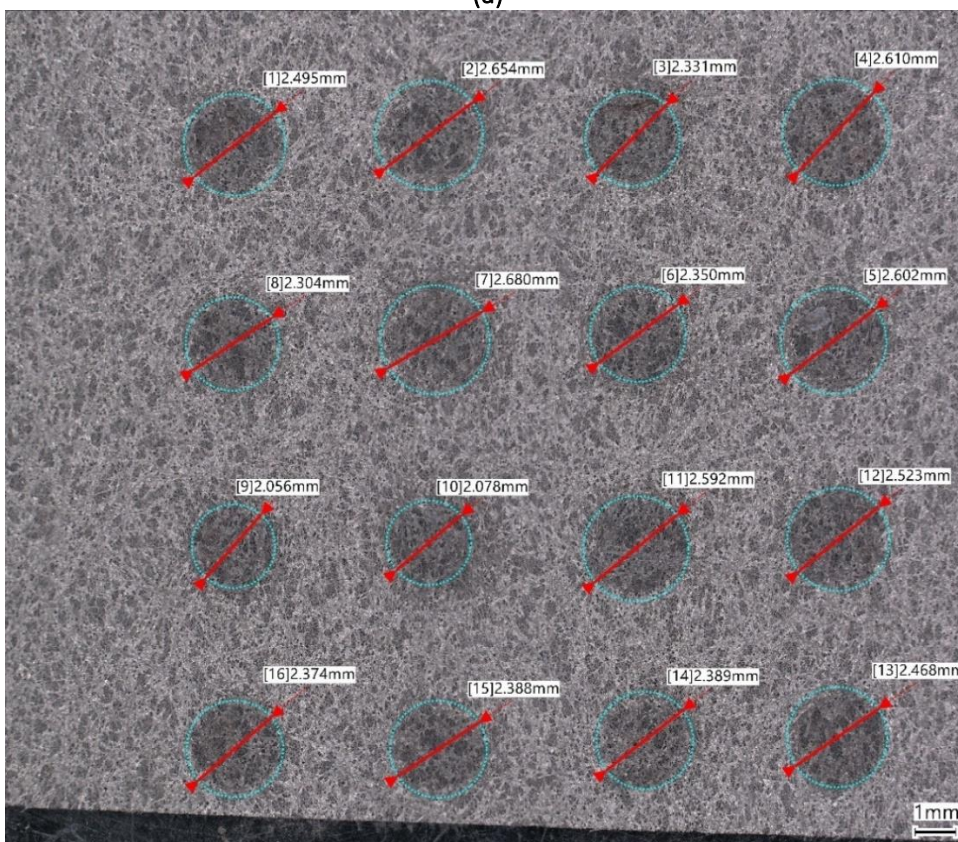
(b)

Figure A.8 A2 variant: (a) sample A (b) sample B

A3 Pattern (design diameter = 2 mm)



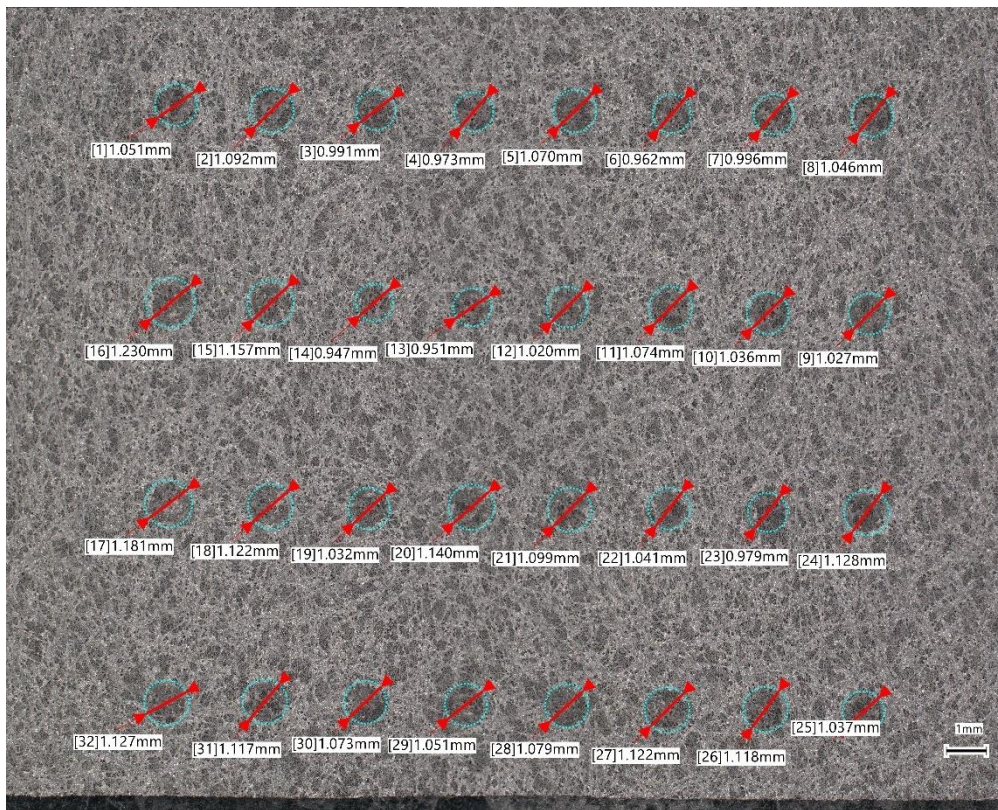
(a)



(b)

Figure A.9 A3 variant: (a) sample A (b) sample B

A4 Pattern (design diameter = 1 mm)



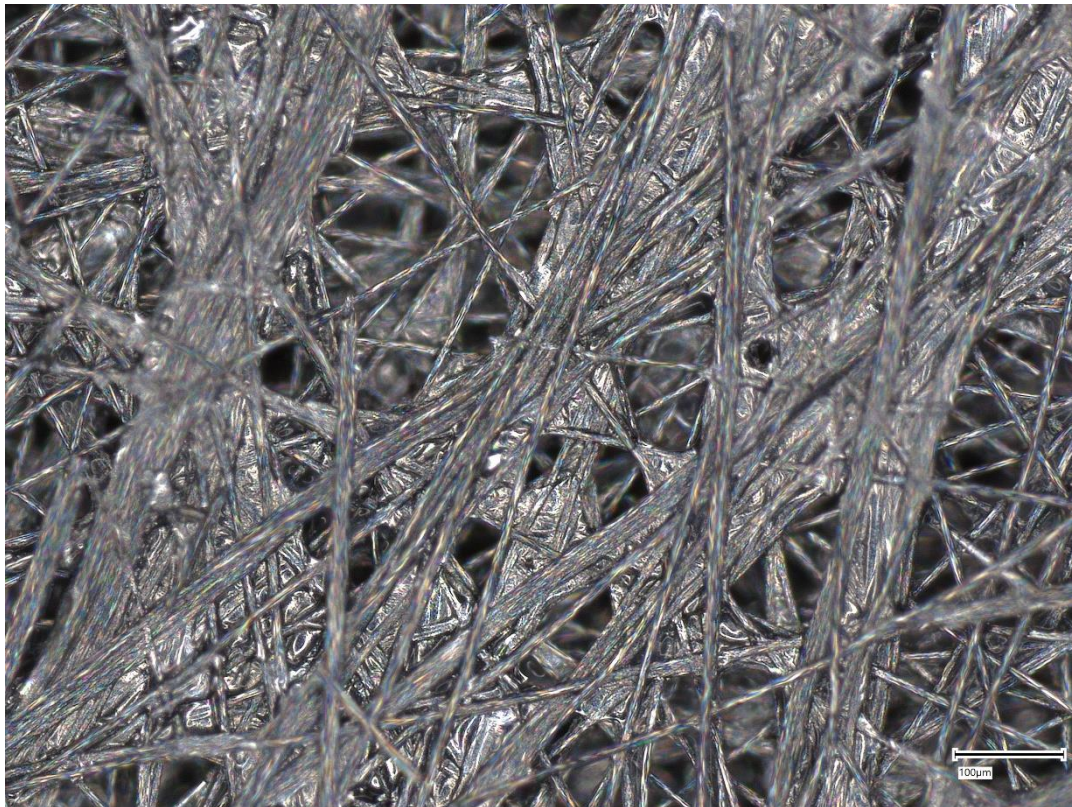
(a)



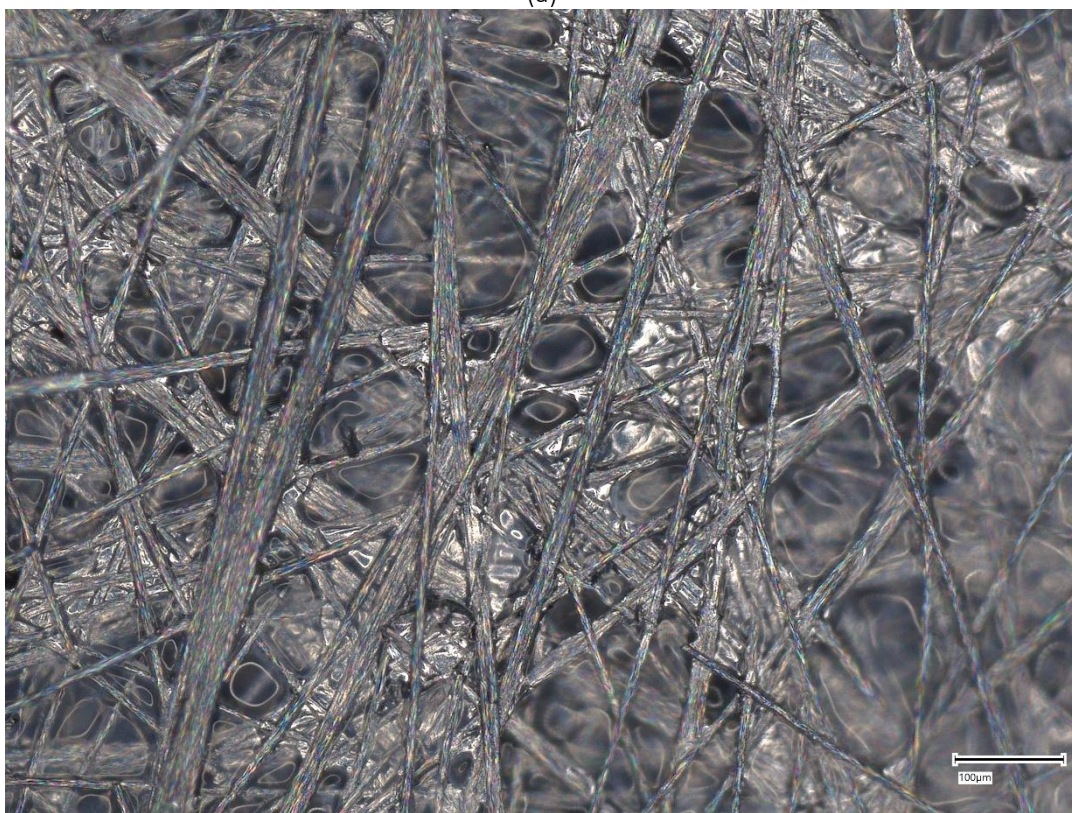
(b)

Figure A.10 A4 variant: (a) sample A (b) sample B

A.4. Dip-Coating Variations



(a)



(b)

Figure A.11 PTFE dip-coated CFP variants: (a) 20% mass PTFE (b) 60% mass PTFE

Appendix B - SEM Images and EDX Mappings

Note: not all of the elements can be mapped by EDX. The reason is due to EDX's limit in detecting low presence of the element

B.1. Bare Carbon

Post-Experiment Bare Carbon B

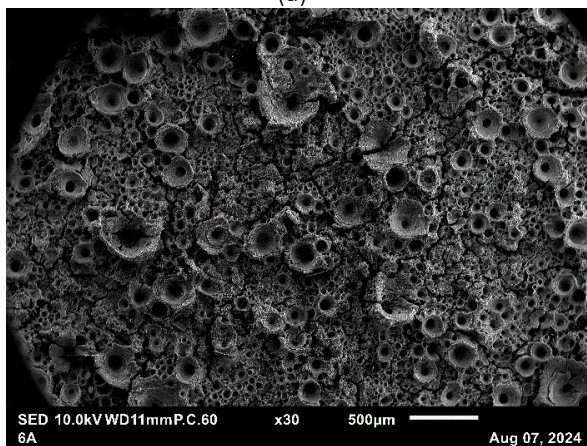
A more extreme case of post-experiment bare carbon sample. The analyte color becomes white indicating a reaction happened due to the high concentration of H_2O_2 with Na_2SiO_3 . The holes that appeared on the silicon layers might caused by the formation of O_2 bubbles.



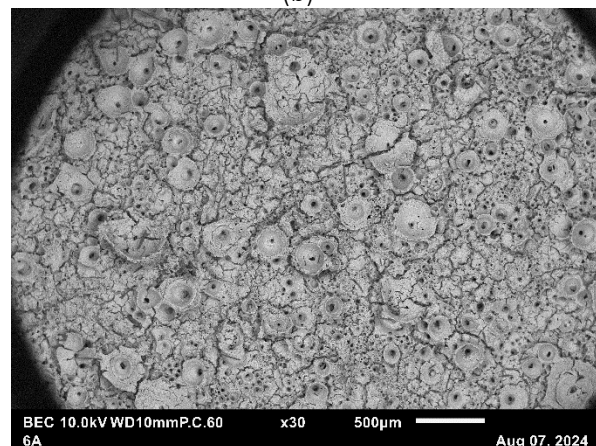
(a)



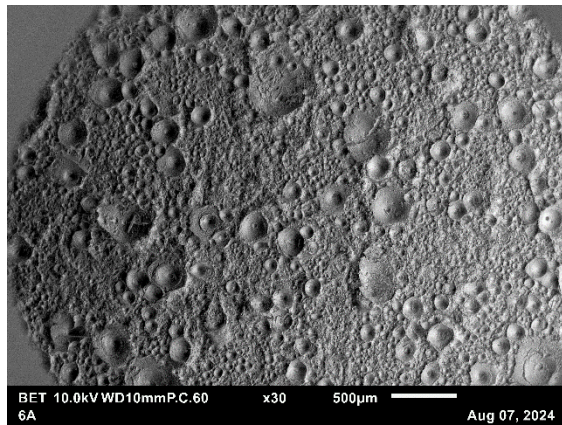
(b)



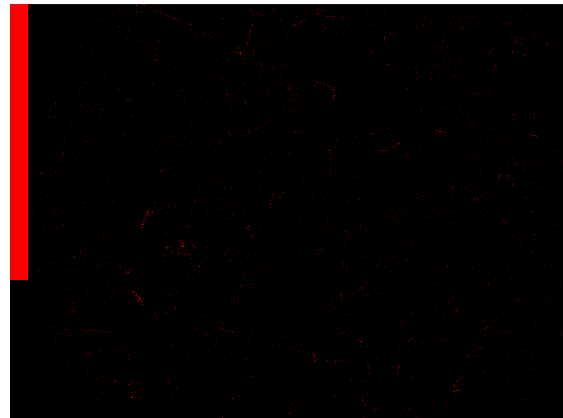
(c)



(d)



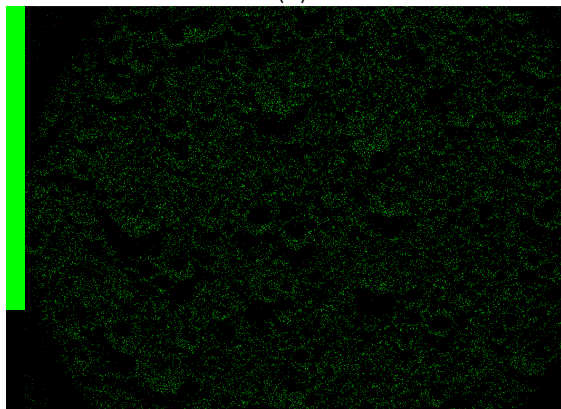
(e)



1.0 mm

C K

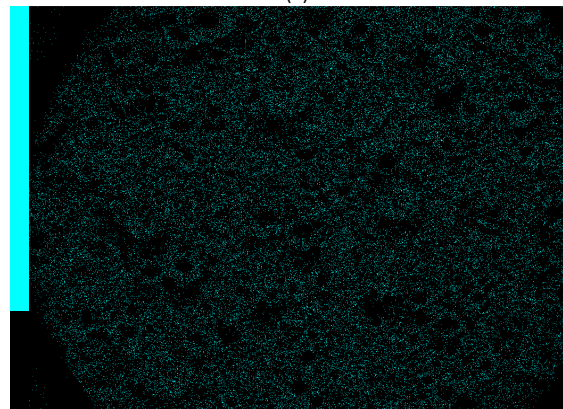
(f)



1.0 mm

O K

(g)



1.0 mm

Si K

(h)



1.0 mm

Na K

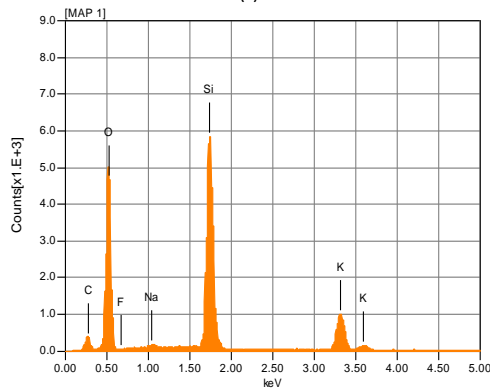
(i)



1.0 mm

K K

(j)



(k)

Formula	mass%	Atom%	Sigma	K ratio	Line
C	6.63	11.43	0.02	0.0005282	K
O	42.34	54.82	0.09	0.0242655	K
F	nd	nd			K
Na	0.35	0.32	0.02	0.0003331	K
Si	31.71	23.38	0.12	0.0405678	K
K	18.97	10.05	0.13	0.0246746	K
Total	100.00	100.00			

(l)

Figure B.1 Post-experiment electrode bare carbon B: (a) a silicon layer covered the whole electrode (b) the analyte becomes whiter after the operation reached the lifetime (c) SED image (d) BEC image (e) BET image; EDX mappings: (f) Carbon (g) Oxygen (h) Silicon (i) Sodium (j) Potassium (k) EDX spectrum (l) EDX chemical composition summary

B.2. PTFE-patterned Electrode

Pre-Experiment A4 sample A (x60)

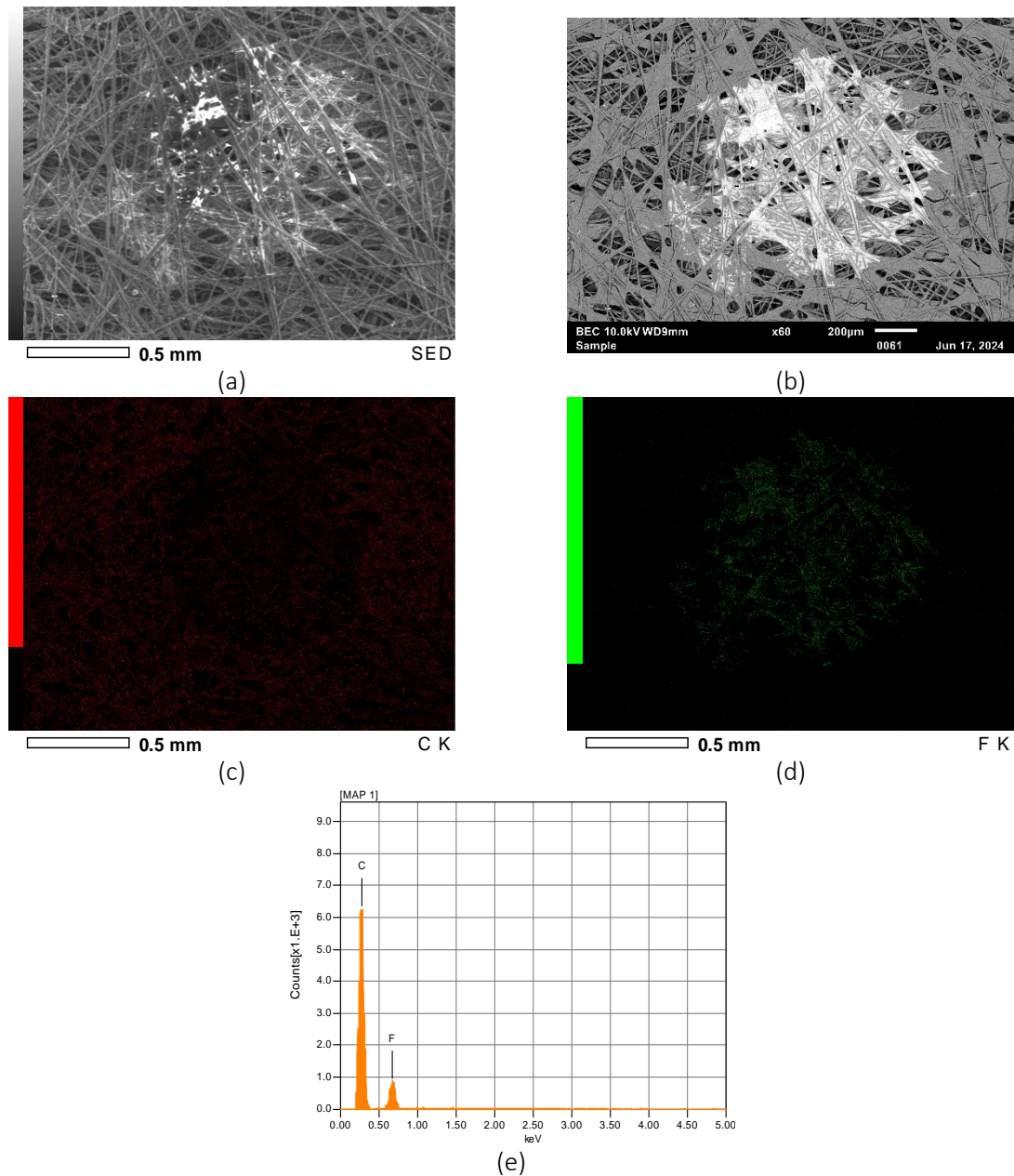
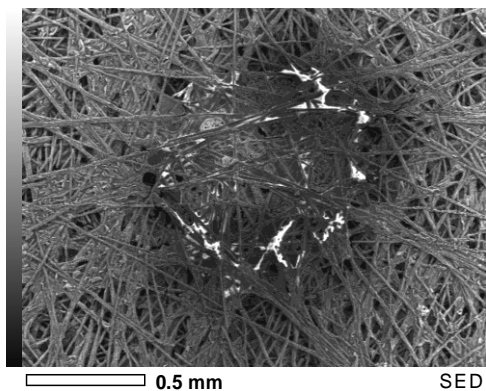
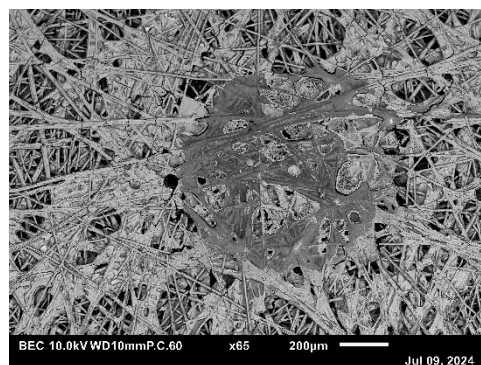


Figure B.2 SEM/EDX images of a PTFE pattern on CFP (A4 sample A) prior to the experiment: (a) SED image at x60; EDX mappings: (b) Carbon (c) Fluorine (d) EDX spectrum (ratio of F/C = 0.194)

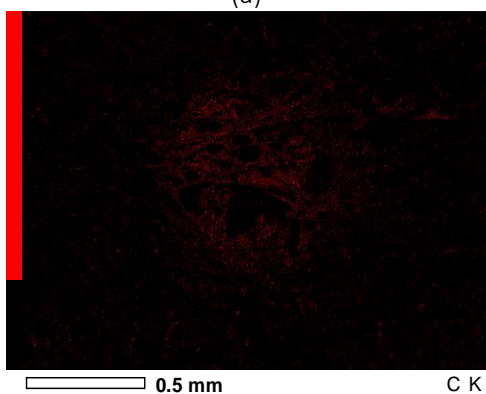
Post-Experiment A4 sample A (x65)



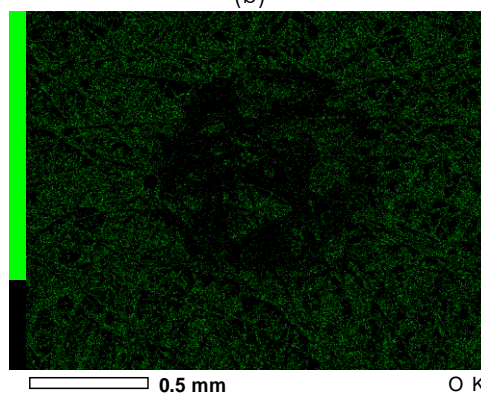
(a)



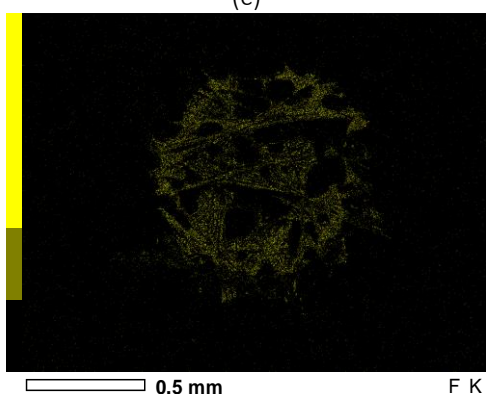
(b)



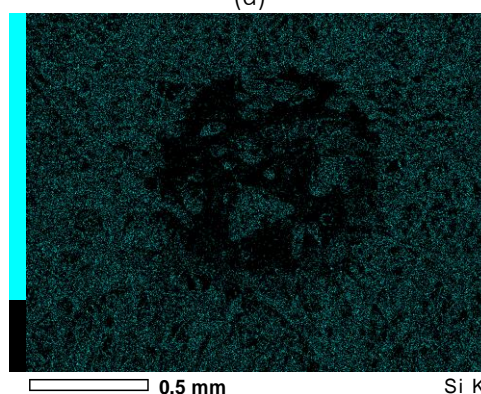
(c)



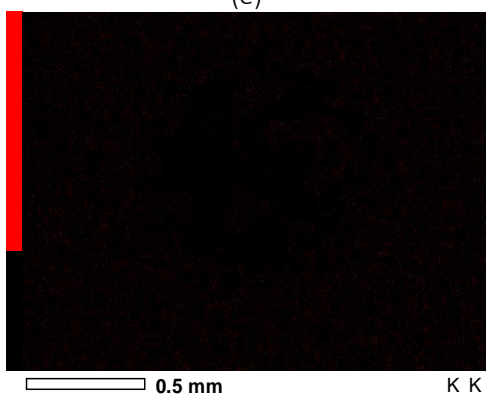
(d)



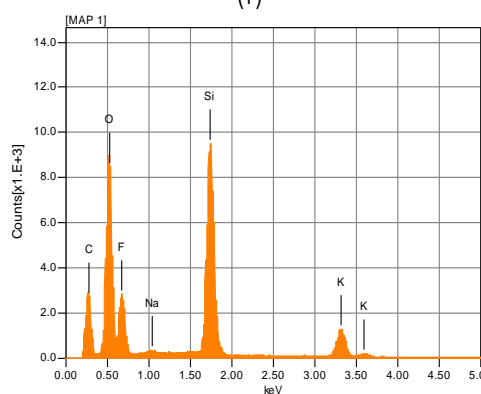
(e)



(f)



(g)



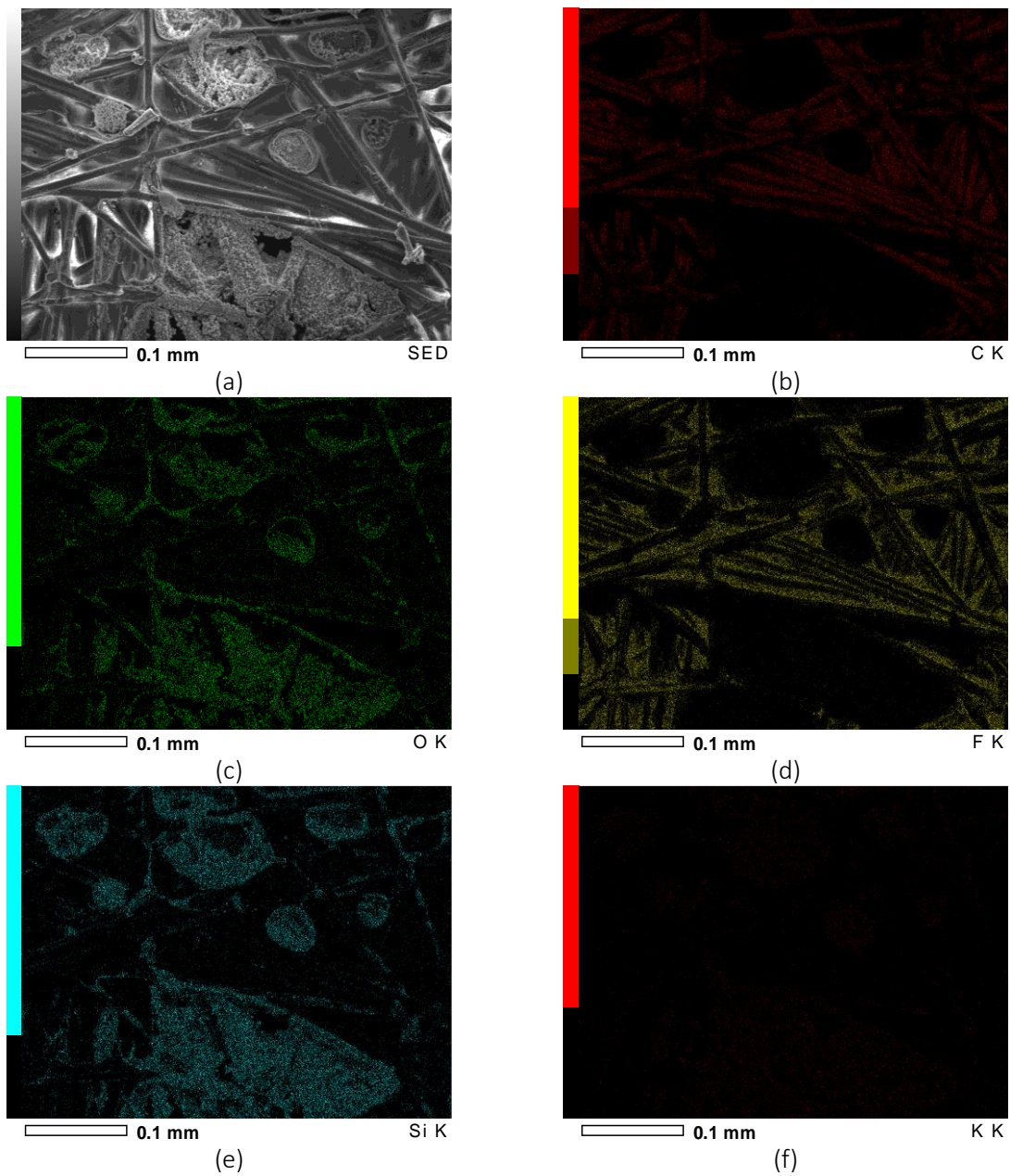
(h)

Formula	mass%	Atom%	Sigma	K ratio	Line
C	20.71	31.12	0.02	0.0037213	K
O	35.83	40.42	0.07	0.0391866	K
F	8.14	7.73	0.04	0.0195125	K
Na*	0.28	0.22	0.02	0.0005024	K
Si	23.96	15.40	0.08	0.0594033	K
K	11.07	5.11	0.08	0.0283614	K
Total	100.00	100.00			

(i)

Figure B.3 SEM/EDX images of a PTFE pattern on CFP (A4 sample A) after the experiment: (a) SED image at x65 (b) BEC image at x65; EDX mappings: (c) Carbon (d) Oxygen (e) Fluorine (f) Silicon (g) Potassium (h) EDX spectrum (i) EDX chemical composition summary

Post-Experiment A4 sample A – Center part (x300)



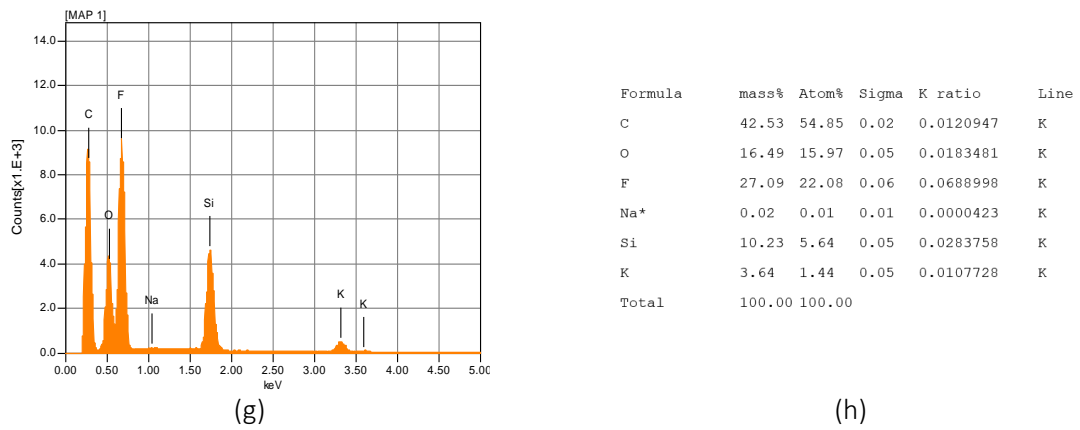
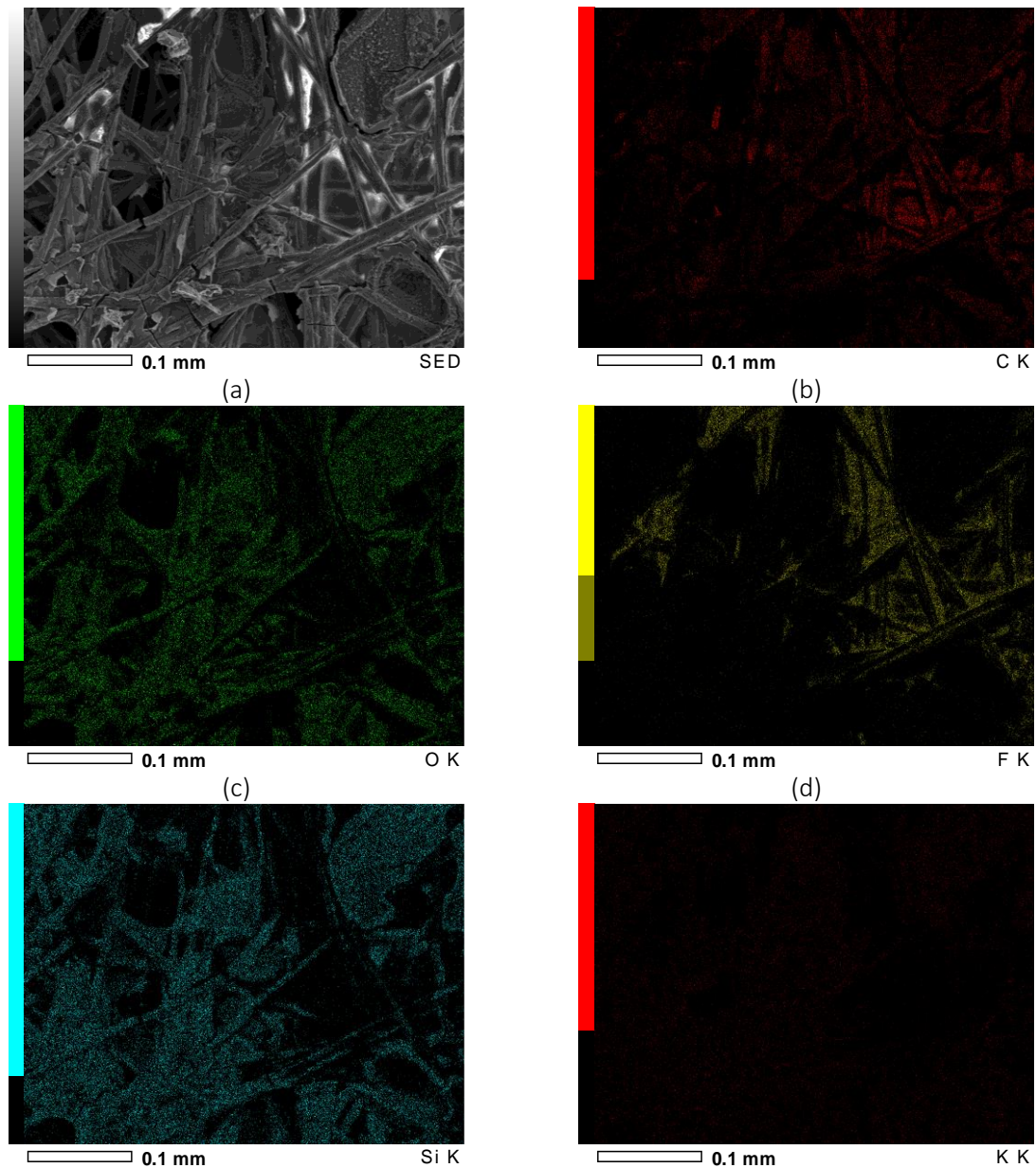


Figure B.4 SEM/EDX images of a PTFE pattern on CFP (A4 sample A) after the experiment on the center of the pattern: (a) SED image at x300; EDX mappings: (b) Carbon (c) Oxygen (d) Fluorine (e) Silicon (f) Potassium (g) EDX spectrum (h) EDX chemical composition summary

Post-Experiment A4 sample A – Near center part (x300)



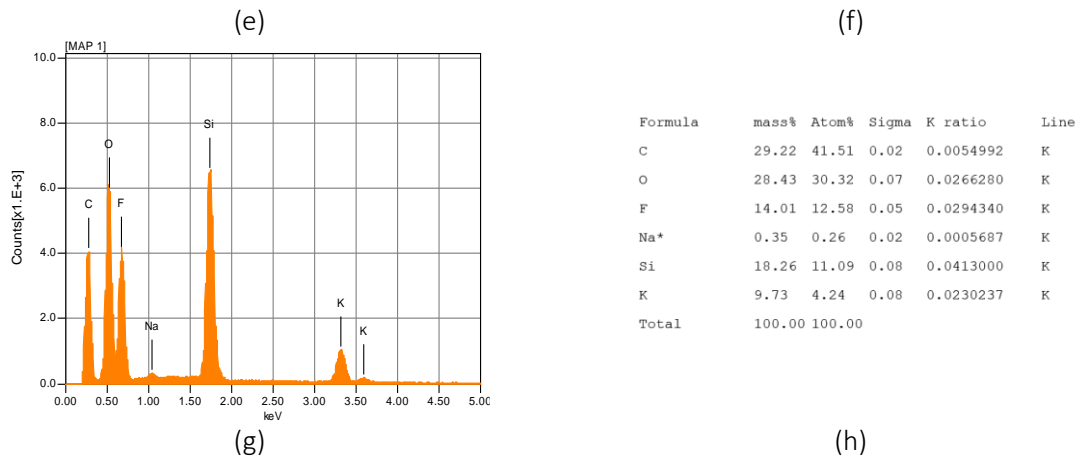
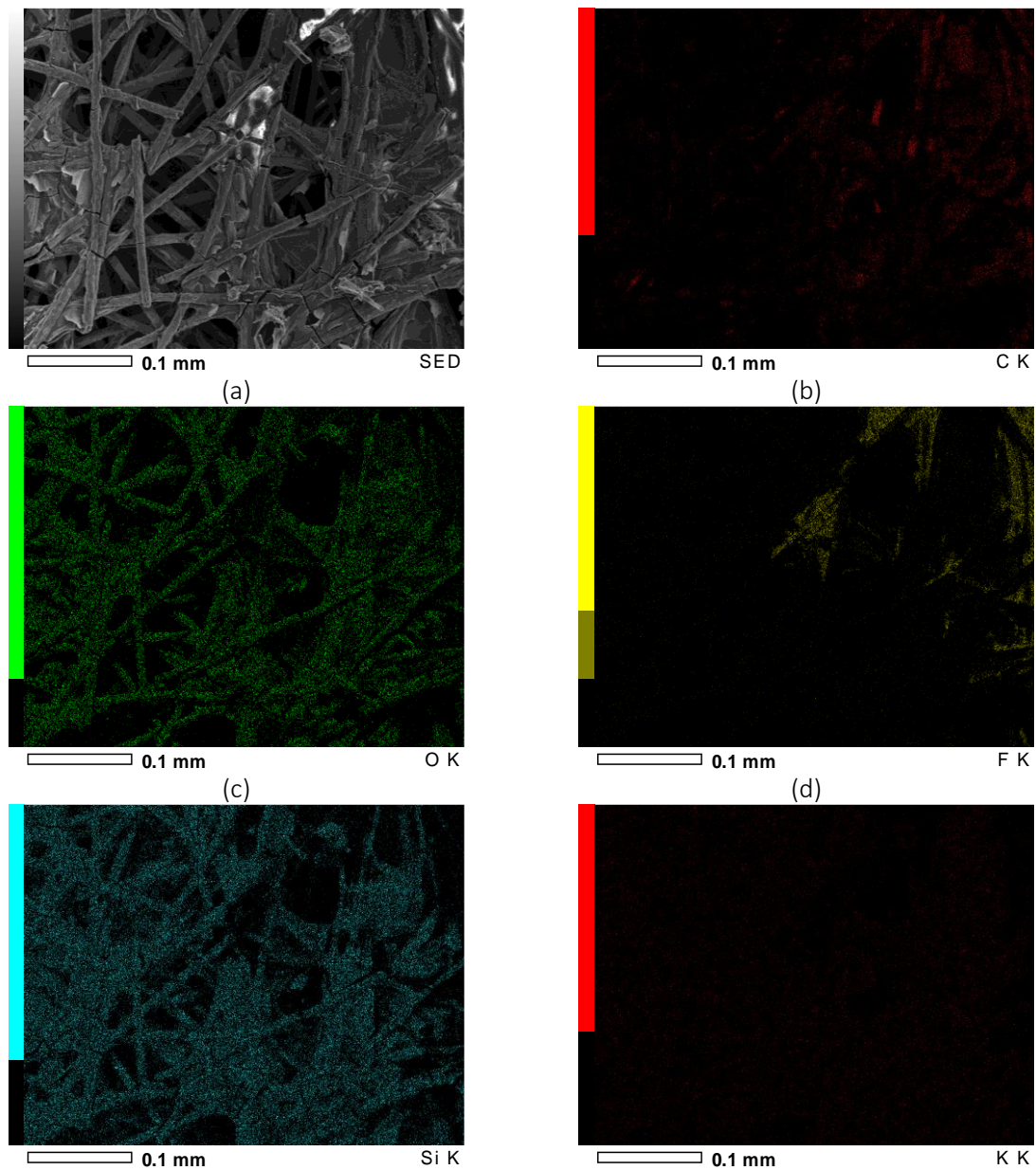


Figure B.5 SEM/EDX images of a PTFE pattern on CFP (A4 sample A) after the experiment on the near-center of the pattern: (a) SED image at x300; EDX mappings: (b) Carbon (c) Oxygen (d) Fluorine (e) Silicon (f) Potassium (g) EDX spectrum (h) EDX chemical composition summary

Post-Experiment A4 sample A – Edge part (x300)



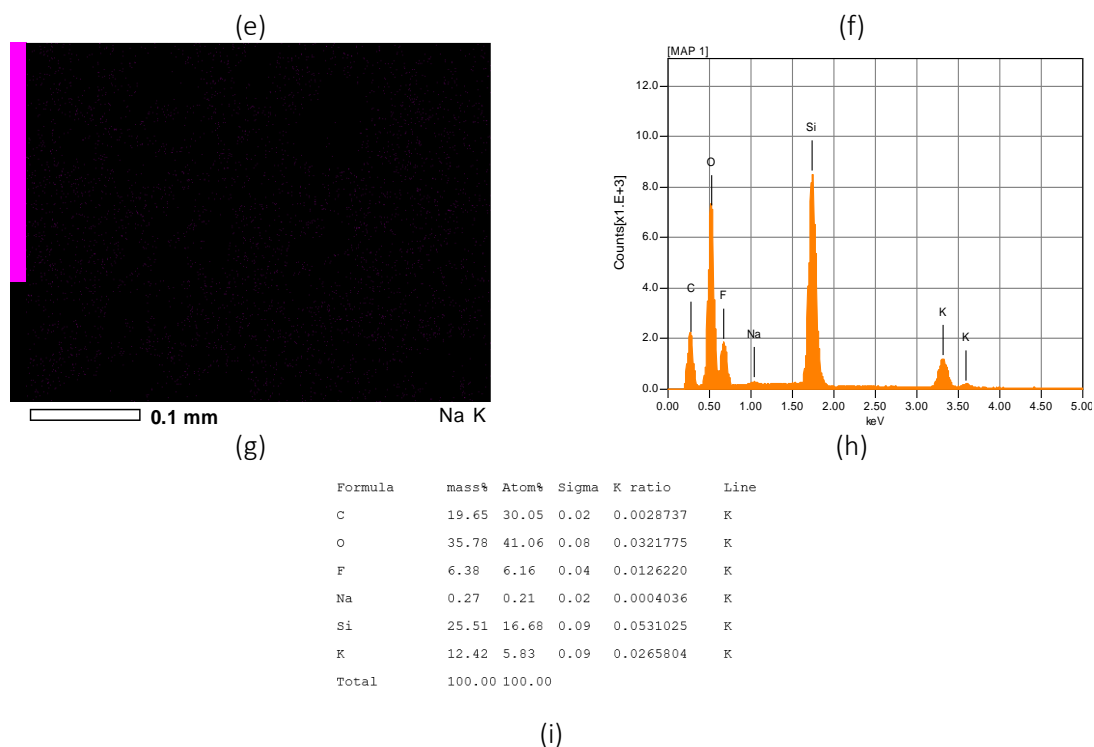
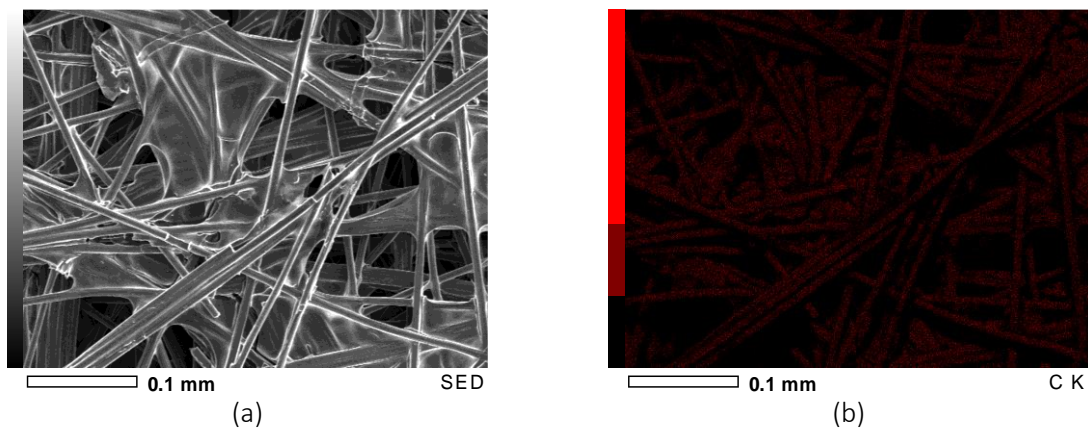


Figure B.6 SEM/EDX images of a PTFE pattern on CFP (A4 sample A) after the experiment on the edge of the pattern: (a) SED image at x300; EDX mappings: (b) Carbon (c) Oxygen (d) Fluorine (e) Silicon (f) Potassium (g) Sodium (h) EDX spectrum (i) EDX chemical composition summary

B.3. Dip-coated Electrode

Pre-Experiment 1% PTFE dip-coated CFP (sample A)



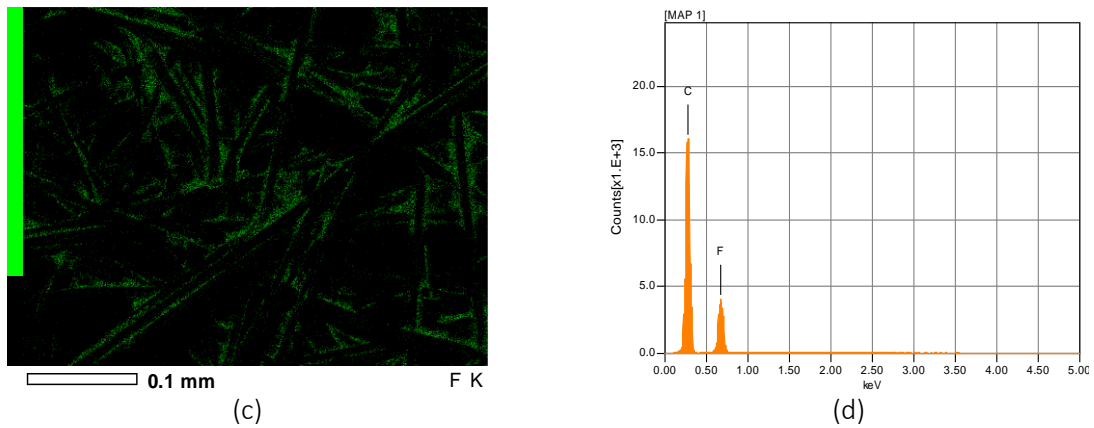


Figure B.7 SEM/EDX images of 1% PTFE dip-coated CFP (sample A) prior to the experiment: (a) SED image at x300; EDX mappings: (b) Carbon (c) Fluorine (d) EDX spectrum (ratio of F/C = 0.307)

Pre-Experiment 20% PTFE dip-coated CFP

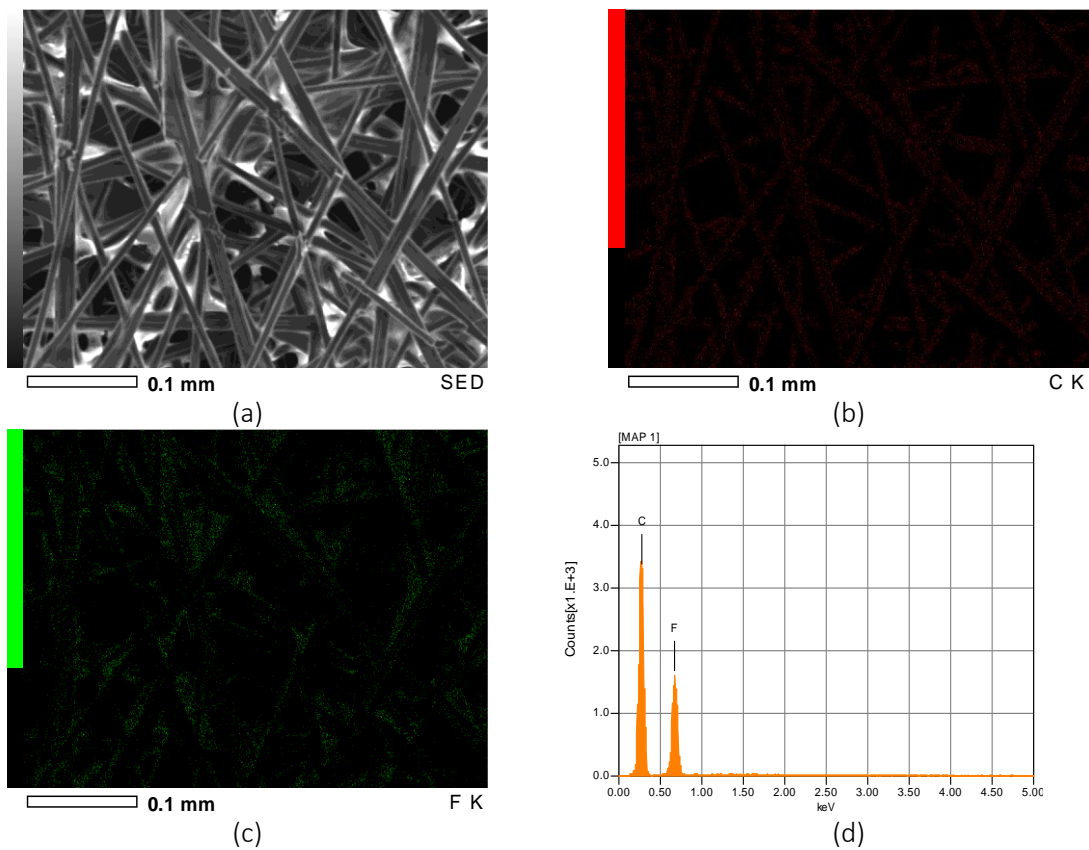


Figure B.8 SEM/EDX images of 20% PTFE dip-coated CFP prior to the experiment: (a) SED image at x300; EDX mappings: (b) Carbon (c) Oxygen (d) Fluorine (e) Silicon (f) Potassium (g) EDX spectrum (ratio of F/C = 0.492)

Pre-Experiment 60% PTFE dip-coated CFP

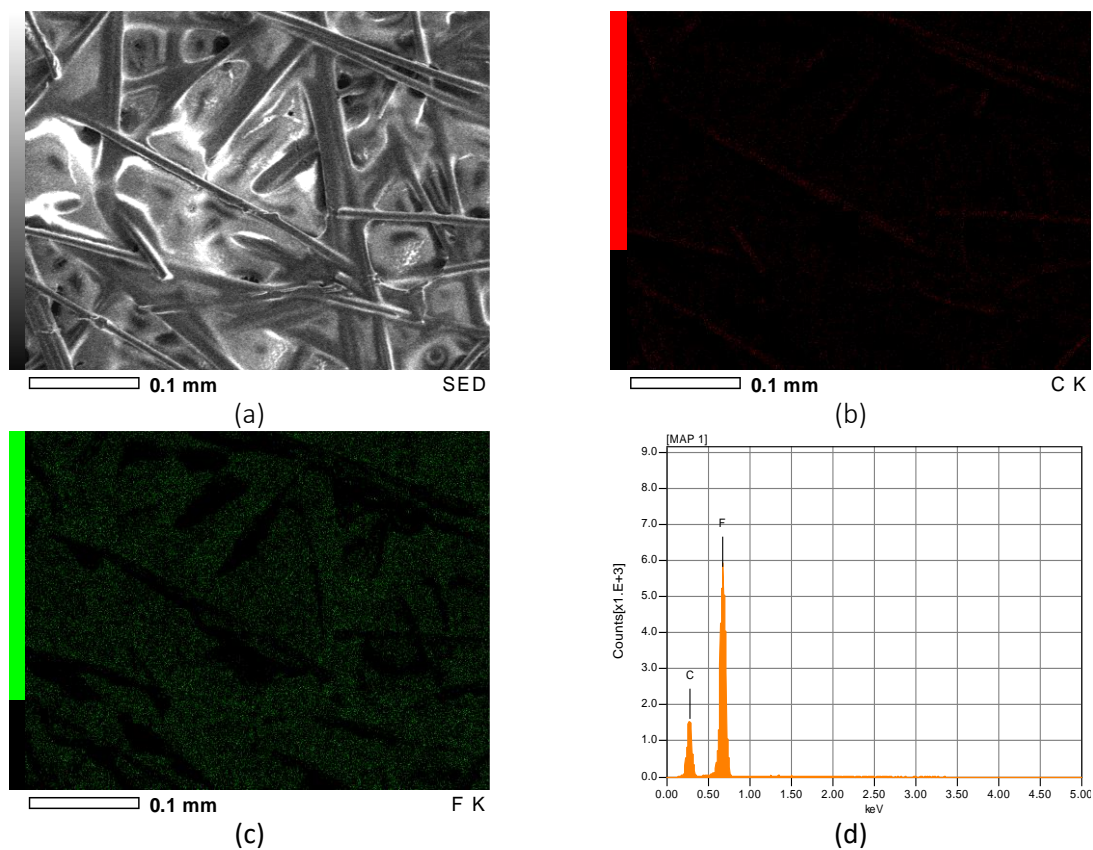
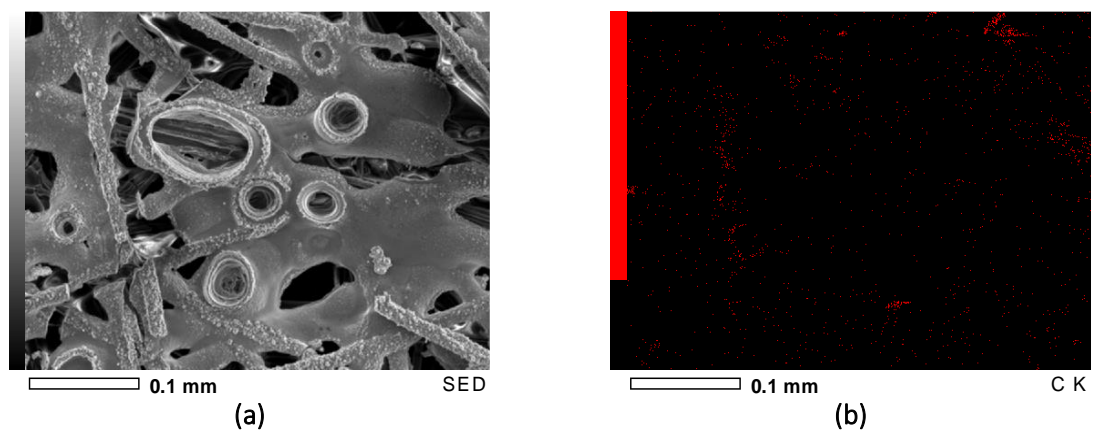


Figure B.9 SEM/EDX images of 60% PTFE dip-coated CFP prior to the experiment: (a) SED image at 300x; EDX mappings: (b) Carbon (c) Fluorine (d) EDX spectrum (ratio of F/C = 2.134)

Post Experiment – 20% PTFE dip-coated CFP (x300)



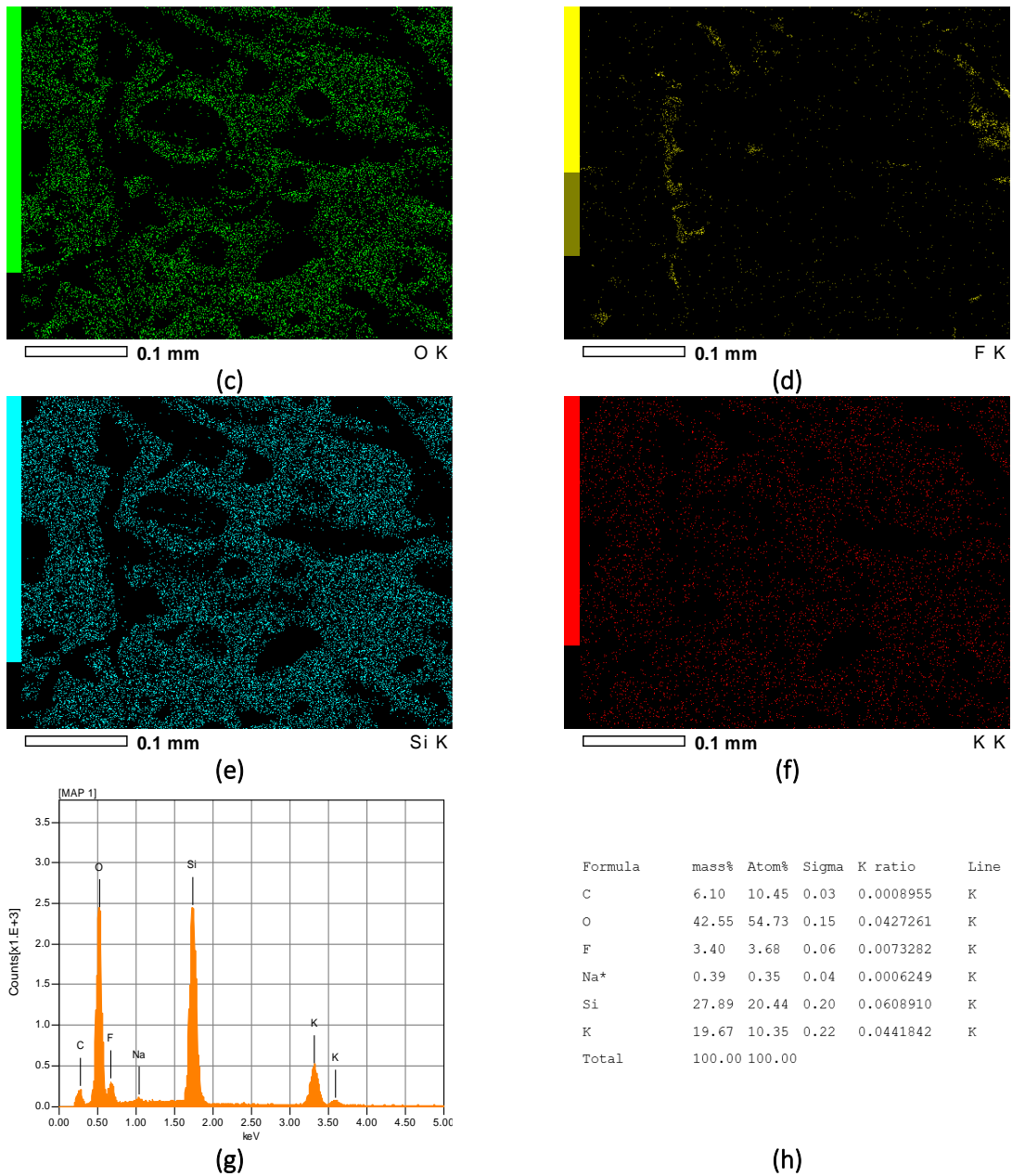
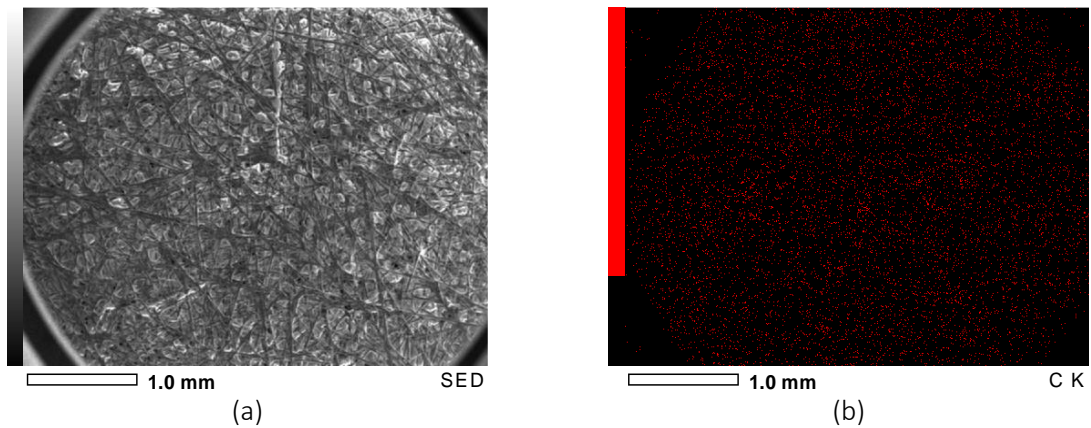


Figure B.10 SEM/EDX images of 20% PTFE dip-coated CFP after the experiment: (a) SED image at x300; EDX mappings: (b) Carbon (c) Oxygen (d) Fluorine (e) Silicon (f) Potassium (g) Sodium (h) EDX spectrum (i) EDX chemical composition summary

Post-Experiment – 60% PTFE dip-coated CFP (x30)



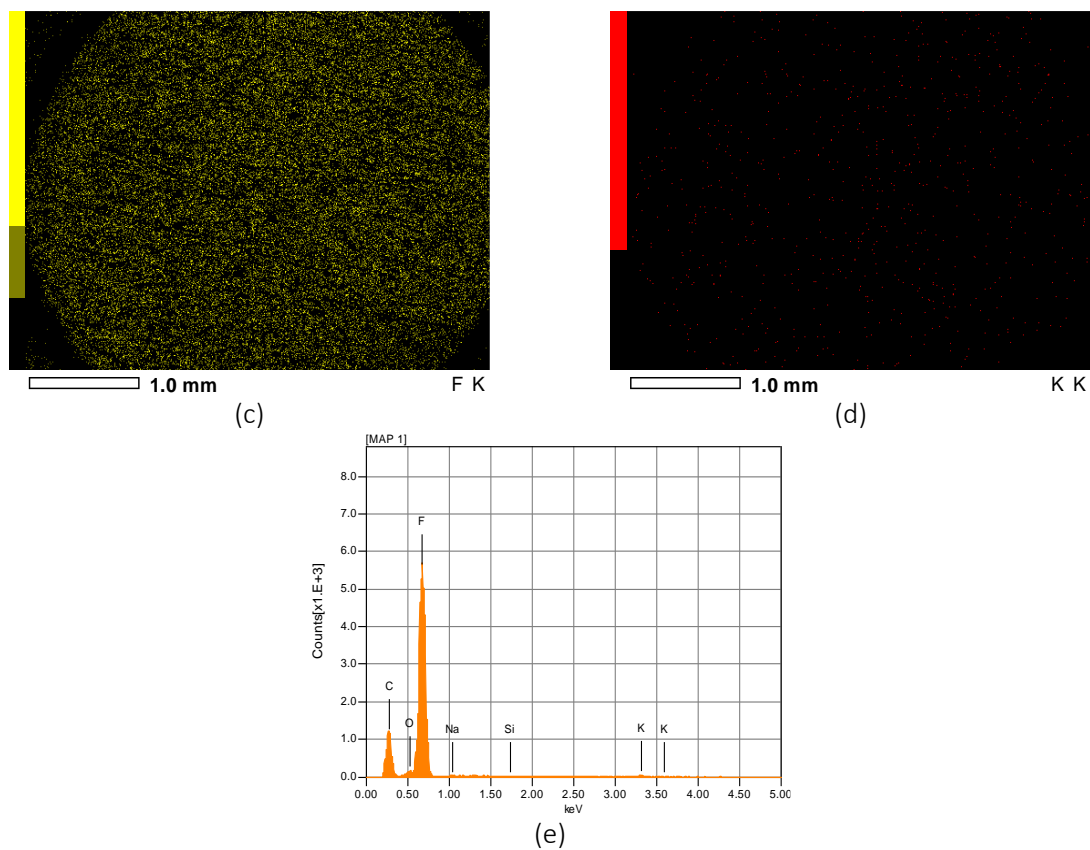
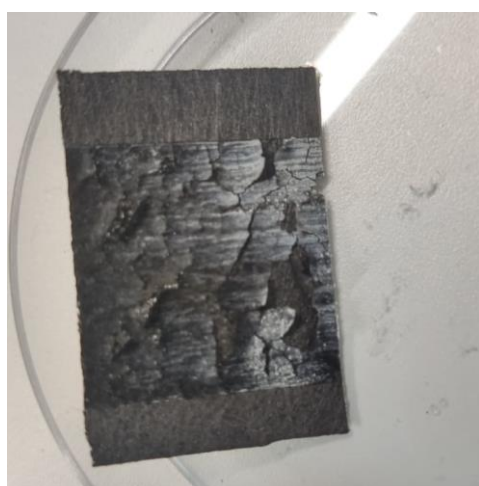


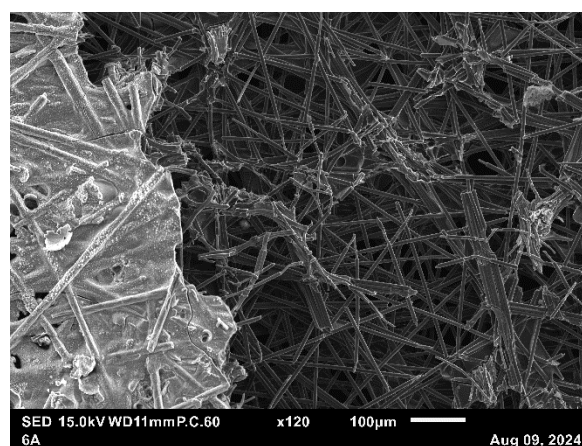
Figure B.11 SEM/EDX images of 60% PTFE dip-coated CFP after the experiment: (a) SED image at x30; EDX mappings: (b) Carbon (c) Fluorine (d) Potassium (d) EDX spectrum. No silicon elements appeared implying that the electron is not able to be transferred across the electrode, which would not trigger the migration of ions. (Other elements mappings are not included due to low indication)

Additional

The layers of Na_2SiO_3 from 1% carbon A can be removed from the carbon electrode after a certain of time.



(a)



(b)

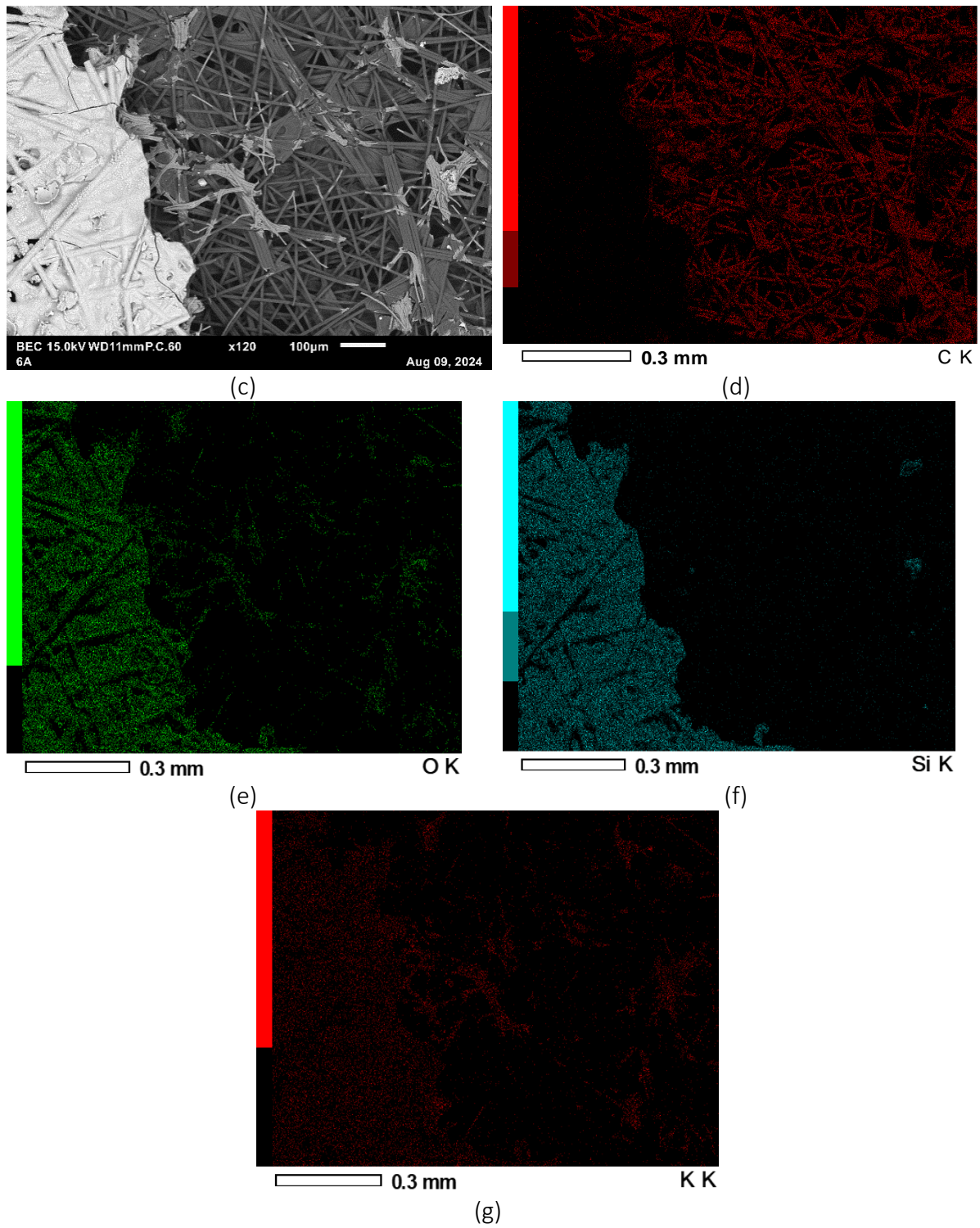


Figure B.12 Observing the post-experiment dip-coated 1%A partially removed of metasilicate layer: (a) the front metasilicate layers are exfoliated from the electrode (b) SED image at x120 (c) BEC image at x120; EDX mappings: (d) Carbon (e) Oxygen (f) Silicon (g) Potassium. (Note: Sodium and Fluorine are in a trace amount of 0.12% and 0.36% in mass)